Sex-specific Changes in Neonatal Cardiac Mitochondria in Response to Perinatal Iron Deficiency

by

Claudia Diana Holody

A thesis submitted in partial fulfillment of the requirements for the degree of

Master of Science

Medical Sciences – Pediatrics
University of Alberta

Abstract

Introduction: Iron deficiency (ID) during gestation has been shown to alter growth and developmental trajectories, consequentially increasing the risk of long-term cardiovascular dysfunction in offspring. The heart becomes energetically dependent on mitochondria soon after birth and disturbances in energy metabolism could impact cardiac development. Given that iron is essential for oxygen transport and an important component of the electron transport system, we hypothesized that perinatal ID would alter cardiac mitochondrial function in the neonatal period.

Objectives: In hearts of neonatal control and iron-deficient offspring, we sought to (1) perform untargeted proteomics analysis; (2) assess changes in mitochondrial function and reactive oxygen species generation, and (3) explore the mechanisms of iron metabolism underlying these changes.

Methods: Female rats were fed an iron-restricted or an iron-replete diet before and during pregnancy. Hearts from neonatal male and female pups underwent quantitative shotgun proteomics analysis. Mitochondrial content and function were assessed by citrate synthase activity and high-resolution respirometry, respectively. Superoxide levels were assessed using dihydroethidium fluorescence. Antioxidant and iron metabolism genes were assessed by RT-qPCR. The effects of ID and postnatal day (PD) were analyzed by fitting a mixed-effects model.

Results: Hemoglobin levels were reduced in ID pups at PD0 and PD14 but recovered by PD28. Body weights of ID pups were reduced at all time points, while heart weights (normalized to body weight) were increased. Shotgun proteomics revealed upregulation of mitochondrion organization proteins in ID male hearts. In ID male hearts only, the mitochondrial content, shown by the citrate synthase activity, was increased by 25% while the mitochondrial respiration through

the NADH-pathway, succinate-pathway, and FAO-pathway, expressed per citrate synthase activity units, was reduced by up to 50%. ID did not change superoxide or antioxidant enzyme mRNA levels in either sex. Transferrin receptor-1 mRNA was increased in ID females; upregulation of this protein was confirmed by proteomics at PD0.

Conclusions: Although male and female neonates experience a similar insult with maternal iron-restriction, only male hearts showed reduced mitochondrial efficiency and compensation by increased mitochondrial content. Lack of changes in other parameters indicate that mitochondria in male ID hearts are likely functional but may have an abnormal protein composition. Further, females may have a greater capacity to prioritize iron for the heart by increasing iron import during ID.

Preface

This thesis is an original work by Claudia Holody. No part of this thesis has been previously published.

Acknowledgements

I would first like to thank my supervisors, Dr. Stephane Bourque and Dr. Hélène Lemieux, for their unwavering support through my master's degree. Their expertise, enthusiasm, and encouragement, especially through challenging times, have been vital to my development as a researcher. Thank you to Dr. Antoine Dufour and Daniel Young at the University of Calgary for their work and guidance on completing the proteomics experiments. Thank you to Chunpeng Nie, for his contribution and knowledge approaching the proteomics analyses and completing RT-qPCR experiments. Thank you to my committee members, Dr. John Seubert and Dr. Jason Dyck. Finally, thank you to the colleagues, friends, and mentors that supported me throughout the years.

Table of Contents

List of Tables

List of Figures

Abbreviations

CS	Citrate synthase
CTL	Control
CVD	Cardiovascular disease
DHE	Dihydroethidium
DMT1	Divalent metal transporter 1
DOHaD	Developmental Origins of Health and Disease
ETF	Electron transferring flavoprotein
ETS	Electron transport system
FAO	Fatty acid oxidation
FCR	Flux control ratio
Fe	Iron
FPN	Ferroportin
FTH	Ferritin heavy chain
FTL	Ferritin light chain
HAMP	Hepcidin antimicrobial protein
Hb	Hemoglobin
ID	Iron deficiency
IDA	Iron deficiency anemia
NCD	Non-communicable disease
OXPHOS	Oxidative phosphorylation
PD	Postnatal day
TFR1	Transferrin receptor 1

Chapter 1
Introduction

1.1 Developmental Origins of Health and Disease

Non-communicable diseases (NCDs) represent an enduring public health concern, affecting countries of all income levels at alarming rates. NCDs are progressive conditions that arise over a prolonged period of time from a combination of biopsychosocial factors and are not caused by inter-individual transmission via a disease vector (World Health Organization, 2018; World Health Organization, 2022a; World Health Organization, 2022b). Shockingly, they are responsible for over 70% of mortalities worldwide and 90% in the industrialized nations like Canada (World Health Organization, 2018; World Health Organization, 2022a). Within NCDs, cardiovascular diseases (CVDs) leads amongst all causes of death at 31% (World Health Organization, 2018). While mortality rates attributed to NCDs tend to be lower in low- and middle-income countries, altogether, these populations comprise over three quarters of NCD deaths (World Health Organization, 2022a). In individuals where NCD does not result in premature death (World Health Organization, 2022a), it reduces quality of life (Van Wilder et al., 2020; Van Wilder et al., 2022) and increases severity of communicable disease, which has become an even greater concern in the era of the COVID-19 pandemic (World Health Organization, 2022a). On a larger scale, the burden of NCDs places substantial strain on governments and health systems, demanding significant financial expenditures and overwhelming potentially ill-prepared and under-resourced healthcare infrastructure (GBD 2015 DALYs and HALE Collaborators, 2016; GBD 2017 DALYs and HALE Collaborators, 2018; Timmis et al., 2022). Currently, the primary method of management and treatment for these diseases includes behavioural, psychological, physical,

nutritional, pharmaceutical, and technical interventions following diagnosis (Timmis et al., 2022). However, prevention remains the ultimate goal and challenge. In this pursuit, the World Health Organization (WHO) urges national policymakers to implement strategies that target modifiable behavioural risk factors for NCDs, focusing on diet, exercise, and substance use (World Health Organization, 2018; World Health Organization, 2022a). Thus far, these recommendations have not produced meaningful progress and various ongoing efforts have stagnated following COVID-19 disruptions (World Health Organization, 2022a). Consequently, many countries are unlikely to meet WHO NCD targets within the suggested timeline (Timmis et al., 2022; World Health Organization, 2022a). Although lifestyle changes are important in mitigating disease risk, research is now advocating for a multifactorial and integrated plan of action, recognizing that the complex origins of NCDs have interfered with the success of control and prevention strategies at all population levels, from individual to global (Baird et al., 2017). The proposed 'lifecourse approach' describes an evolving paradigm that considers the cumulative impact of a lifetime of exposures to NCD risk factors (Baird et al., 2017).

Critical to this understanding and its application is the recognition that early life adversities, be they biological, psychological, and/or social, can influence long-term health outcomes. Though referenced in scientific literature as early as the 1920s, this concept as a concrete field of study was born out of a series of epidemiological studies conducted by David Barker and Clive Osmond in the 1980s (Barker and Osmond, 1986; Barker and Osmond, 1987a; Barker and Osmond, 1987b; reviewed by Bourque and Davidge, 2020). In identifying associations between indices of infant health, namely birth weight and postnatal growth trajectory, and long term cardiovascular health, Barker and Osmond laid the foundation for what is now known as the Developmental Origins of Health and Disease (DOHaD) (Bourque and Davidge, 2020; Fall and Osmond, 2013). Early on,

Barker's observations led him to suspect poor maternal (and thereby fetal) nutrition as a crucial, if not causal, influence explaining their findings (Bourque and Davidge, 2020; Fall and Osmond, 2013). Various famine studies later supported these initial suspicions (Bourque and Davidge, 2020; Fall and Osmond, 2013; Michonska et al., 2022; Padmanabhan et al., 2016) and solidified maternal nutrition as a prominent developmental stressor of interest within DOHaD research. The subsequent evolution of Barker and Osmond's work over the last 40 years has expanded our understanding of maternal nutrition through pregnancy by further exploring facets of both under- and overnutrition and the role of specific macro- and micronutrients in development (Bailey, 2015; Baird et al., 2017; Michonska et al., 2022; Padmanabhan et al., 2016), the latter of which will be explored further. Despite its epidemiological roots, preclinical studies have played a crucial role in elucidating the mechanisms behind the observed associations.

The DOHaD hypothesis posits that challenges during critical developmental periods can fundamentally alter the structure and function of biological systems and thereby predispose an individual to NCDs in later life (Bourque and Davidge, 2020; Nathanielsz et al., 2007). The integration of several key principles underlying developmental biology illuminate the current understanding of this hypothesis. Phenotypic plasticity is the phenomenon by which a single genotype can produce various phenotypes in response to an internal or external stimulus (Burggren and Reyna, 2011; Padmanabhan et al., 2016; West-Eberhard, 2005). This quality confers adaptability and survivability to the living organism when confronted with variations in its environment and/or deviations from homeostasis (Padmanabhan et al., 2016). The term developmental plasticity, then, emphasizes that during development, from preconception to the first postnatal years, the living organism is highly responsive to environmental or physiological stimuli and thus uniquely vulnerable to phenotypic alterations prompted by external influences

(Padmanabhan et al., 2016; West-Eberhard, 2003). Because this level of plasticity progressively declines as the organism matures, phenotypic alterations, originally deployed as a response to a specific stimulus during development, can become solidified as intrinsic functional and anatomical characteristics that persist beyond the presence of the original inciting force (Bourque and Davidge, 2020; Padmanabhan et al., 2016). This, in turn, can shift the organism's developmental trajectory, that is, the progression of physiological functional capacity across the lifespan, from early development (i.e., organogenesis, growth, transition to adult phenotype, and maturation), through to adulthood, age-related decline, and death (Bourque and Davidge, 2020; Burggren and Reyna, 2011). Exposures capable of influencing development in this way can grant an organism greater resilience over its lifetime, i.e., a more favourable developmental trajectory (Bourque and Davidge, 2020). However, perhaps of more concern are the stressors that alter developmental trajectory in an unfavourable manner and produce an increased risk of NCDs in adulthood. The potential impact of such an exposure on the lifelong health and disease of an individual is augmented when considering that developmental plasticity spans across levels of biological organization, meaning that the effect(s) of a single stressor to which any level responds can be amplified outward, above and below its origin (Burggren and Reyna, 2011; Padmanabhan et al., 2016; West-Eberhard, 2005). Further, the transience of developmental plasticity also brought about the idea of critical windows of development; indeed, it is well known that even the same stressor applied at different developmental periods can affect developmental trajectory differently (Burggren and Reyna, 2011). Mid-development may be considered most vulnerable since at both ends of the developmental process, the organism is either too undeveloped for anything to become permanent or too old to be plastic enough to incite changes that would cause programming (Burggren and Reyna, 2011; Dötsch, 2014; Padmanabhan et al., 2016). Thus, the perinatal period,

the time surrounding birth, may be of particular interest as it represents the physiological disconnection between the fetus and the mom. Even after the fetus is fully formed, the perinatal period still represents an important period of organogenesis and tissue differentiation and shifts from in utero to ex utero life (Padmanabhan et al., 2016). The physiological adaptations that occur during this time when superimposed with a stressor, are likely to have long lasting effects.

Preclinical DOHaD research has not only offered potential for early intervention strategies to prevent disease but has also provided valuable insights into the complexities of pathophysiological mechanisms, namely, the susceptibility of certain subgroups over others, e.g., males vs. females, to NCDs. Sex differences in NCD risk, progression, and severity as they relate to DOHaD were first revealed by epidemiological studies in aging adults in 1993 (Osmond et al., 1993). Hormonal differences have long been at the forefront of trying to explain these differences (Gilbert and Banek, 2012), however, there is evidence of fundamental physiological differences between the two sexes beyond the influence of hormones because sex differences can exist before the appearance of hormonal variations through developmental periods. Preclinical studies have deepened our understanding on this front and revealed how sex differences manifest at the cellular and molecular level (Bourque and Davidge, 2020; Gilbert and Banek, 2012). Sex differences not only exist in normal physiology but become even more apparent in the unique reactions of males and females to similar developmental stressors (Gilbert and Banek, 2012; Ostadal et al., 2019). Males and females show very different growth trajectories, even in the first trimester crown-rump length (Alur, 2019), different nutrient requirements, with male infants being more susceptible to anemia (Domellöf et al., 2002; Wieringa et al., 2007), and differences in mitochondrial physiology (Ostadal et al., 2019), all of which contribute to explaining sex differences in DOHaD.

Within preclinical DOHaD research, mitochondria are gaining traction as a central player in the developmental programming of CVDs (Leduc et al., 2010; Ostadal et al., 2019; Rodríguez-Rodríguez et al., 2018). These organelles are at the intersection of multiple metabolic pathways and cellular processes, and it is suggested that they may drive or contribute to developmental programming in a variety of ways. These include: (1) nutrient sensing and environmental adaptation, (2) reactive oxygen species production and oxidative stress, (3) mitochondrial DNA mutations, (4) mediation of metaboloepigenetic processes, and (5) sex differences (Baird et al., 2017; Hsu, C. N., & Tain, 2019). Their intricate relationship with iron is explored in Section 1.3 Iron in Mitochondria. Their dynamic nature and transformation over the course of cardiac development are explored in Section 1.7 Perinatal Cardiac Metabolism.

1.2 Iron Homeostasis

Iron, as an essential micronutrient, is required to sustain normal biological processes in living organisms, playing a critical role in various physiological, cellular, and molecular functions (Bailey, 2015). As the central component of the functional unit of hemoglobin (Hb) and myoglobin, heme, iron is involved in oxygen transport and storage across and within corporal compartments (Abbaspour et al., 2014; Muckenthaler et al., 2017). While 70% of the body's iron is in erythrocytes and myocytes transporting or storing oxygen, respectively (Briguglio et al., 2020; Muckenthaler et al., 2017), the remaining iron supply, still largely protein-bound, fulfills several cellular functions within DNA (Puig et al., 2017) and energy metabolism (Paul et al., 2017), among others. Iron's role in these fundamental processes makes it vital for healthy growth and development, i.e., when cell proliferation and growth are especially high. As with all nutrients, however, bodily iron must remain at an optimal level, since either deficiency or excess can be

harmful (Bailey, 2015). Thus, to safely leverage iron's chemistry for biological purposes, the human body has evolved both systemic and cellular strategies to precisely regulate iron.

1.2.1 Systemic Iron Homeostasis

Systemic iron homeostasis is the process by which the body balances iron availability with iron demand for cellular functions through the coordinated action of key proteins in specific organs and tissues (Brannon and Taylor, 2017). Management of bodily iron supply can be said to begin in the small intestine, where dietary iron is absorbed from the intestinal lumen by enterocytes and released into the bloodstream (Katsarou and Pantopoulos, 2020; Muñoz et al., 2009). While iron is regularly trafficked in and out of cells, there is no way for the human body to excrete iron, and thus systemic strategies to regulate iron levels are limited to restricting its absorption. Under normal conditions, only 1-2 mg of iron per day (Katsarou and Pantopoulos, 2020) are absorbed to match what is passively lost from excretory processes like perspiration and epithelial shedding (Abbaspour et al., 2014). Iron absorption is predominantly controlled by the hepcidin–ferroportin axis, whereby circulating hepcidin, produced by the liver, inhibits ferroportin at the basolateral surface of duodenal enterocytes and limits iron entry into the plasma from the intestinal lumen (Abbaspour et al., 2014; Katsarou and Pantopoulos, 2020; Muñoz et al., 2009).

Circulating iron has several possible destinations. The liver is the primary site of iron storage (Katsarou and Pantopoulos, 2020) from which it can be mobilized back into the circulation in conditions of scarcity. Most circulating iron is destined for the bone marrow to supply erythropoiesis (Katsarou and Pantopoulos, 2020). The greatest source of iron feeding erythropoiesis is not newly absorbed dietary iron, but rather recycled iron from senescent erythrocytes. Macrophages in the liver, kidneys, and spleen, phagocytose red blood cells to replenish the pool of circulating iron (Katsarou and Pantopoulos, 2020). Finally, lower quantities

of iron are supplied to peripheral tissues to fulfill various cellular functions (Katsarou and Pantopoulos, 2020). Whether newly absorbed, mobilized from storage, or recycled, transferrin is the main protein used for trafficking iron systemically in the blood; it binds plasma iron to keep it in a soluble and inert state (Anderson and Frazer, 2017; Katsarou and Pantopoulos, 2020).

1.2.2 Cellular Iron Homeostasis

Cellular iron metabolism can be categorized into four processes that regulate iron level and distribution in the cell: (1) iron import, (2) iron storage, (3) iron usage, (4) iron export (Fig. 1.2.1).

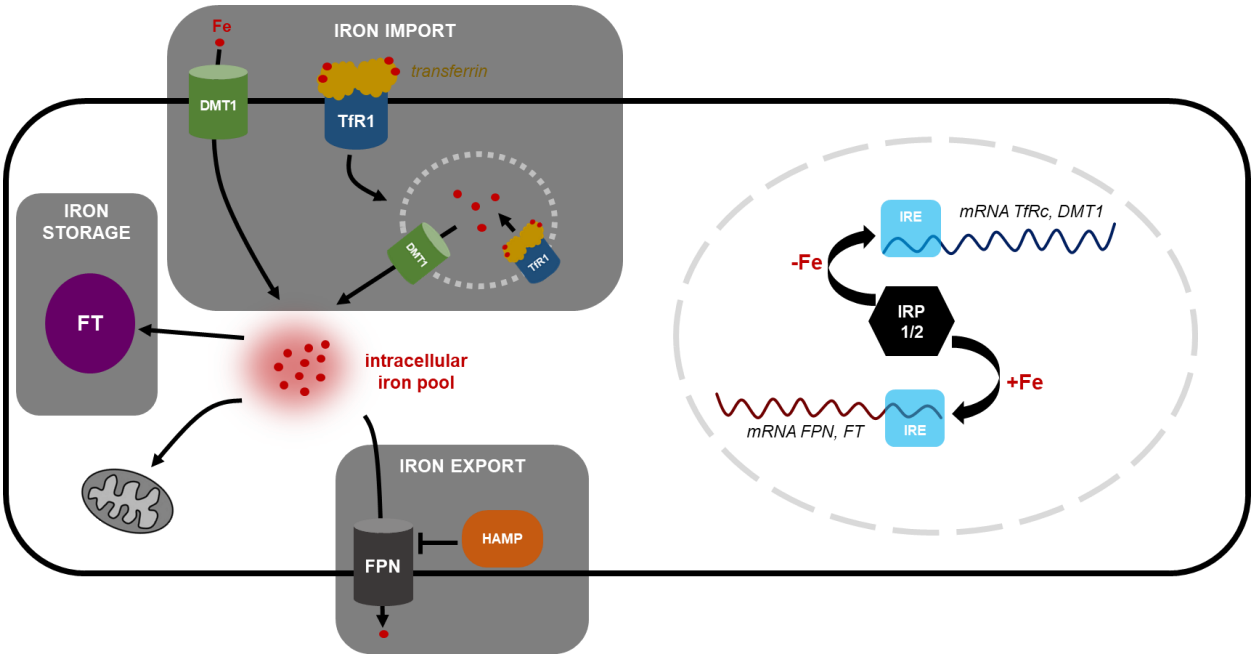

Figure 1.2.1: Summary of cellular iron metabolism and transcriptional regulation of iron homeostasis proteins. Transferrin receptor 1 (TfR1) linked to circulatory transferrin carrying iron is internalized into an endosome. Divalent metal transporter 1 (DMT1) can both import iron from outside of the cell but also exports iron from the endosome. Iron reaches an intracellular iron pool where it can be stored in ferritin (FT), used for synthesis of prosthetic groups in the mitochondria or exported by ferroportin (FPN). The latter can be inhibited by an endogenous hepcidin (HAMP) protein. The expression of these proteins is controlled mainly at the post-transcriptional level by iron-regulatory protein (IRP) interactions with iron-responsive elements (IRE). Adapted from (Anderson and Frazer, 2017; Lakhal-Littleton, 2019; Ravingerová et al., 2020).

Various forms of circulating iron (see section 1.2.1 on Systemic Iron Homeostasis) enter the cell via differing mechanisms. Free ferrous iron (Fe^{2+}) in the bloodstream enters the cell via divalent metal transport 1 (DMT1); this importer is not specific to iron but can also take up other divalent metals (Katsarou and Pantopoulos, 2020). Transferrin-bound iron is recognized by transferrin-receptor 1 (TFR1); upon receptor-ligand binding, the complex is engulfed into the cell (Anderson and Frazer, 2017). Now sequestered in an endosome, acidification releases ferric iron from transferrin and transforms the free iron into its ferrous form; free ferrous iron exits the endosome via DMT1. The intracellular (or labile) iron pool, is the central point of iron metabolism in the cell, serving as a point of exchange. Most iron in the cell, about 95%, is bound to proteins while the remaining 5% forms the labile iron pool (Prabhakar, 2022). Ferritin is the intracellular iron storage protein, storing iron in a nontoxic form and maintaining a reservoir of iron in the cell (Anderson and Frazer, 2017; Muckenthaler et al., 2017).

Ferroportin (FPN) is the only protein known to export iron from the cell (Anderson and Frazer, 2017; Muckenthaler et al., 2017). It releases iron from the cell and into the bloodstream to prevent intracellular iron accumulation or overload (Katsarou and Pantopoulos, 2020). FPN's inhibitor, hepcidin, is most recognized for its role in systemic iron regulation (see section 1.2.1 on Systemic Iron Homeostasis), but accumulating evidence indicates production of intracellular hepcidin in various organs beyond the liver (Lakhal-Littleton, 2019; Lakhal-Littleton et al., 2016); these include the brain (McCarthy and Kosman, 2014), the kidney (Kulaksiz et al., 2005), the placenta (Evans et al., 2011), and the heart (Lakhal-Littleton et al., 2016; Merle et al., 2007). As opposed to circulating hepcidin meant to reduce iron export from intestinal cells and thereby limit iron import into the bloodstream, it is suggested that intracellular hepcidin is meant to sequester iron in tissues, preventing its release from cells when exogenous iron is scarce. This mechanism is

suggested to hold particular importance in the heart (Lakhal-Littleton, 2019; Lakhal-Littleton et al., 2016).

Most proteins responsible for intracellular iron metabolism described herein, i.e., FT, FPN, DMT1, and TFR1, are post-transcriptionally regulated by iron-regulatory proteins (IRP) 1 and 2 via iron-responsive elements (IREs) on untranslated regions of their mRNA (see Fig. 1.2.1 for details on the IRP/IRE system) (Anderson and Frazer, 2017; Katsarou and Pantopoulos, 2020). Though hepcidin is also transcriptionally regulated, its regulation is complicated by a responsiveness to stimuli beyond iron levels, such as erythropoiesis, hypoxia/hypoxemia, and inflammation (Katsarou and Pantopoulos, 2020).

1.3 Iron in Mitochondria

Iron is involved in the biosynthesis of two major protein prosthetic groups, heme and iron-sulfur clusters (ISC) (Paul et al., 2017; Ward and Cloonan, 2019). Proteins containing the prosthetic groups dependent on iron have functions in almost all intracellular compartments and are involved in various metabolic pathways (e.g. drug, lipid, and vitamin metabolism), cell stress responses (e.g. apoptosis and DNA repair), and regulatory pathways (e.g. cell cycle initiation and progression and gene expression) (Andreini et al., 2018). Heme biosynthesis begins and ends in the mitochondria. ISC biogenesis occurs through two separate pathways depending on whether the ISC is destined for mitochondrial or cytosolic proteins; both pathways depend on mitochondria. Then, the mitochondria are a primary site of iron use in the cell. If mitochondrial iron is not used to synthesize either of these prosthetic groups, it can be stored by mitochondrial ferritin to help maintain cellular iron homeostasis (Paul et al., 2017; Ward and Cloonan, 2019).

Beyond their role in intracellular iron homeostasis and utilization, mitochondria themselves contain numerous proteins that incorporate iron in the form of a prosthetic group (heme

and/or ISC) or as the iron ion directly. Seven percent of all mitochondrial proteins will incorporate iron in one of these forms, most of these proteins are involved in cellular respiration (Andreini et al., 2018). Mitochondrial complexes I, II, III, and IV are responsible for creating the proton gradient that drives ATP production, will each incorporate multiple heme groups and ISCs into their structure. Cytochrome *c*, which shuttles electrons between complexes III and IV, contains a heme group (Musallam and Taher, 2018). These proteins are part of the electron transport system (ETS), and consequently the production of ATP by oxidative phosphorylation (OXPHOS), depends on iron.

Given the interconnectedness of iron and mitochondria, it is not surprising that iron availability modulates many mitochondrial processes and that these organelles are sensitive to conditions of iron imbalance, like iron deficiency (ID). ID and iron deficiency anemia (IDA) have been shown to alter mitochondrial dynamics, energy metabolism, morphology, and mtDNA integrity (Paul et al., 2017; Ward and Cloonan, 2019). As a highly metabolically active organ, largely depending on OXPHOS for energy production, the heart is vulnerable to mitochondrial perturbations. Indeed, ID associated cardiac dysfunction has been linked to abnormalities in the aforementioned mitochondrial elements (Kobak et al., 2019; Rines and Ardehali, 2013).

1.4 Perinatal Iron Metabolism and Deficiency

Iron deficiency (ID) is the most common nutritional disorder worldwide and a widespread public health problem across low-, middle-, and high-income countries. It affects approximately one third of the world's population, amounting to several billion people (World Health Organization, 2015). ID results from an imbalance of iron uptake and iron demand (World Health Organization, 2001). It is the primary cause of anemia, which is defined as a reduced concentration of Hb in the blood, below set thresholds (World Health Organization, 2017). Anemia

affects half a billion women 14-49 years of age and 269 million children 6-59 months of age worldwide (World Health Organization, 2017).

Since iron plays a ubiquitous role in various physiological functions, symptoms of ID, such as weakness, fatigue, irritability, and poor concentration, tend to be generalized and go easily unnoticed (Balendran and Forsyt, 2021). Symptoms also change with severity of ID (World Health Organization, 2001). As iron stores are depleted but overall iron supply remains adequate, symptoms are mild, if at all present. If the imbalance between iron demands and supply persists such that iron stores are deplete, supply of iron to the circulation is reduced and consequently so is the saturation of its transport protein (World Health Organization, 2001). Finally, a long-term negative iron balance results in iron-deficiency anemia once Hb production is impaired (World Health Organization, 2001; World Health Organization, 2017). Iron status, stage and severity of ID, and presence of anemia are established using circulating biomarkers (World Health Organization, 2001; World Health Organization, 2017). Where comprehensive assessment of iron status biomarkers may not be available, serum ferritin alone can be used as an indicator of ID with some caveats (i.e. inflammation) while the combination of serum ferritin and Hb indicates IDA (World Health Organization, 2001; World Health Organization, 2017) Among the many possible causes and types of anemia, nutritional ID is the most common, accounting for at least 50% of cases (World Health Organization, 2017). Rates of IDA in relation to other anemias will vary based on age, sex, geographical region, socioeconomic status, race (Han et al., 2022; Kassebaum et al., 2014; Miller, 2016; World Health Organization, 2017)..

Despite widespread supplementation efforts, preventing and treating ID and its associated anemia remains a challenge, particularly in certain populations most vulnerable to ID. Worldwide, 38%, or approximately 32 million, pregnant women are estimated to be anemic (Stevens et al.,

2013). In high-income regions, estimates are upwards of 20% (Stevens et al., 2013). Middle and low income countries typically report higher occurrence of IDA in pregnant women, from 30% to upwards of 60% (Stevens et al., 2013). In Canada, it is estimated that 23% of women will be anemic during pregnancy (Stevens et al., 2013). An Alberta, study reported that 40% of their study participants qualified as anemic (Gragasin et al., 2021), coinciding with another Alberta study which reported rates of ID of 40% by the third trimester (O'Brien and Ru, 2017). One Canadian centre (Toronto, Canada) reported rates of ID upwards of 90% in their pregnant population, with approx. 50% of these being characterized as severe and ~30% of women with a clinical diagnostics of IDA (combo of low ferritin and Hb) through the course of their care (Tang et al., 2019). Variability in these numbers could be due to varying definitions and diagnostic criteria for these conditions, and challenges inherent in estimating epidemiological prevalence (World Health Organization, 2001), but altogether emphasize the pervasiveness of ID and IDA in the pregnant population in an industrialized setting.

Seventy five percent of anemias in pregnancy are caused by IDA (Horowitz et al., 2013). While ID and IDA are highly prevalent in their own right in pregnant women, they are also a commonly diagnosed comorbidity (Watkins et al., 2021). Several conditions complicate or augment the underlying risk of ID for mother and baby; these include overweight or obesity before and during pregnancy (Wawer et al., 2021), preexisting or gestational diabetes, multifetal pregnancies (Zgliczynska and Kosinska-Kaczynska, 2021), and adolescent pregnancies (Jeha et al., 2015). Even without these complications, the normal physiology of pregnancy creates an inherent risk of ID and increase the opportunity for ID to act as a perinatal developmental stressor. Risk of IDA increases as pregnancy progresses (Stevens et al., 2013), and the perinatal period holds the highest risk for women and infants (Bailey, 2015). Pregnancy is a physiologically anemic

state during which Hb threshold for anemia is lowered (Benson et al., 2021). The expansion of blood volume to support fetal growth results in a dilution of Hb in relation to plasma and consequently a reduced Hb per blood volume (Means, 2020). The developmental context further complicates the maintenance of iron homeostasis in several ways where both mother and baby are concerned.

First, growth and development increase iron demand, which cannot always be sustained by increasing iron intake due to the safeguard of limited iron absorption in the gut (see Section 1.2.1 Systemic Iron Homeostasis). Second, the propensity for ID and IDA in pregnant women and in young children may seem maladaptive given the associated pregnancy and developmental complications (see Section 1.5 Developmental Programming of Cardiovascular Disease by Perinatal Iron Deficiency), it has nevertheless been suggested to be evolutionarily beneficial (Miller, 2016). Because pathological organisms (e.g., *Plasmodium* (malaria), influenza, *Yersinia Pestis* (Black Death, Plague of Justinian) require iron for replication and pathogenesis, ID may confer protection against infectious disease and increase survival, especially in populations vulnerable to infection and illness, such a pregnant women and children (Miller, 2016). Third, maternal iron metabolism is altered to prioritize iron for fetal growth (Benson et al., 2021; Juul et al., 2019; Rao and Georgieff, 2002). Fourth, during fetal development, not only does iron transport across the placenta add a level of regulation to iron homeostasis for mother and fetus (Lakhal-Littleton, 2021; Rao and Georgieff, 2002), but placental iron retention is prioritized over fetal iron needs, to maintain vital placental processes and promote fetal survival (Benson et al., 2021; Sangkhae et al., 2020). Finally, fetal and newborn (i.e., perinatal) iron metabolism is unique to that of the adult. Fetal iron demands are inherently high throughout gestation due to ongoing growth and development, but even more so in the third trimester where the fetus prioritizes accumulation

of iron stores that will support growth post birth (Lönnerdal et al., 2015; Rao and Georgieff, 2002). This is required since iron homeostasis mechanisms are not mature in the newborn; for example, newborns cannot increase intestinal uptake of iron to compensate for ID (Brannon and Taylor, 2017; Lipiński et al., 2010). Altogether, these factors highlight why pregnant women and young children are the subgroup most susceptible to ID and IDA.

Prior to discussing the short- and long-term consequences of perinatal ID, a discussion on the inherent differences between humans and rodents with respect to iron metabolism and the propensity to develop ID during gestation is warranted. This discussion is important because the consequences of perinatal ID, particularly the long-term programming effects, have largely been reported in rats, and an understanding of the limitations of such models provides important context. First, while rats and humans are both omnivorous, rats absorb inorganic iron more efficiently than humans (Cao et al., 2013; Cao et al., 2014). Second, the rodent estrous cycle does not include menstruation, and therefore rats do not experience periodic phases of iron loss associated with this process (Miller, 2016). As such, it is likely that ID occurs less frequently in rats than it does in humans, and rodents are less likely to begin pregnancy with depleted iron stores, whereas humans often do (Miller, 2016). For these reasons, in the present studies, dams allocated to the ID group are fed an iron-restricted diet for 2 weeks before mating as a means to induce a state of latent ID (i.e., ID without concomitant anemia) to model this scenario. However, there are additional challenges in modeling human pregnancies in rats. For example, given that the gestational period for rats is much shorter and pregnancies are multiparous (typically consisting of 10-20 offspring in a single litter) (Andersen et al., 2018), maternal and offspring growth trajectories (and the associated iron demands) throughout pregnancy differ markedly from those in humans. As such, the circulatory adaptations, including expansions in blood volume that give rise to anemia, as well

as demands from the growing conceptus can cause a more rapid and pronounced anemia than that which typically occurs in humans. Finally, from a teleological perspective, the high prevalence of ID among pregnant women and young children has been hypothesized to stem from the evolutionary advantage it confers against infectious diseases (since many infectious organisms require iron for replication and pathogenesis, as described in the preceding paragraph). However, the same is likely untrue for rodents, whose immune function has evolved to enable survival in environments unequivocally lethal to humans, where the deleterious effects of ID in gestation likely outweigh any benefits. Notwithstanding, these limitations do not invalidate their utility as a model of human development (Marcela et al., 2012). Indeed, organ development, e.g., kidneys, heart, brain, etc., is similar in rats and in humans (Marcela et al., 2012), and by carefully manipulating the availability of dietary iron to the dam throughout pregnancy to recapitulate the salient features of gestational ID in humans (Noble et al., 2023; Woodman et al., 2017), the biochemical effects on organ development can be studied, even if the epidemiology of ID in rats and humans differs. A final caveat is that by virtue of the longstanding and intimate evolutionary relationship humans have with ID, which presumably does not exist in rats, the developmental consequences of ID may be different between species; this limitation warrants consideration but is beyond the purview of the present study.

1.5 Developmental Programming of Cardiovascular Disease by Perinatal Iron Deficiency

Maternal and perinatal ID and the associated anemia are well-known risk factors for poor maternal and birth outcomes. Mothers are at risk of poor weight gain (Miller, 2016), greater perinatal bleeding (Lakhal-Littleton, 2021), postpartum hemorrhage (Young et al., 2019), preeclampsia (Lakhal-Littleton, 2021; Young et al., 2019), blood transfusion (Young et al., 2019),

cardiovascular insufficiency (Lakhal-Littleton, 2021), reduced maternal fitness (Miller, 2016; World Health Organization, 2017), placenta previa and placental abruption (Tzu-hsi Lao et al., 2022). Furthermore, developing infants are at risk of intrauterine growth restriction (Watkins et al., 2021), low birth weight (M G Figueiredo et al., 2018; Young et al., 2019), small-for-gestational-age (Young et al., 2019), perinatal mortality (Watkins et al., 2021; Young et al., 2019), and preterm birth (Lakhal-Littleton, 2021; Watkins et al., 2021; Young et al., 2019). Even in the absence of overt clinical complications, ID during critical stages of organogenesis and organ maturation may affect the function and resilience of various organ systems in the offspring long-term, with poorer neurodevelopmental outcomes being of particular prominence in the literature (Brannon and Taylor, 2017; Lonnerdal, 2017; Markova et al., 2019; Miller, 2016; Quezada-Pinedo et al., 2021). Additionally, and in line with the DOHaD hypothesis, preclinical studies strongly support that, when present during gestation and/or early development, ID is one such insult that can impact growth and alter developmental trajectories, and in turn affect lifelong susceptibility to chronic disease, including CVD (Alwan and Hamamy, 2015).

Offspring of ID dams reliably demonstrate increased blood pressure in adulthood compared to their iron-sufficient counterparts (Bourque et al., 2008a; Bourque et al., 2012; Crowe et al., 1995; Gambling et al., 2003; Komolova et al., 2008; Lewis et al., 2002; Lisle et al., 2003; Woodman et al., 2020). This hypertension is accompanied by vascular dysfunction (Woodman et al., 2019), cardiomegaly (Bourque et al., 2008a; Lewis et al., 2002; Woodman et al., 2020), altered renal hemodynamics (Bourque et al., 2008a), altered kidney metabolism (Woodman et al., 2020), glomerular morphology (Lisle et al., 2003; Woodman et al., 2020), and greater salt-sensitivity (Bourque et al., 2008a). Studies also report greater occurrence of other risk factors for CVD, such as increased visceral adiposity (Bourque et al., 2012; Komolova et al., 2008), sedentary behaviour

(Bourque et al., 2012; Komolova et al., 2008), and elevated stress (Bourque et al., 2008b). Interestingly, despite both sexes exhibiting similar degrees of anemia and impaired growth at birth, male offspring are more susceptible to these cardiovascular programming effects than females (Gambling et al., 2003; Woodman et al., 2019; Woodman et al., 2020). The few studies done in humans have not yet identified a clear association between developmental ID and/or the associated anemia and cardiovascular risk profile (Alwan and Hamamy, 2015; Quezada-Pinedo et al., 2021), though this body of work is subject to considerable heterogeneity, limitations, and confounders. Available evidence includes indirect connections, whereby maternal ID is associated with altered placental development (Godfrey et al., 1991; Gragasin et al., 2021; Roberts et al., 2020), growth restriction, preterm birth, and fetal hypoxia (Bourque and Davidge, 2020), factors that have clearer epidemiological evidence linking them to worse cardiovascular outcomes in adulthood. Further, two separate studies following survivors of fetal anemia secondary to hemolytic disease reported altered cardiac morphology in childhood (Dickinson et al., 2010) and adulthood (Wallace et al., 2017); adults had evidence of premature cardiovascular dysfunction and worse lipid profiles, but these parameters were not studied in children. The differential cause of anemia limits translation of these results to the potential effects of ID in utero, but they nonetheless suggest an effect of anemia on cardiovascular development in humans (Wallace et al., 2017). Given the reproducibility of later life cardiovascular complications in animal models of maternal iron restriction, greater focus on illuminating this relationship in humans is warranted; indeed, a 2015 narrative review (Alwan and Hamamy, 2015) and a 2021 systematic review and meta-analysis (Quezada-Pinedo et al., 2021) on the subject concluded similarly. Meanwhile, the specific mechanisms by which perinatal ID affects long-term cardiovascular function are not clear, thus prompting our study of early developmental timepoints in affected offspring.

Cardiac enlargement, absolute and/or relative to body weight, is a prominent phenotypic feature of young offspring subjected to perinatal ID (Andersen et al., 2006; Bourque et al., 2008a; Gambling et al., 2003; Kochanowski and Rothman, 1985; Woodman et al., 2018). Despite a profound morphological change, cardiac development in the context of ID is not well studied (see previous paragraph). A recently published study from our laboratory, which was conducted in parallel to the work included herein, has provided some insight into the effect of perinatal ID on cardiac function in the neonate (Noble et al., 2023). Echocardiographic studies of neonatal offspring exposed to perinatal ID revealed functional alterations indicative of an inadequate compensation to anemia; while ID offspring had proportionally larger hearts relative to body weight, cardiac output was unchanged and thus tissue oxygen delivery was reduced in conjunction with lower Hb levels. The cardiac defects were characterized by a greater systolic dysfunction in male ID offspring, and a greater diastolic dysfunction in female ID offspring. These studies provide a clear impetus to explore the cellular mechanisms that may underlie neonatal cardiac dysfunction secondary to perinatal ID to both understand how the heart's own development may be impacted and illuminate why functional alterations are different between male and female offspring.

Understanding how the heart adapts to ID conditions in early life may illuminate aspects of its own function and development within the DOHaD context. Further, beyond the heart's own lifelong health, by virtue that it supports all other organs via maintenance of blood supply, its function and development and alterations are linked to nearly all other developmental and physiological processes. Thus, an integrative approach to early organ development and how it may result in chronic disease in later life requires an understanding of cardiac development in the

context of ID to begin understanding how this may impact development of other organs (e.g., the kidneys, see previous paragraph) in the DOHaD context.

1.6 Perinatal Cardiac Metabolism

The primordial human heart first beats at gestational day 22 (Tan and Lewandowski, 2020); in the rat, this happens at about embryonic day 9-10 (Goss, 1938; Kobayashi et al., 2011). By gestational week 7, the 4-chambered human heart is fully formed (Tan and Lewandowski, 2020). In the rat, this corresponds to approximately embryonic day 16 (Marcela et al., 2012), with no discernable organization within the myocyte. From then until birth, the heart will undergo few morphological changes but continue to grow by expanding the cardiomyocyte number (Günthel et al., 2018; Marcela et al., 2012). The highly proliferative nature of the fetal myocardium along with substrate availability, low oxygen availability, and connection to placental circulation, altogether create a comparatively modest cardiac workload and ATP demand which shapes fetal cardiac metabolism (Lopaschuk and Jaswal, 2010; Piquereau and Ventura-Clapier, 2018; Sánchez-Díaz et al., 2020; Schrepper, 2016). Compared to the adult heart, the fetal heart is highly dependent on glycolysis which accounts for just under 50% of ATP produced (Lopaschuk and Jaswal, 2010). However, more than 50% of ATP is produced by oxidative metabolism of lactate, glucose, and fatty acids preferentially in that order. Thus, mitochondria are still the leading source of ATP in the cardiomyocyte at this stage of development despite being less active than those of the adult myocardium (Lopaschuk and Jaswal, 2010). The fetal heart contains significantly less mitochondria with lower enzyme activities (Rolph, Jones, & Parry, 1982). These mitochondria are initially small and round with few cristae and are poorly organized within the myocyte (Rolph et al., 1982). As gestation progresses, fetal mitochondria take on a variety of sizes and shapes (e.g. cylindrical, vermiform, horseshoe, doughnut) and in late gestation will aggregate around the

nucleus before being distributed between myofibrils. In rodents and humans, this occurs more slowly and to a lesser extent before birth than it does in the ovine heart, which is more mature at birth (Brook et al., 1983; Kim et al., 1992; Rolph et al., 1982; Sheldon et al., 1976; Smith and Page, 1977; Sordahl et al., 1972). Regardless of species, it is clear that cardiomyocyte mitochondria and cytoarchitecture mature synchronously (Anmann et al., 2014). Although birth will be the primary trigger causing cardiac mitochondria to mature, fetal mitochondria are not static but continue developing throughout gestation. The developing heart seemingly prepares for the impending metabolic transition by gradually increasing mitochondrial content, size, oxidative capacity, and transcription of genes related to fatty acid metabolism as the fetus approaches full-term (Iruretagoyena et al., 2014; Piquereau and Ventura-Clapier, 2018; Rolph et al., 1982; Schrepper, 2016; Sordahl et al., 1972). Mitochondria and the network they create within cells and tissues are regarded as highly dynamic due to their constant remodeling, their metabolic flexibility, and their adaptability in the face of environmental changes; these features are prominent in the adult heart. The dynamic nature of cardiac mitochondria is further highlighted by their functional evolution over the course of a lifetime, from embryonic to elderly life (Schrepper, 2016). Arguably, the most dramatic transformation occurs over the perinatal period, during which time the myocardium transforms its metabolic profile from highly glycolytic to almost completely mitochondria dependent (Lopaschuk and Jaswal, 2010). During this window of time, the heart will require substantial amounts of iron and may be vulnerable to deleterious functional changes by perinatal ID.

Birth is arguably the defining event of perinatal cardiac development. Transition from intrauterine to extrauterine life constitutes a significant change of environment which incites profound physiological changes and by necessity, a metabolic makeover in the heart. Loss of

placental circulation and establishment of independent circulation quickly increases cardiac workload, driving up ATP demand in cardiomyocytes (Tan and Lewandowski, 2020). Circulatory changes coupled with initiation of breathing increase oxygen available to cells (Schrepper, 2016; Tan and Lewandowski, 2020). Nutrient and substrate availability are altered such that circulating fatty acid concentrations rise after a brief starvation period before the first feeding and introduction of a milk diet (Sánchez-Díaz et al., 2020; Schrepper, 2016). Immediately after birth, cardiac metabolism and mitochondria retain a fetal phenotype for a short period but soon adapt to their new conditions. Timing of the metabolic switch in large mammals, including humans, is still unclear and seems to vary greatly between species (Velayutham et al., 2019). In rodents, this transition seems to take place over the first three weeks after birth but is not complete until 3 months of age when cardiomyocytes reach their full capacity for energy metabolism (Anmann et al., 2014; Gong et al., 2015; Lopaschuk and Jaswal, 2010). A hallmark of this transition is the shift to oxidative metabolism and a significantly greater contribution of fatty acids to ATP production. This is accomplished by increasing expression and activity of enzymes involved in fatty acid β-oxidation, the citric acid cycle, and OXPHOS (Marin-Garcia et al., 1997). Additionally, the newborn heart will quickly expand its mitochondrial population through mitochondrial biogenesis. Mitochondrial fusion, fission, and mitophagy also become more active in the postnatal period (Dorn et al., 2015). Mitochondrial dynamics are critical to remodeling of the heart's bioenergetic profile; disruption of various dynamic processes often results in perinatal death or abnormal cardiac development and prevents metabolic transition. One study specifically interrupted Parkin-mediated mitophagy in hearts of newborn mice which prevented metabolic transition, caused retention of fetal mitochondria, and repressed the genetic program for fatty acid metabolism (Gong et al., 2015). This led to speculation that early metabolic transition is accomplished by removal

(mitophagy) of fetal mitochondria followed by rapid renewal and replacement (biogenesis) and redistribution (fusion and fission) of mitochondria specialized for fatty acid oxidation (FAO; Dorn et al., 2015). As cardiac tissue develops and myofibrils become more abundant and organized, so do the mitochondria. Subsarcolemmal, interfibrillar, and perinuclear mitochondrial subpopulations emerge during this time (Pohjoismäki and Goffart, 2017). Cristae density increases while matrix volume decreases to create a greater surface area on the inner mitochondrial membrane for OXPHOS enzymes (Smith and Page, 1977). Mitochondrial DNA (mtDNA) content is low in the newborn heart and has a simple structure compared to the adult heart (Pohjoismäki et al., 2010).

Mature mitochondria preferentially oxidize fatty acids but maintain a certain metabolic flexibility, allowing the heart to oxidize different types of fuels depending on availability and to maintain necessary ATP production under a variety of conditions (Karwi et al., 2019). The mature mitochondrial network (also referred to as the mitochondrial reticulum) is highly organized and has accrued a significant complexity since fetal life. Two distinct subpopulations of mitochondria can be observed, the subsarcolemmal (SSM) and interfibrillar mitochondria (IFM) (Palmer et al., 1977; Weinstein et al., 1984). However, the existence of a continuous mitochondrial reticulum brings into question the idea of functionally distinct populations altogether (Lai et al., 2019). While individual mitochondria are present, the majority form a highly interconnected branched network thought to facilitate energy distribution and signaling throughout the densely packed cardiomyocyte (Glancy et al., 2017; Pohjoismäki and Goffart, 2017). Mitochondrial subnetworks protect the network as a whole by limiting spread of local dysfunction (Glancy et al., 2017). Mitochondria within these networks are large and elongated with an ovoid or rectangular shape. They are also densely packed with cristae, a feature that is vital to their high metabolic activity (Schrepper, 2016; Sordahl et al., 1972). Mitochondrial fusion, fission, biogenesis, and mitophagy

processes act as a quality control mechanism to maintain the health of the mitochondrial population. Aberrations in mitochondrial dynamics do not cause same lethality as they would in early development but have been linked to various cardiac pathologies (Dorn et al., 2015; Piquereau et al., 2013). The adult heart contains five times more mtDNA copies than the newborn, most of which will have acquired a complex 'adult-type' organization in the first five to ten years of life; this mtDNA structure including dimeric molecules, branched structures, and four-way junctions is unique to humans (Pohjoismäki et al., 2010).

1.6.1 Role of Iron in Perinatal Cardiac Metabolism

In the healthy heart, there is a substantial increase in cardiac mitochondrial iron in the first six weeks of life (Wofford et al., 2017). This can be attributed to the rapid maturation of cardiac energy metabolism during postnatal life. This mitochondrial maturation occurs at a time when the fetus and neonate are most vulnerable to ID (Rao and Georgieff, 2002). The potential for coincidence of perinatal ID and postnatal remodeling of cardiac mitochondria is high and of great concern given the reliance of mitochondrial function on iron availability. As little is known about the effects of ID in mitochondria of the developing heart, this section briefly summarizes current knowledge of the effects of ID on various mitochondrial activities and applies it to the setting of perinatal cardiac development.

A hallmark of postnatal cardiac development is the increase in mitochondrial content driven by mitochondrial biogenesis. Iron deprivation in cells downregulates mitochondrial biogenesis in a manner that is independent of PGC-1α/β and HIF-1α signaling pathways (Rensvold et al., 2013; Rensvold et al., 2016). Mitochondrial biogenesis under ID conditions will produce lower quality mitochondria. Cardiac and skeletal muscle mitochondria exposed to ID suffer morphological changes and changes in mitochondrial composition as a result of downregulation

of iron-containing mitochondrial proteins (Cartier et al., 1986; Tanne et al., 1994). Further, although no iron-containing proteins are involved directly in fatty acid β-oxidation, some iron-containing proteins are involved in lipid metabolism (Andreini et al., 2018), such as those responsible for fatty acid transport into the mitochondria. Accordingly, acute ISC loss in cells leads to fatty acid synthesis and lipid droplet formation (Crooks et al., 2018). Altogether, ID is known to independently impede several key processes that are expected to be augmented during perinatal cardiac metabolic transition.

1.7 Rationale and Objectives

Perinatal cardiac development, and more specifically, development of mature cardiac metabolism, occurs at a time where the fetus/neonate is most at risk for ID and IDA. Despite cardiac enlargement in young ID offspring indicating cardiovascular adaptation, the heart's response to these conditions at a cellular level has not been adequately explored nor has it been clarified whether this morphological change is physiological or pathological, particularly in the neonatal period when the developing heart is undergoing adaptation to extrauterine life. We hypothesized that perinatal ID would cause mitochondrial dysfunction and oxidative stress in the hearts of neonatal offspring.

The objectives of this work were as follows:

1. To assess the global molecular responses of the neonatal heart to perinatal ID before and after perinatal metabolic transition using quantitative shotgun proteomics, determine if and how mitochondrial proteins are altered, and see whether these responses differed between male and female offspring hearts.

2. To assess the effect of perinatal ID on cardiac mitochondrial function in neonatal offspring, from birth to Hb restoration, using high-resolution respirometry.
3. To assess whether perinatal ID is associated with changes in oxidative stress that may coincide with alterations in mitochondrial function.
4. To assess whether perinatal ID is associated with changes in mitochondrial morphology that coincide with alterations in mitochondrial function.
5. To explore differences in cardiac iron metabolism as a possible mechanism of sex-specific effects in the hearts of perinatal ID offspring.

Chapter 2
Methods

2.1 Animal Model of Perinatal Iron Deficiency

The protocols described herein were approved by the University of Alberta Animal Care and Use Committee in accordance with guidelines established by the Canadian Council for Animal Care. Female Sprague-Dawley rats aged 6 weeks were purchased from Charles River (Saint-Constant, QC, Canada) and housed at the University of Alberta Animal Care Facility which maintains a 12-hour light/dark cycle and an ambient temperature of 23°C. Rats had ad libitum access to food and water throughout the study. All purified diets used in this study were based on the AIN-93G formula (Reeves et al., 1993) and differed only by the amount of ferric citrate added (see below).

The experimental design is illustrated in Figure 2.1.1. Two weeks before mating, female rats were randomly assigned to one of two groups: control rats (CTL; n=10) were fed the control diet (containing 37 mg/kg elemental iron), and iron-deficient rats (ID; n=12) were fed an iron-restricted diet (containing 3 mg/kg elemental iron). After two weeks on their respective diets, rats were housed overnight with male rats (fed a standard rodent chow) until pregnancy was confirmed by presence of sperm in a vaginal smear. Upon confirmation of pregnancy (defined as gestational day [GD] 0), dams were individually housed, and those in the ID group were fed a moderately iron-restricted diet containing 10 mg/kg elemental iron, whereas CTL dams remained on their prescribed CTL diet. From GD0, food intake, body weight, and hemoglobin (Hb) levels were assessed weekly. Maternal Hb levels were assessed using a HemoCue Hb201+ hemoglobinometer from approximately 10μL of blood collected via saphenous venipuncture.

On the day of birth (defined as postnatal day [PD] 0), all dams were switched to standard rodent chow for the remainder of the study. At this time, litters were standardized to ten offspring (five males and five females). At PD 0, 14, and 28, pups were weighed, and 1 male and 1 female from each litter were euthanized. At PD0, pups were euthanized by decapitation and Hb was assessed from the free-flowing blood (Hemocue Hb201+); at PD14 and PD28, pups were first anesthetized by isoflurane (5% induction, 3% maintenance in 100% oxygen) prior to euthanasia by cardiac excision. Offspring hearts were excised, weighed, and used fresh for mitochondrial respiration experiments (described below). Hb levels and hearts were collected from an additional 1-2 pups at each time point; these tissues were either immediately flash-frozen in liquid nitrogen or embedded in Tissue-Tek optimal cutting media and subsequently frozen in liquid nitrogen. All tissues were stored at -80 °C prior to analyses. At PD21, pups were separated from their mothers, housed with their same-sex littermates, and fed the standard rodent chow until PD28.

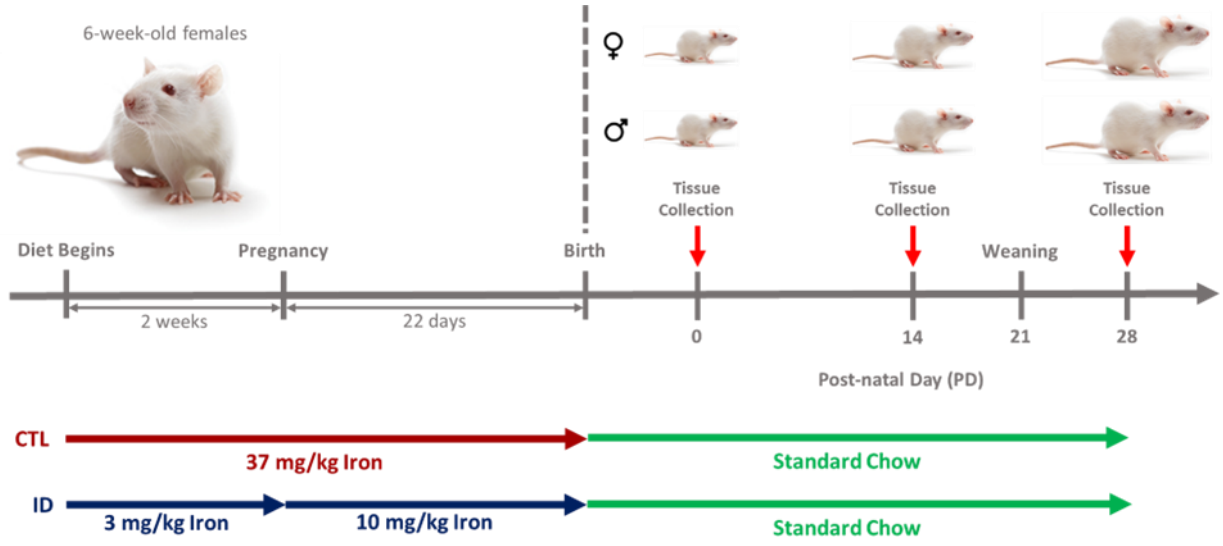

Figure 2.1.1: Rodent model of perinatal iron deficiency (ID). 6-week-old female Sprague-Dawley rats were fed either a control (CTL; 37 mg/kg iron) or iron-deficient (ID; 3 mg/kg iron) diet for two weeks before breeding. Upon confirmation of mating, the ID group was given a 10 mg/kg iron diet. At birth, both CTL and ID dams were switched to standard rodent chow. Tissues were collected from male and female pups at postnatal days (PD) 0, 14, and 28.

2.2 Quantitative Shotgun Proteomics

2.2.1 Sample Preparation

Flash frozen cardiac ventricles from PD 0 and 28 male and female offspring were crushed into a powder with a liquid nitrogen cooled mortar and pestle and stored at -80 °C. Pulverized tissue samples were aliquoted into 0.6mL microcentrifuge tubes and shipped on dry ice to Dr. Antoine Dufour at the University of Calgary for processing and data acquisition; the latter were performed by Daniel Young. Subsequent bioinformatics analysis and data visualization were performed by Claudia D. Holody and Chunpeng Nie. All steps are described in detail below, as previously published (Das et al., 2021), and summarized in Figure 2.2.1.

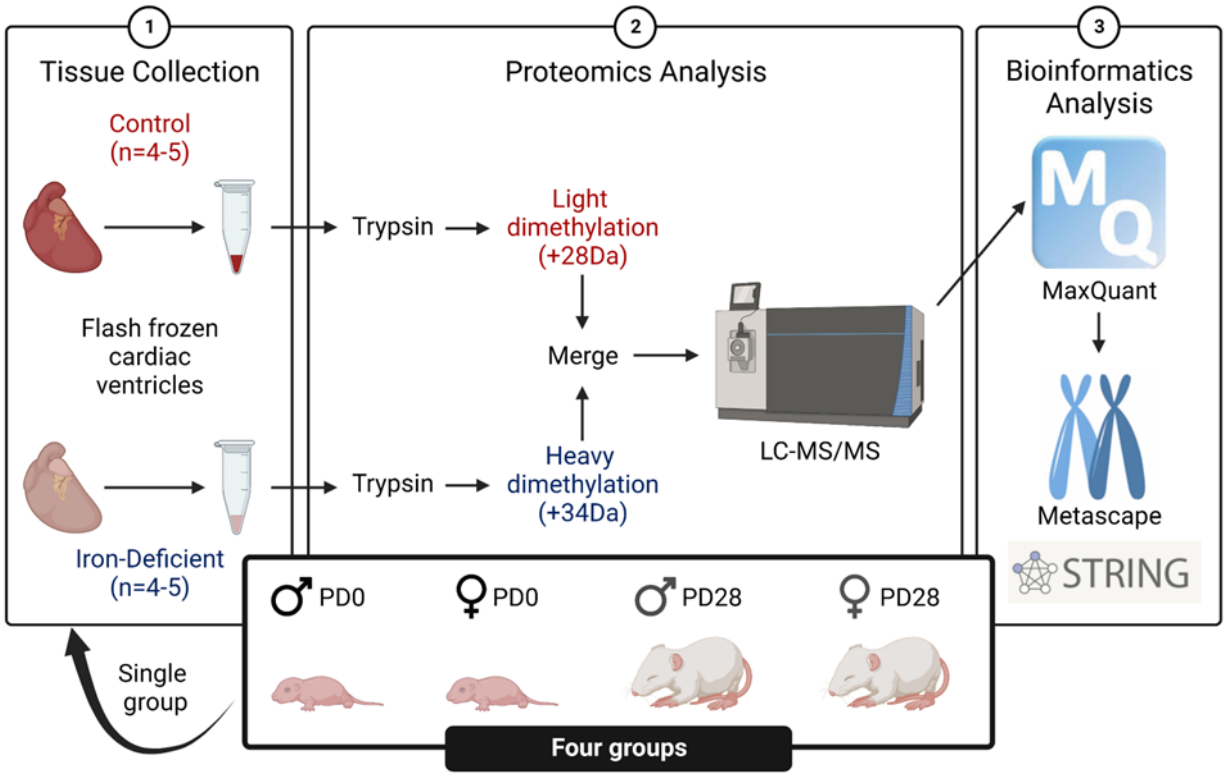

Figure 2.2.1: Schematic of proteomics workflow. Cardiac ventricles from either postnatal day (PD) 0 or 28, male or female offspring were analyzed simultaneously using formaldehyde labeling to measure relative protein expression. Created with BioRender (https://biorender.com/) and modified from (Das et al., 2021).

Samples were lysed with 1% SDS, 0.1 M EDTA in 200 mM HEPES (pH 8), and protease cOmplete™ inhibitor tablets (Sigma-Aldrich, ON, Canada). Proteins were denatured using a final concentration of 10 mM dithiothreitol (DTT). Samples were alkylated by incubation with a final concentration of 15 mM iodoacetamide (IAA) in the dark for 25 min at room temperature. Samples were digested with trypsin (Promega, Madison, WI, USA); the pH was adjusted to 6.5 using HCl. Peptide α- and ε-amines were labeled by incubating CTL and ID samples for 18 h at 37 °C with isotopically heavy (final concentrations of 40 mM formaldehyde [$^{13}CH_2O$] + 20mM sodium cyanoborohydride [$NaBH_3CN$]) or light labels (final concentrations of 40 mM light formaldehyde [CH_2O] + 20 mM $NaBH_3CN$), respectively. Finally, samples were subjected to C18 chromatography using Pierce™ C18 columns (Thermo Chromatography™, ON, Canada) before being undergoing liquid chromatography and tandem mass spectrometry (LC-MS/MS).

2.2.2 High Performance Liquid Chromatography (HPLC) and Mass Spectrometry (MS)

Liquid chromatography and mass spectrometry was carried out by the Southern Alberta Mass Spectrometry (SAMS) core facility at the University of Calgary, Canada. Analysis was performed on an Orbitrap Fusion Lumos Tribrid mass spectrometer (Thermo Scientific, ON, Canada) operated with Xcalibur (version 4.0.21.10) and coupled to a Thermo Scientific Easy-nLC (nanoflow Liquid Chromatography) 1,200 system. Tryptic peptides (2 µg) were loaded onto a C18 trap (75 um x 2 cm; Acclaim PepMap 100, P/N 164,946; Thermo Scientific, ON, Canada) at a flow rate of 2 µl/min of solvent A (0.1% formic acid and 3% acetonitrile in LC-MS grade water). Peptides were eluted using a 120 min gradient from 5 to 40% (5–28 % in 105 min followed by an increase to 40 % B in 15 min) of solvent B (0.1 % formic acid in 80 % LC-MS grade acetonitrile) at a flow rate of 0.3 µl/min and separated on a C18 analytical column (75 um x 50 cm; PepMap RSLC C18; P/N ES803; Thermo Scientific). Peptides were then electrosprayed using 2.3 kV

voltage into the ion transfer tube (300 °C) of the Orbitrap Lumos operating in positive mode. The Orbitrap first performed a full MS scan at a resolution of 120,000 FWHM to detect the precursor ion having an m/z between 375 and 1,575 and a +2 to +7 charge. The Orbitrap AGC (Auto Gain Control) and the maximum injection time were set at 4 × 105 and 50 ms, respectively. The Orbitrap was operated using the top speed mode, with a 3 s cycle time for precursor selection. The most intense precursor ions presenting a peptide-specific isotopic profile and having an intensity threshold of at least 5,000 were isolated using the quadrupole and fragmented with HCD (30 % collision energy) in the ion routing multipole. The fragment ions (MS^2) were analyzed in the ion trap at a rapid scan rate. The AGC and respectively, for the ion trap. Dynamic exclusion was enabled for the maximum injection time were set at 1 × 104 and 35 ms, 45 s to avoid the acquisition of the same precursor ion having a similar m/z (±10 ppm).

2.2.3 Proteomic Data Analysis

Spectral data were matched to peptide sequences in the human UniProt protein database using the Andromeda algorithm (Cox et al., 2011) as implemented in the MaxQuant (Cox and Mann, 2008) software package v.1.6.10.23, at a peptide-spectrum match FDR of < 0.01. Search parameters included a mass tolerance of 20 p.p.m. for the parent ion, 0.5 Da for the fragment ion, carbamidomethylation of cysteine residues (+57.021464 Da), variable N-terminal modification by acetylation (+42.010565 Da), and variable methionine oxidation (+15.994915 Da). N-terminal and lysine heavy (+34.063116 Da) and light (+28.031300 Da) dimethylation were defined as labels for relative quantification. The cleavage site specificity was set to trypsin/p for the proteomics data, with up to two missed cleavages allowed. Significant outlier cutoff values were determined after log (2) transformation by boxplot-and-whiskers analysis using the BoxPlotR tool (Spitzer et al., 2014).

2.2.4 Bioinformatics Analysis

Data were integrated, analyzed, and graphed to determine pathway enrichment with STRING v11.5 (Search Tool for the Retrieval of Interacting Genes; https://string-db.org/) (Mering et al., 2005; Szklarczyk et al., 2018; Szklarczyk et al., 2021) and Metascape (https://metascape.org) (Zhou et al., 2019); the program used to generate a given proteomics figure is identified in the corresponding figure description. For both programs, data were analyzed using *Homo sapiens* as the organism due to the larger protein interactome available for this species (Zhou et al., 2019). The false discovery rate was set at 5 %.

2.3 Mitochondrial Function

At PD 0, 14, and 28, hearts from one male and one female offspring per litter were collected, separated from their atria, and either the remaining ventricles (PD 0) or the apex (PD 14 and 28) were immediately immersed in ice-cold biopsy preservation solution (BIOPS) (Lemieux et al., 2011). Cardiac fibers were then mechanically permeabilized in ice-cold BIOPS using forceps, followed by gentle agitation for 30 min on ice in BIOPS supplemented with 50 mg/ml saponin (Lemieux et al., 2017a). Finally, fibers were rinsed in mitochondrial respiration medium (Mir05) (Gnaiger E et al., 2000) for ten minutes on ice on a stirring platform before being blotted dry, weighed, and immediately used for respirometry.

Respirometry was performed at 37°C using 2 to 5 mg of permeabilized cardiac ventricular fibers per chamber of an Oxygraph-2K (Oroboros Instruments, Innsbruck, Austria) filled with 2 ml of MiR05. DatLab software (Oroboros Instruments, Innsbruck, Austria) was used for data acquisition and analysis. Artificial oxygen diffusion limitation was avoided by maintaining oxygen levels over 200 μM (Lemieux et al., 2017a); instrumental oxygen background fluxes were calibrated as a function of oxygen concentration and subtracted from the total volume-specific

oxygen flux using DatLab. Two substrate-uncoupler-inhibitor titration (SUIT) protocols were applied to the permeabilized fibers to evaluate the mitochondrial function; the assessed pathways are depicted in Figure 4. These protocols included two respiratory states (Gnaiger, 2020): (1) LEAK respiration in the non-phosphorylating state without ADP present, and (2) oxidative phosphorylation (OXPHOS), i.e., coupled respiration in the presence of saturating ADP. Concentrations of the substrates, uncouplers, or inhibitors used in the SUIT protocols are final concentrations present in the Oxygraph-2k chamber.

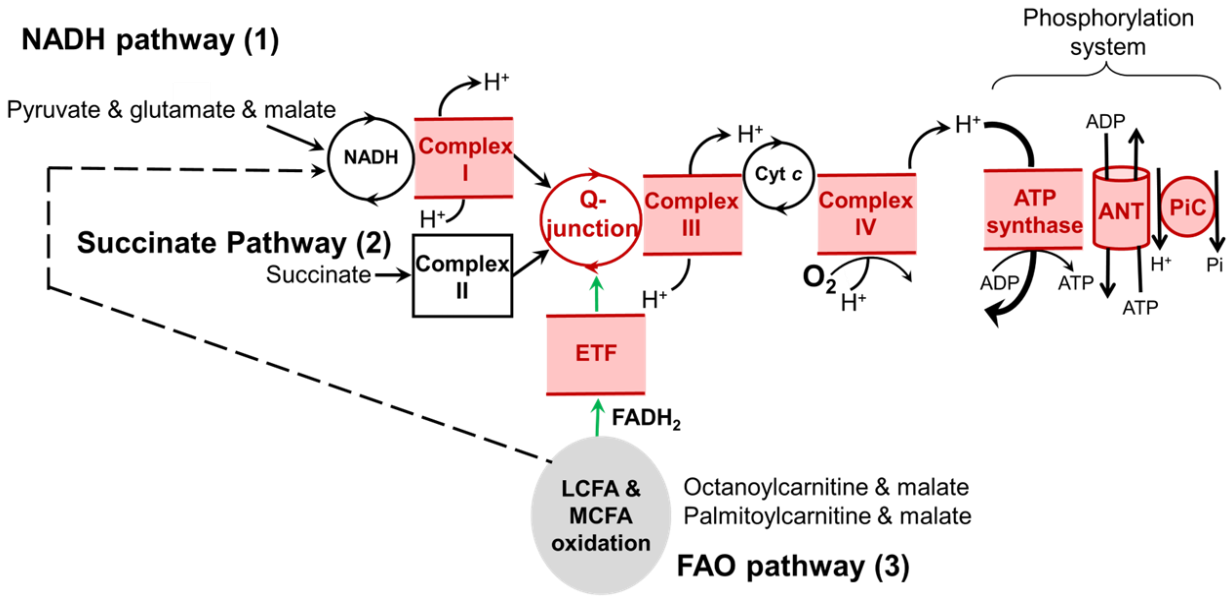

Figure 2.3.1: Schematic of select oxidative phosphorylation (OXPHOS) pathways depicting electron entrance into the electron transport system (ETS) via the NADH (1), succinate (2), and fatty acid oxidation (3; FAO) pathways. Components in red are in the inner mitochondrial membrane while black solid lines indicate peripheral association to the inner mitochondrial membrane. (1) A combination of pyruvate, glutamate, and malate promotes electron entry into the ETS via complex I specifically, allowing assessment of the NADH-pathway. (2) The presence of succinate promotes electron entry into the ETS at complex II. (3) The presence of octanoylcarnitine, palmitoylcarnitine, or both, alongside malate promotes electron flow through the fatty acid oxidation (FAO) pathway for medium-chain (MCFA) and long-chain fatty acids (LCFA), respectively. Electrons from all three pathways converge at the Q-junction before passing through complex III and complex IV to the final electron acceptor, oxygen (O_2). Oxidation of electrons across the ETS generates a protonmotive force between the intermembrane space and the mitochondrial matrix; this force is used by ATP synthase of the phosphorylation system to produce ATP. Figure is modified from (Lemieux and Blier, 2022).

The first protocol, for the assessment of carbohydrate oxidation capacity, proceeded as follows: (1) LEAK respiration in the presence of 5 mM pyruvate and 5 mM malate; (2) OXPHOS capacity for the NADH (N) pathway (electron flux through complex I) after the addition of 2.5 mM ADP and 10 mM glutamate; (3) integrity of the mitochondrial outer membrane by addition of 10 µM cytochrome *c*; (4) OXPHOS capacity for the combined NADH & Succinate pathway (NS-pathway, convergent electron flux through complex I and II) after the addition 10 mM succinate; (5) OXPHOS capacity for the Succinate pathway (S-pathway; electron flux through complex II) after inhibition of complex I with 0.5 µM rotenone; (6) residual oxygen consumption (ROX) after inhibition of complex III with 2.5 µM antimycin A; (7) complex IV activity using 2 mM ascorbate and 0.5 mM tetramethylphenylenediamine (TMPD); and (8) chemical background with 100 mM sodium azide (subtracted from complex IV activity). A variation of this SUIT protocol included the addition of the uncoupler DNP (10 µM steps up to 30 µM) after succinate on a reduced number of animals to confirm no limitation of the OXPHOS capacity by the phosphorylation system in cardiac fibers from the rat, as previously measured in the heart of rat (Lemieux et al., 2010), mice (Lemieux et al., 2017b), and Nile rat (Schneider et al., 2020).

The second SUIT protocol allowed the evaluation of FAO capacity. It included the sequential measurement of: (1) LEAK respiration in the presence of 5 mM malate and 0.2 mM octanoylcarnitine, a medium chain fatty acid; (2) OXPHOS capacity of the FAO pathway after addition of 2.5 mM ADP; (3) integrity of the outer mitochondrial membrane by addition of 10 µM cytochrome *c*; (4) OXPHOS capacity with combined medium chain and long chain FAO pathway after the addition of 0.04 mM palmitoylcarnitine; (5) combined FAO and N-pathway capacities after the addition of 5 mM pyruvate; and (6) combined FAO and NS-pathway capacities by the addition of 10 mM succinate.

2.4 Citrate Synthase Activity

Citrate synthase (CS) activity was used as a marker of mitochondrial content (Larsen et al., 2012). As previously described (Woodman et al., 2018), a UV/Vis spectrophotometer equipped with a heated cell holder and circulating water bath was used to measure CS activity at 37°C. Aliquots of homogenized tissue were thawed and vortexed. Absorbance was measured for 5 min at 412 nm after the reduction of 0.1 mM dithiobis-2- nitrobenzoic acid (ε: 13.6ml/cm × mM) in the presence of 0.25% Triton X-100, 0.5 mM oxaloacetic acid, 0.31 mM acetyl coenzyme A, 100 mM Tris-HCl, and triethanolamine-HCl buffer (pH 8.0).

2.5 Transmission Electron Microscopy

Quickly after euthanasia, a portion of the apex was cut down to pieces approximately 1 mm^3 in size, which were immediately placed in cold fixative solution (2% paraformaldehyde, 2.5% glutaraldehyde, 0.1M cacodylate buffer). Samples were stored at 4 °C before undergoing processing and imaging at the Cross Cancer Institute, University of Alberta; sample processing and imaging were performed by Pinzhang (Priscilla) Gao. The microscope operator was blinded to the experimental groups of the study. Four to five photos were taken at random of a single sample for each group (n=1 per group). Representative images are shown in Figure 3.4.6. We performed a qualitative assessment of mitochondria present in these photos with assistance from Dr. Hisashi Fujioka at Case Western University.

2.6 Fluorescence Microscopy

Superoxide levels were assessed as previously described (Woodman et al., 2018). Slides of heart cryosections (8 μm thickness) from male and female pups at PD 0, 14, and 28 were thawed, washed three times with Hank's Balanced Salt Solution (HBSS), and warmed to 37°C in a humidified chamber for 10 min. Slides were then washed and incubated with 20 μM

dihydroethidium (DHE) for 30 min. Fluorescence was visualized using an Olympus IX81 fluorescence microscope. Adobe Photoshop was used to determine the intensity of fluorescence, referred to as mean fluorescence intensity.

2.7 RT-qPCR

Flash frozen cardiac ventricles from PD 0, 14, and 28 male and female offspring were crushed into a powder with a liquid nitrogen cooled mortar and pestle and stored at -80 °C. Approximately 10 mg of powdered cardiac tissue was placed in 1 mL of TRIzol reagent (Life Technologies, Carlsbad, CA, USA) and homogenized in 2 mL tubes containing ceramic beads for four intervals of 15 s using a homogenizer (Precellys Minilys Tissue Homogenizer; Bertin Instruments, France) (Woodman et al., 2023). After centrifugation at 12 000 X g for 10 min at 4°C, the supernatant was transferred into sterile 1.5 mL microcentrifuge tubes. Two hundred µL of chloroform was added to each sample after which tubes were vigorously shaken for 15 s and subsequently incubated at room temperature for 2 min before centrifugation at 12 000 X g for 10 min at 4 °C. The upper colorless phase was transferred into new tubes, 500 µL of isopropanol was added to each tube, samples were mixed by inverting tubes several times and incubated at -20 °C overnight. Samples were then centrifuged at 12 000 X g for 10 min at 4°C; the supernatant was discarded, and the remaining pellet was dislodged and mixed with 70 % ethanol by pipetting up and down. After centrifugation at 7500 X g for 5 min at 4°C, the supernatant was removed, and the pellet was air dried for 10 min before RNA was dissolved with 12 µL of water. cDNA was synthesized from extracted RNA using the High-Capacity cDNA Reverse Transcription Kit (Applied Biosystems); all reactions contained 2000 ng of RNA. RNA concentration and purity were confirmed by measuring absorbance at $A260_{nm}$ and $A280_{nm}$ with a NanoDrop1000 spectrophotometer (Thermo Fisher). cDNA was diluted 40-fold and stored at -80°C. Sequences

for genes of interest were obtained from NCBI's Gene Database (https://www.ncbi.nlm.nih.gov/gene/) and primer sequences (Table 2.7.1) were designed using LightCycler Probe Design Software 2.0 (Roche Diagnostics Corporation); if a given gene possessed multiple transcript variants or isoforms, the primer sequence was designed to recognize all variants. All primers were purchased from Thermo Fisher (https://www.thermofisher.com/order/custom-standard-oligo). qPCR reactions were carried out in duplicate in clear 384-well optical reaction plates using a LightCycler 480 (Roche Diagnostics Corporation); reaction volumes per well totaled 20 µL consisting of 5 µL cDNA, 0.2 µL primers, 4.8 µl water and 10 µL PowerUP SYBR Green Master Mix (Applied Biosystems). Thermal cycling conditions for DNA amplification were as follows: an initial step of 50 °C for 120 s, 40 denaturation cycles at 95 °C for 15 s each and annealing and extension at 60 °C for 60 s. Cycle thresholds (CT) were used to calculate relative gene expression using *Actb* as the reference gene. Relative gene expression was calculated using the following formula: 2^(-[CT of gene of interest]-[CT of Actb]).

Table 2.7.1. Primers sequences used for RT-qPCR in *Rattus norvegicus*.

Gene (Other Names) [Gene ID]	Official Full Gene Name	Primer Sequences (5' to 3')	
Actb (*Actx*) [81822]	actin, beta	Fwd Rev	CTA CAA TGA GCT GCG TGT GG GGG TGT TGA AGG TCT CAA ACA TGA T
Sod1 (*CuZnSOD*) [24786]	superoxide dismutase 1	Fwd Rev	GCA GAA GGC AAG CGG TGA GGT ACA GCC TTG TGT ATT GTC CC
Sod2 (*MnSOD*) [24787]	superoxide dismutase 2	Fwd Rev	GTC TGT GGG AGT CCA AGG TT GTT CCT TGC AGT GGG TCC TGA TTA
Cat (*CS1; Cas1; Catl; Cs-1; Cat01*) [24248]	catalase	Fwd Rev	CGG ATT CCT GAG AGA GTG GTA CA TGT GGA GAA TCG GAC GGC AAT AG
Dmt1 (*Slc11a2; Nramp2*) [25715]	solute carrier family 11 member 2	Fwd Rev	GGC TTA TCT GGG CTT TGT GTT CT GCC TAG CGG TCA GTC CGA
Tfrc (*Trfr*) [64678]	transferrin receptor	Fwd Rev	CAG CAA AGT CTG GCG AGA TG GCC TCC ACT GGG TCA ATG TTA C
Ftl (*Ftl1*) [29292]	ferritin light chain 1	Fwd Rev	TTG CAC CTG CGG GCC TCT TA GGC CAA TTC GCG GAA GAA GT
Fth (*Fth1*) [25319]	ferritin heavy chain 1	Fwd Rev	CGC CAG ATC AAC CTG GAG T AAG TAT TTG GCA AAG TTC TTC AGG G
Fpn1 (*Slc40a1; Slc11a3; Slc39a1*) [170840]	solute carrier family 40 member 1	Fwd Rev	TGG CCT TCA CTT GGC TAC G ACG GAG ATC ACA CAC AAG ATC AAA C
Hamp (*Hepc*) [84604]	hepcidin antimicrobial peptide	Fwd Rev	GTG CGC TGC TGA TGC TGA A AGG CAG TGT GTT GAG AGG T

2.8 Data Analysis

In these experiments, the litter/dam was considered the experimental unit; thus, data obtained from offspring of the same sex and litter were considered experimental replicates, and averages were taken and treated as n=1. Data were also paired for analysis by litter (i.e., pups from the same dam were paired for analysis across time). Data were analyzed by paired two-way ANOVA or by fitting a mixed-effects model for the effects of iron-restriction and time as implemented in GraphPad Prism 8.3.0. Sidak's post-hoc test was used for multiple comparisons of CTL and ID groups within age groups. The Mann-Whitney U test was used for noncontinuous data (i.e., litter size and mortality). Outliers were identified using Grubb's test and excluded from analysis.

Chapter 3
Results

3.1 Maternal and Litter Outcomes

Maternal iron restriction resulted in a reduced Hb level at GD 0, which persisted through gestation ($P_{ID} < 0.0001$; Fig. 3.1.1A). ID dams had an overall reduction in body weight at all GD monitored ($P_{ID} = 0.0007$; Fig. 3.1.1B). Food intake normalized to body weight was similar between CTL and ID dams throughout the gestation period (P=0.07; Fig. 3.1.1C). Maternal iron restriction did not affect litter sizes (P=0.58; Fig. 3.1.2A) nor the ratio of male to female pups in litters (P=0.48; Fig. 3.1.2C), though 1-2 pups per ID litter died within the first 24 hours after birth (Fig. 3.1.2B).

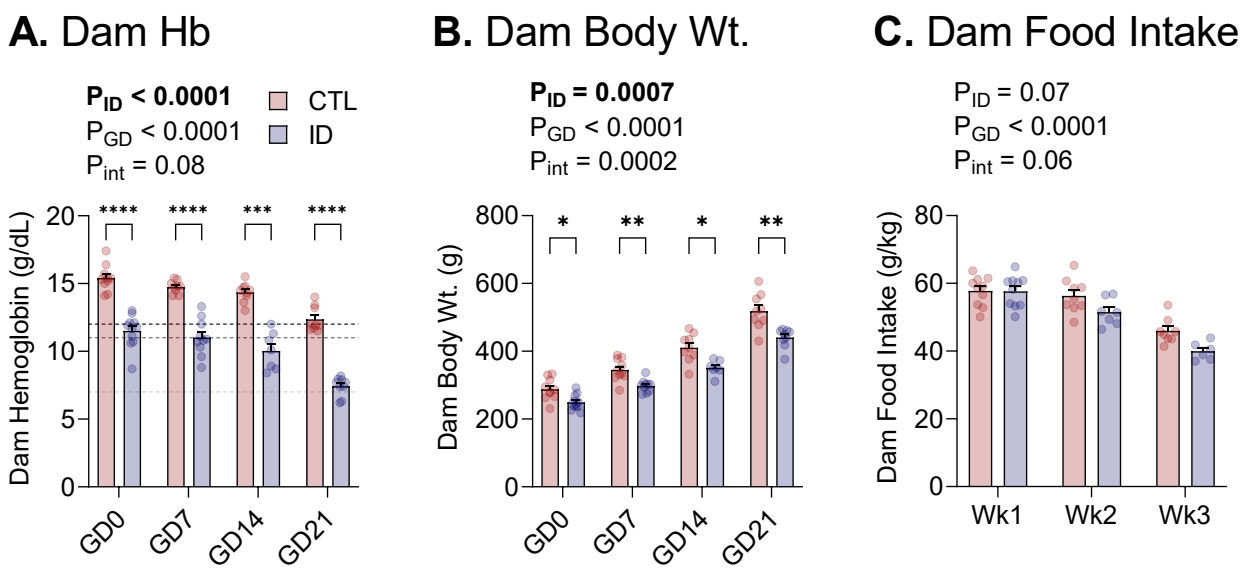

Figure 3.1.1: Effects of maternal iron restriction on dams. (A) Hemoglobin (Hb [g/dL]; horizontal dashed lines indicate Hb cutoffs for iron deficiency anemia in women ([12g/dL in black], in pregnant women [11 g/dL in dark grey], and severe ID anemia in women [7 g/dL in light grey]), (B) body weight (Wt; g), and (C) food intake (normalized to body weight; g/kg) through gestation (n=7-11). Bars show mean±SEM with individual data points. CTL: control; ID: iron-deficient; GD: gestational day; Wk: week. *P<0.05, **P<0.01, ***P<0.001, ****P<0.0001 for multiple comparisons.

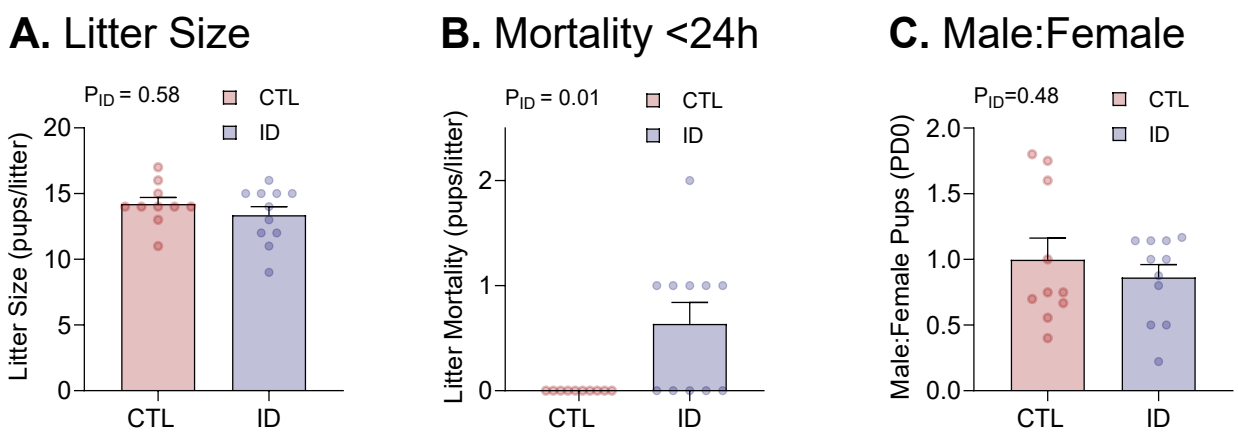

Figure 3.1.2: Effects of maternal iron restriction on litter outcomes. (A) Litter size (pups/litter at birth), (B) mortality under 24 hours (pups/litter), and (C) male:female ratio of neonatal pups in litters. Bars show mean±SEM with individual data points. CTL: control; ID: iron deficient. *P<0.05, **P<0.01, ***P<0.001, ****P<0.0001 for multiple comparisons.

3.2 Offspring Outcomes

Hb levels, body weights, and heart weights were measured in pups at PD 0, 14, and 28. Hb levels (Fig. 3.2.1A, B) were reduced in ID pups at PD 0 ($P_{ID} < 0.0001$ for both males and females) and PD 14 ($P_{ID} = 0.008$ for males; $P_{ID} = 0.02$ for females) but were no longer different at PD 28 ($P_{ID} = 0.85$ for males; $P_{ID} = 0.58$ for females). ID pups of both sexes were growth restricted compared to CTLs ($P_{ID} < 0.0001$; Fig. 3.2.1C, D). Hearts of ID animals were enlarged relative to body weight at all timepoints (Fig. 3.2.1E, F), despite absolute heart weights remaining largely unchanged ($P_{ID} = 0.17$ for males, Fig. 3G; $P_{ID} = 0.08$ for females; Fig. 3.2.1H). Organ weights, both relative to body weight and absolute weights, for kidneys, livers, and brains are shown in Fig. 3.2.2 and Fig. 3.2.3, respectively. Brains of ID animals were also enlarged relative to body weight (Fig. 3.2.2E, F), while relative liver weights remained unchanged (Fig. 3.2.2C, D).

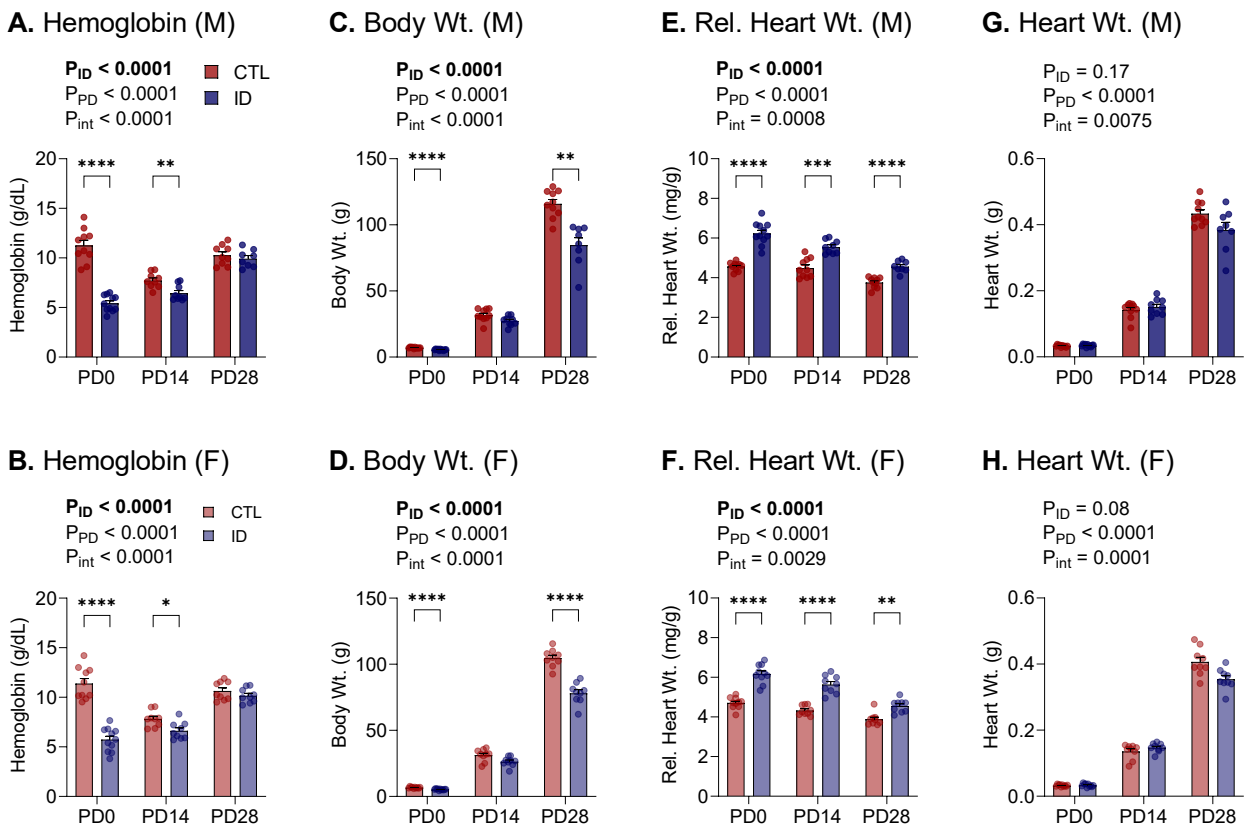

Figure 3.2.1: Effects of maternal iron restriction on male (M; top row comprising panels A, C, E, and G) and female (F; bottom row comprising panels B, D, E, F) pup (A, B) hemoglobin (Hb; g/dL), (C, D) body weight (Wt; g), (E, F) relative heart weight (normalized to body weight; mg/g), and (G, H) absolute heart weight (g) at postnatal days (PD) 0, 14, and 28 (n=8-11). Bars show mean±SEM with individual data points. CTL: control; ID: iron deficient. *P<0.05, **P<0.01, ***P<0.001, ****P<0.0001 for multiple comparisons.

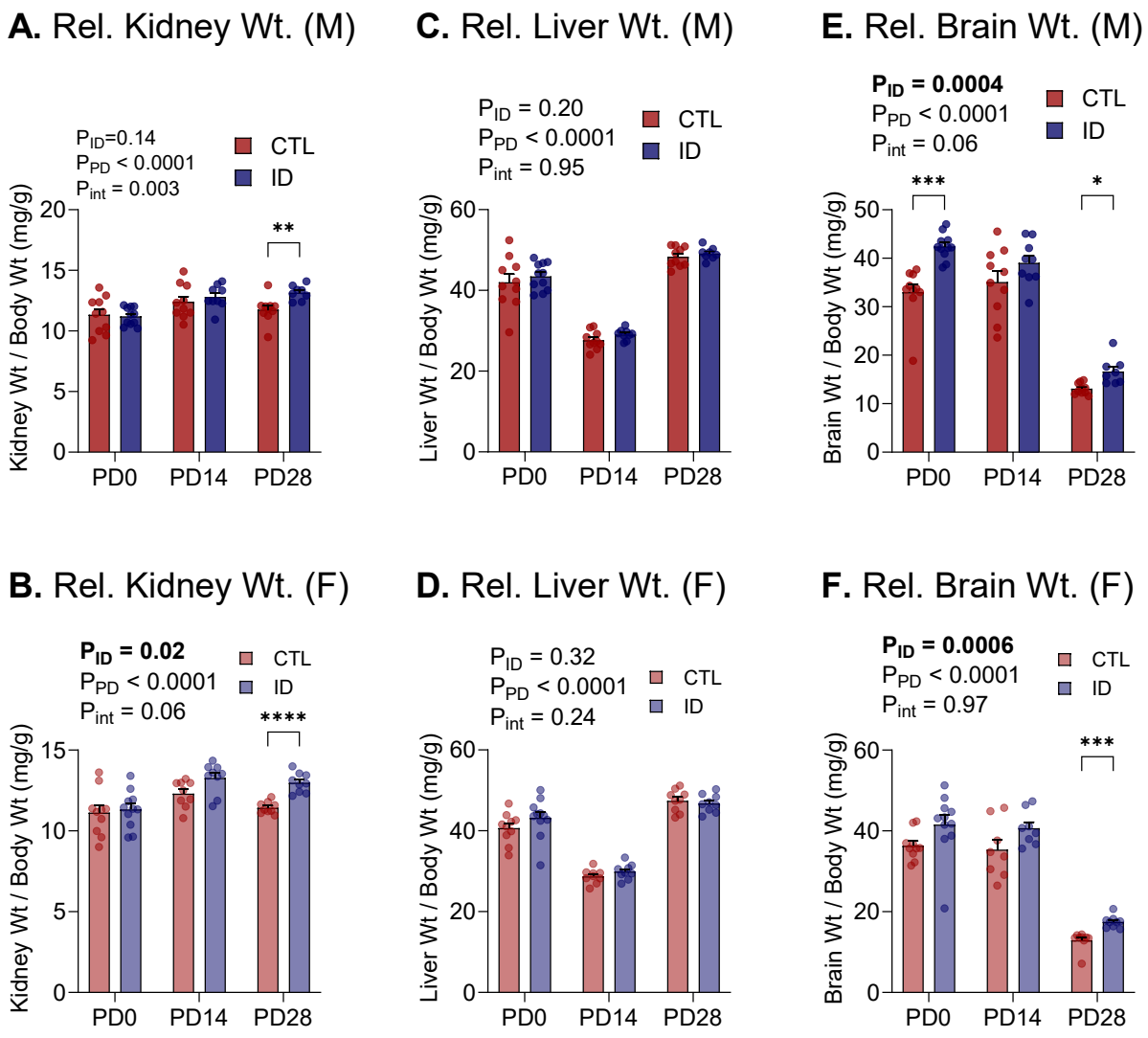

Figure 3.2.2: Effect of maternal iron restriction on male (M; top row comprising panels A, C, E) and female (F; bottom row comprising panels B, D, F) pup (A, B) kidney weight relative to body weight (mg/g), (C, D) liver weight relative to body weight (mg/g), and (E, F) brain weight relative to body weight (mg/g) at postnatal days (PD) 0, 14, and 28 (n=8-11). CTL: control; ID: iron deficient. *P<0.05, **P<0.01, ***P<0.001, ****P<0.0001 for multiple comparisons.

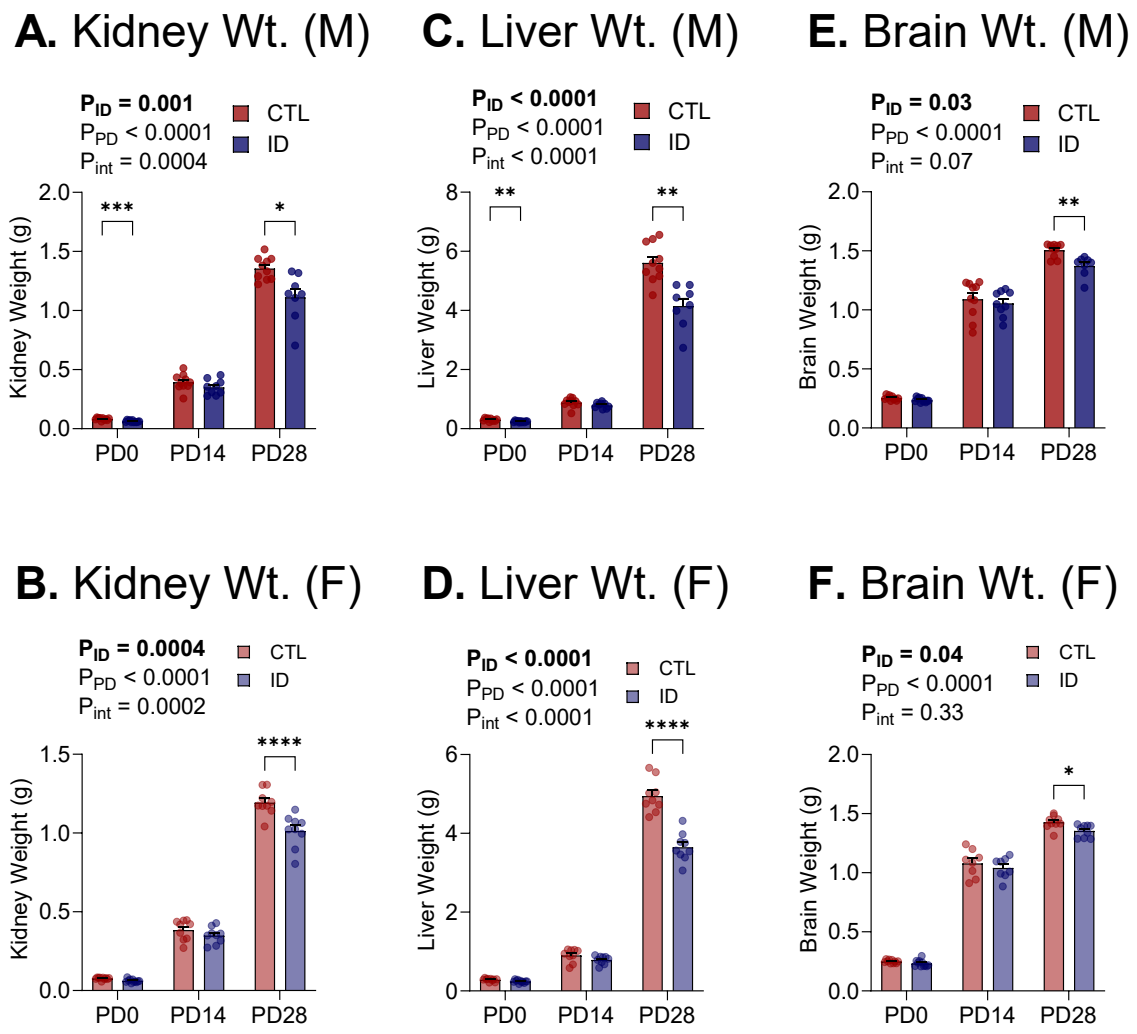

Figure 3.2.3: Effect of maternal iron restriction on male (M; top row comprising panels A, C, E) and female (F; bottom row comprising panels B, D, F) pup (A, B) absolute kidney weight (g), (C, D) absolute liver weight (g), and (E, F) absolute brain weight (g) at postnatal days (PD) 0, 14, and 28 (n=8-11). CTL: control; ID: iron deficient. *P<0.05, **P<0.01, ***P<0.001, ****P<0.0001 for multiple comparisons.

3.3 Quantitative Shotgun Proteomics of Neonatal Hearts

To characterize the impact of perinatal ID on global proteome changes in neonatal hearts, we performed quantitative shotgun proteomics analyses of male and female offspring hearts at PD 0 and 28 (Fig. 3.3.1). From the complete list of identified proteins, interquartile boxplot analysis was used to set outlier cutoffs, thus determining the two sets of proteins: those significantly downregulated by ID and those significantly upregulated by ID. Changes in protein abundance are represented as $\log_2$ fold change (ID over CTL), thus, $\log_2 > 0$ indicates the protein is upregulated by ID, whereas $\log_2 < 0$ indicates downregulation of the protein by ID (Fig 3.3.1A, C for males and Fig. 3.3.1B, D for females).

In male offspring hearts, at PD 0, we identified 54 proteins that were downregulated by ID, compared to CTL, and 45 upregulated proteins (Fig. 3.3.1A). At PD 28, the number of significantly altered proteins increased, with 59 proteins being downregulated and 67 proteins being upregulated, compared to CTLs (Fig. 3.3.1C). A similar pattern emerged in female offspring hearts whereby we observed an increased amount of significantly altered proteins from PD 0 to PD 28. In female offspring hearts, at PD 0, 63 proteins were downregulated; but only 18 proteins were upregulated by ID in female offspring hearts (Fig. 3.3.1B). At PD 28, 82 proteins were downregulated proteins, and 56 proteins were upregulated by ID in female offspring hearts (Fig. 3.3.1D).

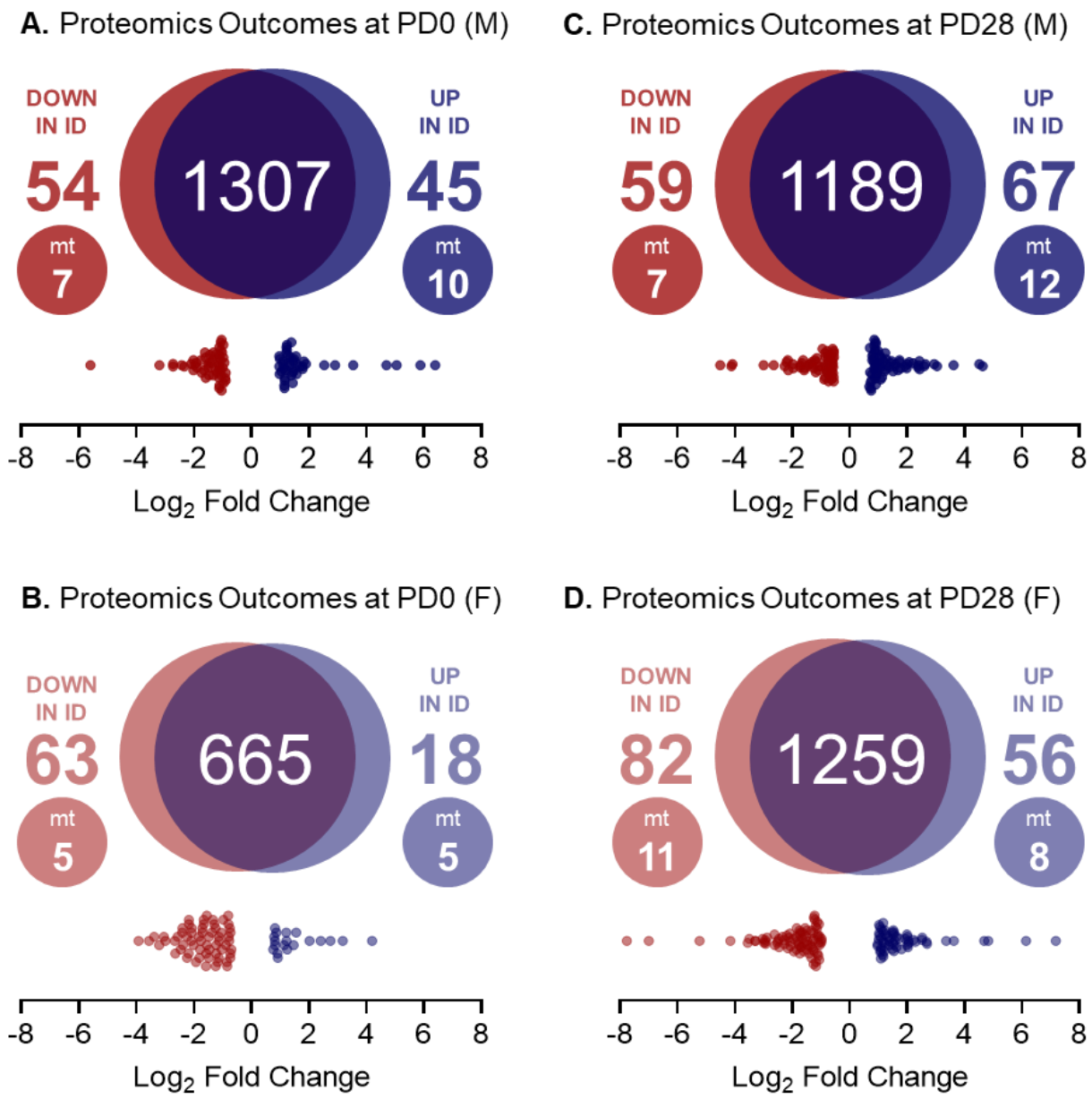

Figure 3.3.1: Summary of proteomics outcomes in male (M; upper panels, A and C) and female (F; lower panels, B and D) offspring hearts at postnatal days (PD) 0 (left panels, A and B) and 28 (right panels, C and D). For each panel, the sum of the three values presented in the Venn diagram is equal to the total number of peptides identified and quantified by mass spectrometry in the hearts of control (CTL) and iron-deficient (ID) pairs (n=4-5). The center value on the overlapping portion of the Venn diagram represents the number of peptides expressed at similar levels between CTL-ID pairs (i.e., not significant outliers); significant outliers were identified using interquartile

boxplot analysis and are presented on the left and right of the Venn diagrams as the number of proteins down- or up-regulated in ID, respectively. The number of mitochondria (mt) related proteins from each of these lists is presented in the colored circle below the number of total down- or upregulated proteins. Finally, under each Venn diagram, the relative expression of all proteins determined as down- or upregulated in ID is shown as a dot plot and presented as the Log_2 fold change relative to CTL.

We then used the Metascape meta-analysis tool to explore the identities and functions of altered proteins before performing pathway enrichment analysis. Given our initial hypotheses suggesting mitochondrial disturbances in perinatal ID hearts, we first investigated whether any of the altered proteins were related to mitochondria or their function. Proteins were defined as mitochondria-related if the term 'mitochondria' was referenced in the protein description, top associated gene ontology terms, the protein function, or the subcellular location. In male offspring hearts, at PD 0, 7 of 54 downregulated proteins and 10 of 45 upregulated proteins were mitochondria-related (Table 3.3.1). In PD 28 male hearts, 7 of 59 downregulated proteins and 12 of 67 upregulated proteins were mitochondria-related (Table 3.3.2). In female offspring hearts at PD 0, 5 of 63 downregulated proteins and 5 of 18 upregulated proteins were mitochondria-related (Table 3.3.3) while at PD 28, 11 of 82 downregulated proteins and 8 of 56 upregulated proteins were mitochondria-related (Table 3.3.4). Each group had unique mitochondria-related proteins altered, which are highlighted within the overall protein network in Figures 3.3.2 and 3.3.3. Overall, functions of mitochondria-related proteins included energy and/or nutrient metabolism, protein processing, and organelle organization. Of note, PD 0 and PD 28 male hearts showed an upregulation of several complex I subunits.

Table 3.3.1: Mitochondria-related proteins altered by ID in PD 0 male hearts.

Gene [Gene ID] Description	Associated Biological Process Gene Ontology (GO) Terms		Change in ID vs. CTL
NDUFB7 [4713] NADH:ubiquinone oxidoreductase subunit B7	GO:0006120 GO:0010257 GO:0032981	mitochondrial electron transport, NADH to ubiquinone NADH dehydrogenase complex assembly mitochondrial respiratory chain complex I assembly	Up
NDUFS8 [4728] NADH:ubiquinone oxidoreductase core subunit S8	GO:0006120 GO:0010257 GO:0032981	mitochondrial electron transport, NADH to ubiquinone NADH dehydrogenase complex assembly mitochondrial respiratory chain complex I assembly	Up
NDUFB9 [4715] NADH:ubiquinone oxidoreductase subunit B9	GO:0006120 GO:0010257 GO:0032981	mitochondrial electron transport, NADH to ubiquinone NADH dehydrogenase complex assembly mitochondrial respiratory chain complex I assembly	Up
ATP5F1C [509] ATP synthase F1 subunit gamma	GO:0042776 GO:0015986 GO:0006754	proton motive force-driven mitochondrial ATP synthesis proton motive force-driven ATP synthesis ATP biosynthetic process	Up
ATAD3A [55210] ATPase family AAA domain containing 3A	GO:0140374 GO:0051607 GO:0140546	antiviral innate immune response defense response to virus defense response to symbiont	Up
HK2 [3099] hexokinase 2	GO:0072656 GO:0006735 GO:0061621	maintenance of protein location in mitochondrion NADH regeneration canonical glycolysis	Up
PDCD5 [9141] programmed cell death 5	GO:1903636 GO:1903638 GO:1903645	regulation of protein insertion into mitochondrial outer membrane positive regulation of protein insertion into mitochondrial outer membrane negative regulation of chaperone-mediated protein folding	Up

TIMM8A [1678] translocase of inner mitochondrial membrane 8A	GO:0045039 GO:0051204 GO:0090151	protein insertion into mitochondrial inner membrane protein insertion into mitochondrial membrane establishment of protein localization to mitochondrial membrane	Up
WDR70 [55100] WD repeat domain 70	GO:2001173 GO:1903775 GO:2001166	regulation of histone H2B conserved C-terminal lysine ubiquitination regulation of DNA double-strand break processing regulation of histone H2B ubiquitination	Up
TTC27 [55622] tetratricopeptide repeat domain 27	GO:0008150	biological process	Up
COX6C [1345] cytochrome c oxidase subunit 6C	GO:0006123 GO:0019646 GO:0042773	mitochondrial electron transport, cytochrome c to oxygen aerobic electron transport chain ATP synthesis coupled electron transport	Down
ACOT2 [10965] acyl-CoA thioesterase 2	GO:0000038 GO:0006637 GO:0035383	very long-chain fatty acid metabolic process acyl-CoA metabolic process thioester metabolic process	Down
SLC22A5 [6584] solute carrier family 22 member 5	GO:0060731 GO:0070715 GO:1900749	positive regulation of intestinal epithelial structure maintenance sodium-dependent organic cation transport (R)-carnitine transport	Down
ZNF608 [57507] zinc finger protein 608	GO:0000122 GO:0045892 GO:1903507	negative regulation of transcription by RNA polymerase II negative regulation of transcription, DNA-templated negative regulation of nucleic acid-templated transcription	Down
C10orf71 [118461] chromosome 10 open reading frame 71	GO:0070886 GO:0106058 GO:0050850	positive regulation of calcineurin-NFAT signaling cascade positive regulation of calcineurin-mediated signaling positive regulation of calcium-mediated signaling	Down
CDC37 [11140] cell division cycle 37, HSP90 cochaperone	GO:0098779 GO:1904925 GO:1904923	positive regulation of mitophagy in response to mitochondrial depolarization positive regulation of autophagy of mitochondrion in response to mitochondrial depolarization regulation of autophagy of mitochondrion in response to mitochondrial depolarization	Down

TAGLN	GO:0007517	muscle organ development	
[6876]	GO:0061061	muscle structure development	
transgelin	GO:0030855	epithelial cell differentiation	Down

Table 3.3.2: Mitochondria-related proteins altered by ID in PD 28 male hearts.

Gene [Gene ID] Description	Associated Biological Process Gene Ontology (GO) Terms		Change in ID vs. CTL
ND3 [4537] NADH dehydrogenase subunit 3	GO:0009642 GO:0006120 GO:0071385	response to light intensity mitochondrial electron transport, NADH to ubiquinone cellular response to glucocorticoid stimulus	Up
NDUFB4 [4710] NADH:ubiquinone oxidoreductase subunit B4	GO:0006120 GO:0010257 GO:0032981	mitochondrial electron transport, NADH to ubiquinone NADH dehydrogenase complex assembly mitochondrial respiratory chain complex I assembly	Up
NDUFA5 [4698] NADH:ubiquinone oxidoreductase subunit A5	GO:0006120 GO:0010257 GO:0032981	mitochondrial electron transport, NADH to ubiquinone NADH dehydrogenase complex assembly mitochondrial respiratory chain complex I assembly	Up
NDUFA8 [4702] NADH:ubiquinone oxidoreductase subunit A8	GO:0006120 GO:0010257 GO:0032981	mitochondrial electron transport, NADH to ubiquinone NADH dehydrogenase complex assembly mitochondrial respiratory chain complex I assembly	Up
NDUFA10 [4705] NADH:ubiquinone oxidoreductase subunit A10	GO:0006120 GO:0010257 GO:0032981	mitochondrial electron transport, NADH to ubiquinone NADH dehydrogenase complex assembly mitochondrial respiratory chain complex I assembly	Up
NDUFA11 [126328] NADH:ubiquinone oxidoreductase subunit A11	GO:0010257 GO:0032981 GO:0042776	NADH dehydrogenase complex assembly mitochondrial respiratory chain complex I assembly proton motive force-driven mitochondrial ATP synthesis	Up
UQCRQ [27089] ubiquinol-cytochrome c reductase complex III subunit VII	GO:0021539 GO:0021548 GO:0021860	subthalamus development pons development pyramidal neuron development	Up

PITRM1			
[10531]	GO:0006626	protein targeting to mitochondrion	
pitrilysin	GO:0072655	establishment of protein localization to mitochondrion	
metallopeptidase 1	GO:0070585	protein localization to mitochondrion	Up
GRPEL1		protein import into mitochondrial matrix	
[80273]	GO:0030150	protein transmembrane import into intracellular	
GrpE like 1,	GO:0044743	organelle	
mitochondrial	GO:0065002	intracellular protein transmembrane transport	Up
STOML2	GO:1900210	positive regulation of cardiolipin metabolic process	
[30968]	GO:1990046	stress-induced mitochondrial fusion	
stomatin like 2	GO:0090297	positive regulation of mitochondrial DNA replication	Up
ZBTB3			
[79842]	GO:0006357	regulation of transcription by RNA polymerase II	
zinc finger and BTB	GO:0006355	regulation of transcription, DNA-templated	
domain containing 3	GO:1903506	regulation of nucleic acid-templated transcription	Up
ALDH7A1			
[501]			
aldehyde	GO:0019285	glycine betaine biosynthetic process from choline	
dehydrogenase 7	GO:0031455	glycine betaine metabolic process	
family member A1	GO:0031456	glycine betaine biosynthetic process	Up
TOMM22			
[56993]			
translocase of outer	GO:0007008	outer mitochondrial membrane organization	
mitochondrial	GO:0045040	protein insertion into mitochondrial outer membrane	
membrane 22	GO:0051204	protein insertion into mitochondrial membrane	Down
APOO	GO:0042407	cristae formation	
[79135]	GO:0007007	inner mitochondrial membrane organization	
apolipoprotein O	GO:0007006	mitochondrial membrane organization	Down
COQ8A	GO:0006744	ubiquinone biosynthetic process	
[56997]	GO:1901663	quinone biosynthetic process	
coenzyme Q8A	GO:0006743	ubiquinone metabolic process	Down
ME2	GO:1902031	regulation of NADP metabolic process	
[4200]	GO:0006108	malate metabolic process	
malic enzyme 2	GO:0006090	pyruvate metabolic process	Down
PDPR			
[55066]			
pyruvate			
dehydrogenase	GO:1904184	positive regulation of pyruvate dehydrogenase activity	
phosphatase	GO:1904182	regulation of pyruvate dehydrogenase activity	
regulatory subunit	GO:0051353	positive regulation of oxidoreductase activity	Down

GARS1 [2617] glycyl-tRNA synthetase 1	GO:0006426 GO:0070150 GO:0015960	glycyl-tRNA aminoacylation mitochondrial glycyl-tRNA aminoacylation diadenosine polyphosphate biosynthetic process	Down
PALLD [23022] palladin, cytoskeletal associated protein	GO:0003334 GO:0070593 GO:0003382	keratinocyte development dendrite self-avoidance epithelial cell morphogenesis	Down

Table 3.3.3. Mitochondria-related proteins altered by ID in PD 0 female hearts.

Gene [Gene ID] Description	Associated Biological Process Gene Ontology (GO) Terms		Change in ID vs. CTL
NDUFA10 [4705] NADH:ubiquinone oxidoreductase subunit A10	GO:0006120 GO:0010257 GO:0032981	mitochondrial electron transport, NADH to ubiquinone NADH dehydrogenase complex assembly mitochondrial respiratory chain complex I assembly	Up
ACADM [34] acyl-CoA dehydrogenase medium chain	GO:0019254 GO:0045329 GO:0051793	carnitine metabolic process, CoA-linked carnitine biosynthetic process medium-chain fatty acid catabolic process	Up
FIS1 [51024] fission, mitochondrial 1	GO:2000192 GO:0032471 GO:0043653	negative regulation of fatty acid transport negative regulation of endoplasmic reticulum calcium ion concentration mitochondrial fragmentation involved in apoptotic process	Up
TFRC [7037] transferrin receptor	GO:0010637 GO:0033572 GO:0010635	negative regulation of mitochondrial fusion transferrin transport regulation of mitochondrial fusion	Up
VDAC3 [7419] voltage dependent anion channel 3	GO:0015853 GO:0006863 GO:0015851	adenine transport purine nucleobase transport nucleobase transport	Up
NDUFB7 [4713] NADH:ubiquinone oxidoreductase subunit B7	GO:0006120 GO:0010257 GO:0032981	mitochondrial electron transport, NADH to ubiquinone NADH dehydrogenase complex assembly mitochondrial respiratory chain complex I assembly	Down
ATP5PB [515] ATP synthase peripheral stalk-membrane subunit b	GO:0021762 GO:0048857 GO:0042776	substantia nigra development neural nucleus development proton motive force-driven mitochondrial ATP synthesis	Down
CPT2 [1376] carnitine palmitoyl-transferase 2	GO:0006853 GO:1902001 GO:0009437	carnitine shuttle fatty acid transmembrane transport carnitine metabolic process	Down

CLUH [23277]			
clustered mitochondria homolog	GO:0048312 GO:0048311 GO:0051646	intracellular distribution of mitochondria mitochondrion distribution mitochondrion localization	Down
SUCLG1 [8802] succinate-CoA ligase GDP/ADP-forming subunit alpha	GO:1901289 GO:0006104 GO:0033869	succinyl-CoA catabolic process succinyl-CoA metabolic process nucleoside bisphosphate catabolic process	Down

Table 3.3.4. Mitochondria-related proteins altered by ID in PD 28 female hearts.

Gene [Gene ID] Description	Associated Biological Process Gene Ontology (GO) Terms		Change in ID vs. CTL
NDUFB6 [4712] NADH:ubiquinone oxidoreductase subunit B6	GO:0006120	mitochondrial electron transport, NADH to ubiquinone	
	GO:0010257	NADH dehydrogenase complex assembly	
	GO:0032981	mitochondrial respiratory chain complex I assembly	Up
UQCRQ [27089] ubiquinol-cytochrome c reductase complex III subunit VII	GO:0021539	subthalamus development	
	GO:0021548	pons development	
	GO:0021860	pyramidal neuron development	Up
ATP6 [4508] ATP synthase F0 subunit 6	GO:0055093	response to hyperoxia	
	GO:0036296	response to increased oxygen levels	
	GO:0042776	proton motive force-driven mitochondrial ATP synthesis	Up
ECHDC2 [55268] enoyl-CoA hydratase domain containing 2	GO:0006635	fatty acid beta-oxidation	
	GO:0019395	fatty acid oxidation	
	GO:0009062	fatty acid catabolic process	Up
CISD1 [55847] CDGSH iron sulfur domain 1	GO:0043457	regulation of cellular respiration	
	GO:0043467	regulation of generation of precursor metabolites and energy	
	GO:0010506	regulation of autophagy	Up
STOML2 [30968] stomatin like 2	GO:1900210	positive regulation of cardiolipin metabolic process	
	GO:1990046	stress-induced mitochondrial fusion	
	GO:0090297	positive regulation of mitochondrial DNA replication	Up
PYROXD2 [84795] pyridine nucleotide-disulphide oxidoreductase domain 2	GO:0007005	mitochondrion organization	
	GO:0006996	organelle organization	
	GO:0016043	cellular component organization	Up
MTX2 [10651] metaxin 2	GO:0007008	outer mitochondrial membrane organization	
	GO:0045040	protein insertion into mitochondrial outer membrane	
	GO:0051204	protein insertion into mitochondrial membrane	Up

COX3 [4514]	GO:0006123	mitochondrial electron transport, cytochrome c to oxygen	
cytochrome c oxidase subunit III	GO:0008535	respiratory chain complex IV assembly	
	GO:0017004	cytochrome complex assembly	Down
ATPAF2 [91647]		mitochondrial proton-transporting ATP synthase	
ATP synthase mitochondrial F1 complex assembly factor 2	GO:0033615	complex assembly	
	GO:0043461	proton-transporting ATP synthase complex assembly	
	GO:0070071	proton-transporting two-sector ATPase complex assembly	Down
PDPR [55066] pyruvate dehydrogenase phosphatase regulatory subunit	GO:1904184	positive regulation of pyruvate dehydrogenase activity	
	GO:1904182	regulation of pyruvate dehydrogenase activity	
	GO:0051353	positive regulation of oxidoreductase activity	Down
CYCS [54205] cytochrome c, somatic	GO:0008635	activation of cysteine-type endopeptidase activity involved in apoptotic process by cytochrome c	
	GO:000612	mitochondrial electron transport, ubiquinol to cytochrome c	
	GO:0097202	activation of cysteine-type endopeptidase activity	Down
PPIF [10105] peptidylprolyl isomerase F	GO:0010849	regulation of proton-transporting ATPase activity, rotational mechanism	
	GO:2000276	negative regulation of oxidative phosphorylation uncoupler activity	
	GO:1902445	regulation of mitochondrial membrane permeability involved in programmed necrotic cell death	Down
PMPCA [23203] peptidase, mitochondrial processing subunit alpha	GO:0006627	protein processing involved in protein targeting to mitochondrion	
	GO:0034982	mitochondrial protein processing	
	GO:0006626	protein targeting to mitochondrion	Down
BCAT2 [587] branched chain amino acid transaminase 2	GO:0009098	leucine biosynthetic process	
	GO:0009099	valine biosynthetic process	
	GO:0006550	isoleucine catabolic process	Down
ALDH7A1 [501] aldehyde dehydrogenase 7 family member A1	GO:0019285	glycine betaine biosynthetic process from choline	
	GO:0031455	glycine betaine metabolic process	
	GO:0031456	glycine betaine biosynthetic process	Down

SLC22A5 [6584] solute carrier family 22 member 5	GO:0060731 GO:0070715 GO:1900749	positive regulation of intestinal epithelial structure maintenance sodium-dependent organic cation transport (R)-carnitine transport	Down
SERPINC1 [462] serpin family C member 1	 GO:2000266 GO:2000257 GO:0030193	 regulation of blood coagulation, intrinsic pathway regulation of protein activation cascade regulation of blood coagulation	Down
FAHD1 [81889] Fumarylaceto- acetate hydrolase domain containing 1	 N/A	 N/A	Down

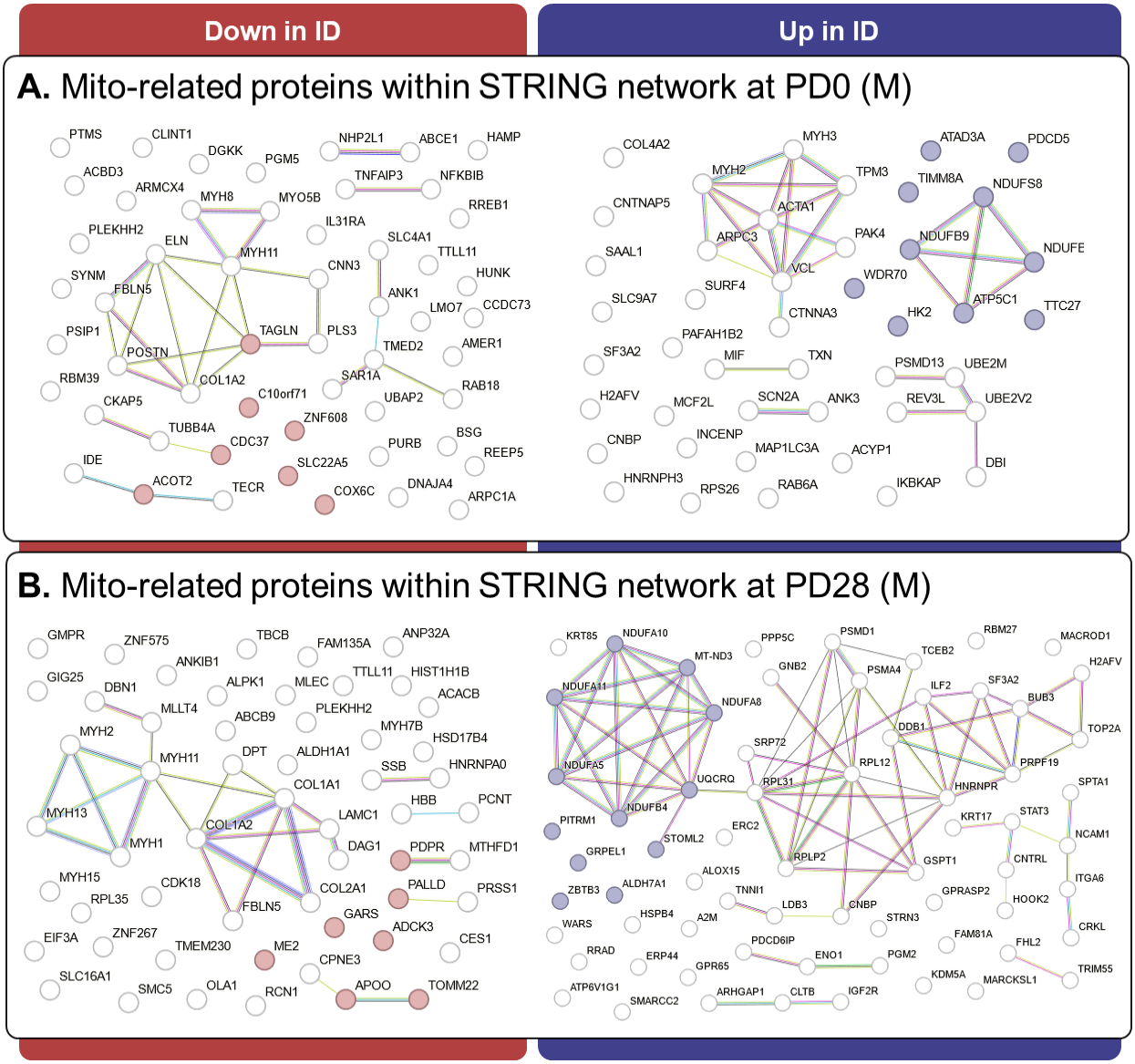

Figure 3.3.2: Protein networks created in STRING v11.5 (string-db.org) show interactions between individual proteins down- or up-regulated by iron deficiency (ID) in male (M) offspring hearts at postnatal days (PD) 0 (upper panel, A) and 28 (lower panel, B). Circles (known as nodes) represent individual proteins; colored nodes (red for downregulated, blue for upregulated) indicate mitochondria-related proteins as identified through Metascape. Connecting lines (known as edges) represent protein-protein interactions and are colored based on interaction evidence: known interactions from curated databases (turquoise), known interactions experimentally determined (fuschia), predicted interactions by gene neighbourhood (green), predicted interactions by gene fusions (red), predicted interactions by gene co-occurrence blue), textmining (yellow), co-expression (black), and protein homology (purple).

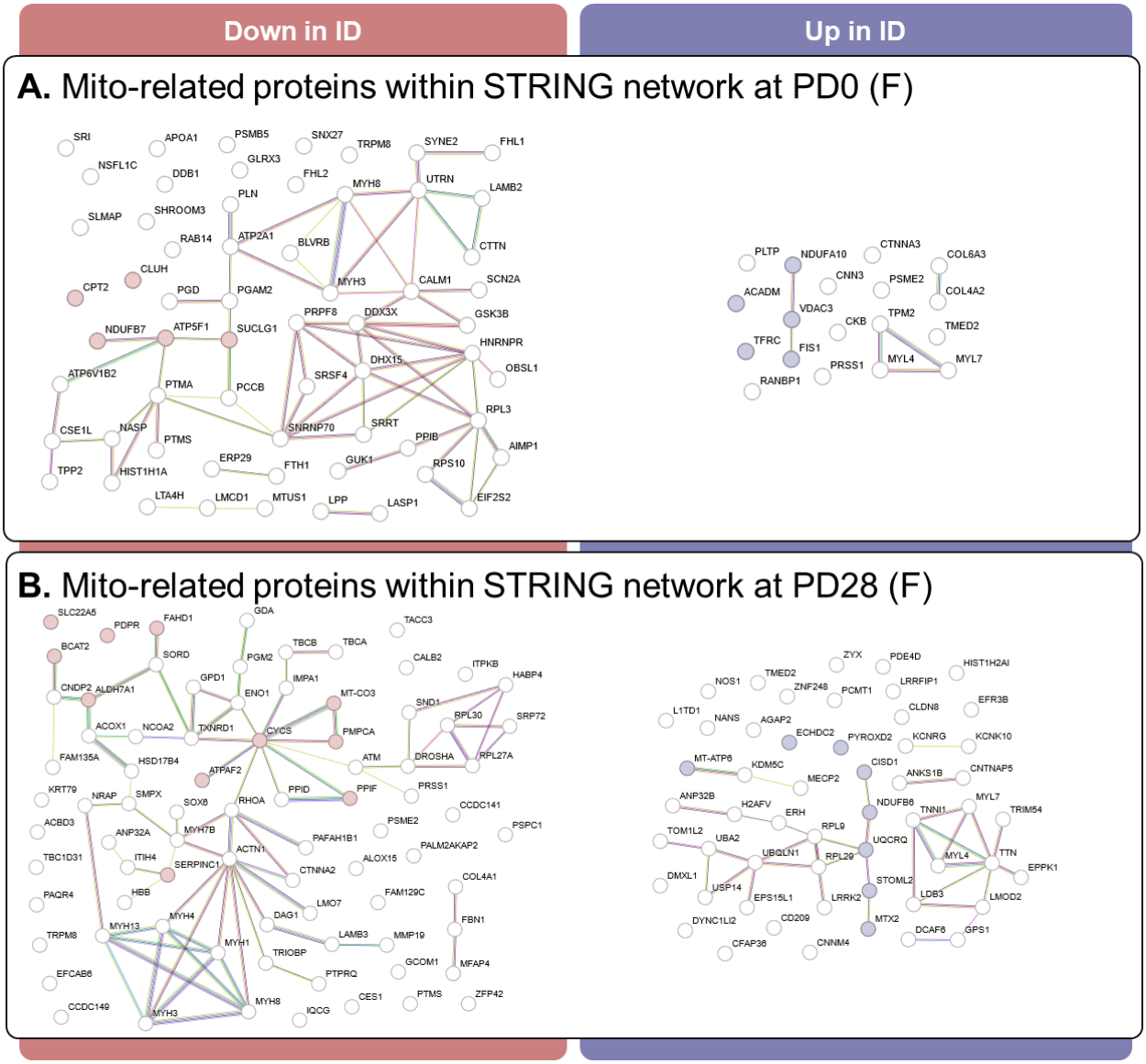

Figure 3.3.3: Protein networks created in STRING v11.5 (string-db.org) show interactions between individual proteins down- or up-regulated by iron deficiency (ID) in female (F) offspring hearts at postnatal days (PD) 0 (upper panel, A) and 28 (lower panel, B). Circles (known as nodes) represent individual proteins; colored nodes (red for downregulated, blue for upregulated) indicate mitochondria-related proteins as identified through Metascape. Connecting lines (known as edges) represent protein-protein interactions and are colored based on interaction evidence: known interactions from curated databases (turquoise), known interactions experimentally determined (fuschia), predicted interactions by gene neighbourhood (green), predicted interactions by gene fusions (red), predicted interactions by gene co-occurrence blue), textmining (yellow), co-expression (black), and protein homology (purple).

Metascape also identified significantly enriched pathways amongst down- and upregulated proteins; the results are summarized in Figure 3.3.4. We noted that the enriched terms could be largely categorized into two groups: (1) biological processes involved in tissue structure and function (e.g., supramolecular fiber organization, extracellular matrix assembly, muscle contraction, adherens junction, etc.), and (2) various intracellular functions. The pathways in the latter category mirror the biological processes identified amongst the mitochondria-related proteins, that is, energy metabolism, nutrient metabolism, organelle organization, and protein processing, including RNA processing and metabolism. Though some pathways are enriched in multiple groups, they present differently. For example, ATP metabolic process is enriched amongst upregulated proteins in males, while it is enriched amongst downregulated proteins in females. Different nutrient pathways are affected between males and females. A list of all proteins associated with a given term in Figure 3.3.4 are listed in Tables 3.3.5-3.3.8.

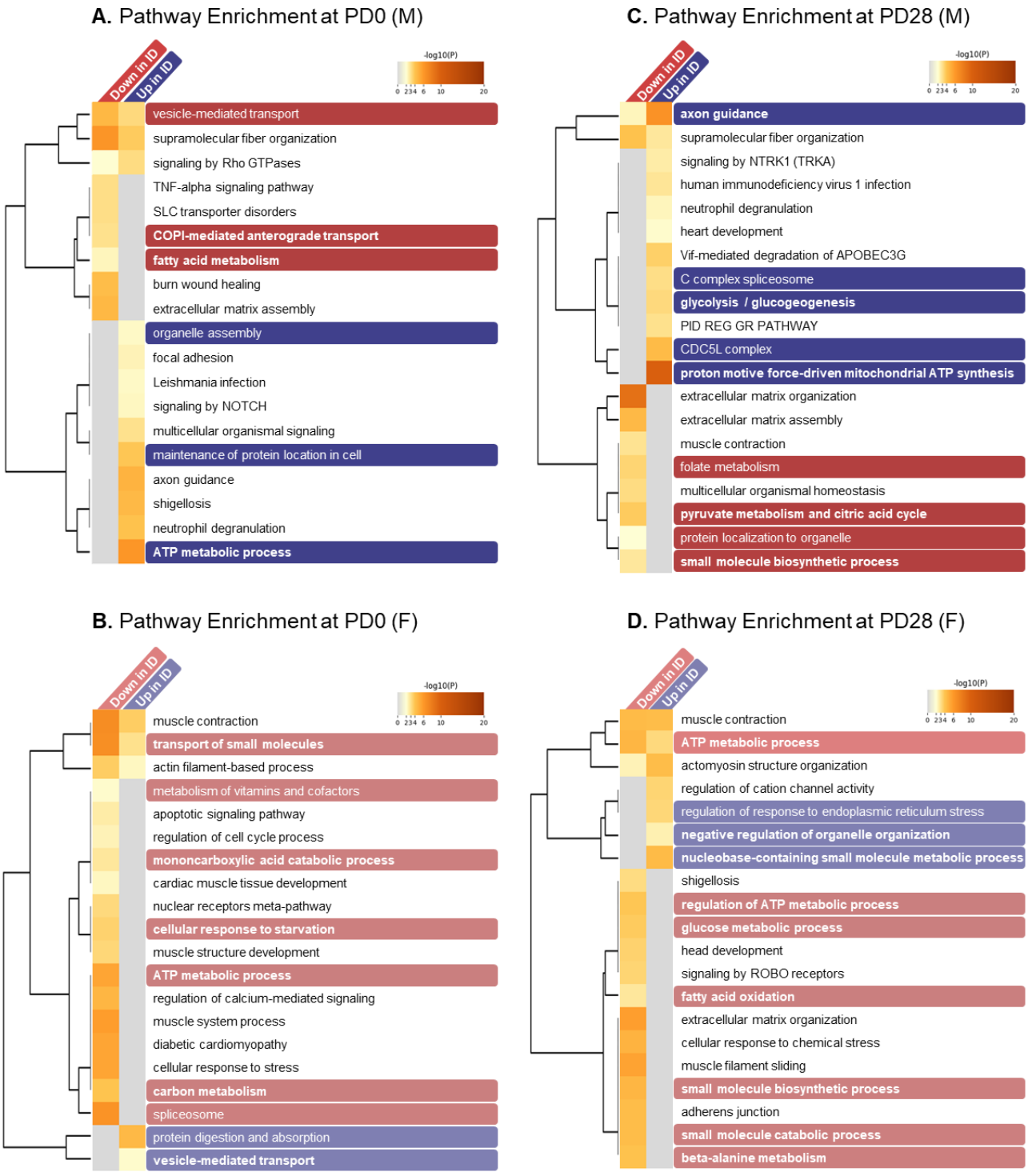

Figure 3.3.4: Pathway enrichment analysis in in male (M; upper panels, A and C) and female (F; lower panels, B and D) offspring hearts at postnatal days (PD) 0 (left panels, A and B) and 28 (right panels, C and D). In Metascape, statistically enriched terms are first identified from input gene lists then clustered based on similarities among their gene memberships; the term with the

best p-value within each cluster becomes the representative (i.e., summary) term for that set of pathways and is displayed in a dendrogram. Heatmap cells indicate term enrichment in that gene list and its associated p value, while grey cells indicate a lack of enrichment. Color-coded pathway labels highlight enriched pathways pertaining to select intracellular functions (e.g., energy metabolism, nutrient metabolism, organelle and protein organization, protein processing, and RNA metabolism) and bolded pathway titles signal the presence mitochondria-related proteins (Tables 3.3.1-3.3.4) amongst membership proteins. Complete lists of proteins responsible for the enrichment of the color-coded representative terms are available in Tables 3.3.5-3.3.8.

Table 3.3.5. Select enriched pathways in PD 0 male hearts.

Representative Summary Pathway [Term]	Change in ID vs. CTL	Cluster Membership Proteins **bolded proteins are mitochondria-related**
Vesicle-mediated transport	Up	ANK3, COL4A2, PAFAH1B2, RAB6A, SURF4, ARPC3
[R-HSA-5653656]	Down	ANK1, COL1A2, CLINT1, TUBB4A, ARPC1A, TMED2, RAB18, ACBD3, REEP5
COPI-mediated anterograde transport	Up	ANK3, **TIMM8A**
[R-HSA-6807878]	Down	ANK1, TUBB4A, TMED2, BSG, SLC4A1, SAR1A
fatty acid metabolism	Up	DBI
[R-HSA-8978868]	Down	**SLC22A5**, TECR, **ACOT2**
organelle assembly	Up	ACTA1, INCENP, MYH3, CEP126, MAP1LC3A
[GO:0070925]	Down	-
maintenance of protein location in cell	Up	ANK3, HK2, TXN, ACTA1, MAP1LC3A, PDCD5
[GO:0032507]	Down	NFKBIB, BSG, TNFAIP3, HAMP
ATP metabolic process	Up	**ATP5F1C**, **HK2**, MYH3, **NDUFB7, NDUFB9, NDUFS8**, PSMD13, TXN, **TIMM8A**, ATAD3A, MAP1LC3A,
[GO:0046034]		COL4A2, REV3L
	Down	**COX6C**, MYH8, BSG, TUBB4A, IDE, COL1A2, TECR, **ACOT2**

Table 3.3.6. Select enriched pathways in PD 28 male hearts.

Representative Summary Pathway [Term]	Change in ID vs. CTL	Cluster Membership Proteins **bolded proteins are mitochondria-related**
axon guidance [R-HSA-422475]	Up	CLTB, GSPT1, NCAM1, PSMA4, PSMD1, RPL12, RPL31, RPLP2, SPTA1, ELOB, RPL35, SRP72, WARS1, SF3A2, HNRNPR, PRPF19, STAT3, ATP6V1G1, H2AZ2, ILF2, **ALDH7A1**
	Down	COL2A1, DAG1, LAMC1, MYH11, **GARS1**, EIF3A, ACACB, ABCB9, HSD17B4
C complex spliceosome [CORUM:1181]	Up	SF3A2, HNRNPR, PRPF19, GSPT1, STAT3, RBM27
	Down	HNRNPA0
glycolysis/gluconeogenesis [hsa00010]	Up	**ALDH7A1**, ENO1, PGM2, STAT3, ELOB
	Down	ACACB
CDC5L complex [CORUM:1183]	Up	ILF2, TOP2A, PRPF19
	Down	-
proton motive force-driven mitochondrial ATP synthesis [GO:0042776]	Up	**ND3**, **NDUFA5**, **NDUFA8**, **NDUFA10**, **NDUFB4**, **STOML2**, **NDUFA11**, **UQCRQ**, NCAM1, PSMA4, PSMD1, ATP6V1G1, ENO1, MACROD1, PGM2, CLTB, GNB2, SMARCC2, PPP5C, STAT3, ELOB, PITRM1, GRPEL1, ALOX15
	Down	ACACB, GMPR, HSD17B4, MTHFD1, SLC16A1, GARS1, COL1A1, COL1A2, **ME2**, **PDPR**
folate metabolism [WP176]	Up	-
	Down	SERPINA3, HBB, MTHFD1, ACACB, PRSS1
pyruvate metabolism and citric acid (TCA) cycle [R-HSA-71406]	Up	SLC16A1
	Down	**ME2**, **PDPR**
protein localization to organelle [GO:0033365]	Up	-
	Down	SERPINA3, ACACB, ALDH1A1, COL2A1, LAMC1
small molecule biosynthetic process [GO:0044283]	Up	-
	Down	ACACB, ALDH1A1, CES1, MTHFD1, **COQ8A**, HSD17B4, **ME2**, HBB

Table 3.3.7. Select enriched pathways in PD 0 female hearts.

Representative Summary Description [Term]	Change in ID vs. CTL	Cluster Membership Proteins **bolded proteins are mitochondria-related**
transport of small molecules	Up	PLTP, PSME2, **TFRC**, **VDAC3**, CKB, FIS1
[R-HSA-382551]	Down	APOA1, ATP2A1, ATP6V1B2, CALM1, FTH1, PLN, PSMB5, SRI, EIF2S2, GLRX3, TRPM8, SCN2A
metabolism of vitamins and cofactors	Up	PRSS1
[R-HSA-196854]	Down	APOA1, CALM1, PCCB, GSK3B, UTRN
monocarboxylic acid catabolic process	Up	**ACADM**
[GO:0072329]	Down	**CPT2**, PCCB, PGD, APOA1, FHL2, LTA4H, RAB14
cellular response to starvation	Up	**ACADM**
[R-HSA-9711097]	Down	ATP6V1B2, RPL3, RPS10, EIF2S2, DDX3X, LTA4H, AIMP1, **SUCLG1**, APOA1, PRPF8
ATP metabolic process	Up	**NDUFA10**, **ACADM**
[GO:0046034]	Down	**ATP5PB**, ATP6V1B2, MYH3, MYH8, **NDUFB7**, PGAM2, GSK3B, PGD, **SUCLG1**, GUK1
carbon metabolism	Up	-
[hsa01200]	Down	PCCB, PGAM2, PGD, **SUCLG1**
spliceosome	Up	-
[CORUM:351]	Down	DDX3X, DHX15, SRSF4, SNRNP70, PRPF8, SRRT, HNRNPR, PSMB5, RPL3, RPS10
protein digestion and absorption	Up	COL4A2, COL6A3, PRSS1, MYL7
[hsa04974]	Down	GSK3B, LAMB2
vesicle-mediated transport	Up	COL4A2, **TFRC**, TMED2
[R-HSA-5653656]	Down	APOA1, CALM1, CTTN, FTH1, RAB14, AIMP1

Table 3.3.8. Select enriched pathways in PD 28 female hearts.

Summary Pathway [Term]	Change in ID vs. CTL	Cluster Membership Proteins **bolded proteins are mitochondria-related**
ATP metabolic process [GO:0046034]	Up	**ATP6**, **NDUFB6**, **UQCRQ**, **STOML2**, LRRK2, NOS1, UBQLN1
	Down	ENO1, **COX3**, MYH3, MYH4, MYH8, **CYCS**, **PDPR**, **FAHD1**, GPD1, ACOX1, **PPIF**, PPID
regulation of response to endoplasmic reticulum stress [GO:1905897]	Up	USP14, UBQLN1, LRRK2, MECP2, NOS1, GPS1, UBA2, TMED2, AGAP2
	Down	-
negative regulation of organelle organization [GO:0010639]	Up	TRIM54, LRRK2, TOM1L2, LMOD2
	Down	ATM, CTNNA2, **PPIF**, TRIOBP
nucleobase-containing small molecule metabolic process [GO:0055086]	Up	**ATP6**, **NDUFB6**, PDE4D, **STOML2**, NANS, LRRK2, MYL4, NOS1, TNNI1
	Down	RHOA, ENO1, ERH, HSD17B4, GDA, PGM2, DAG1, MECP2, **SLC22A5**, ATM, PAFAH1B1, **PPIF**
regulation of ATP metabolic process [GO:1903578]	Up	**CISD1**, NOS1
	Down	RHOA, ENO1, GPD1, **PPIF**, CES1
glucose metabolic process [GO:0006006]	Up	PDE4D, NANS, MECP2
	Down	ENO1, GPD1, SORD, PGM2, IMPA1, GDA, **ALDH7A1**
fatty acid oxidation [GO:0019395]	Up	**ECHDC2**
	Down	ACOX1, ALOX15, HSD17B4, **SLC22A5**, GPD1, TXNRD1, NCOA2, RHOA, SND1
small molecule biosynthetic process [GO:0044283]	Up	MECP2, EFR3B, TTN
	Down	ALOX15, **BCAT2**, CES1, GPD1, IMPA1, ITPKB, SORD, PGM2, ATM, PAFAH1B1, **PPIF**, ACBD3
small molecule catabolic process [GO:0044282]	Up	NOS1, ECHDC2
	Down	ACOX1, **BCAT2**, ENO1, HSD17B4, IMPA1, SORD, GDA
beta-alanine metabolism [hsa00410]	Up	-
	Down	ACOX1, **ALDH7A1**, CNDP2, TXNRD1, NCOA2

Finally, given the model of perinatal ID, we verified the lists of altered proteins and enriched pathways for evidence of changes in cellular iron handling. In PD 0 male hearts, only hepcidin (HAMP) was downregulated. Further, only PD 0 female hearts showed enrichment of iron handling pathways. Notably, transferrin receptor 1 was upregulated in these hearts while ferritin heavy chain was downregulated. A complete list of enriched iron handling pathways and the associated proteins is in Table 3.3.9.

Since we observed changes in mitochondrial proteins and pathways, we then studied mitochondrial function to see if these proteome changes would have functional consequences for cardiac mitochondria.

Table 3.3.9. Cellular iron processing pathways enriched in PD 0 female hearts.

Pathway Description [Term]	Change in ID vs. CTL	Membership Proteins
iron uptake and transport	Up	TFRC,
[R-HSA-917937]	Down	ATP6V1B2, FTH1, GLRX3
cellular iron ion homeostasis	Up	TFRC
[GO:0006879]	Down	FTH1, SRI, GLRX3
iron ion homeostasis	Up	TFRC
[GO:0055072]	Down	FTH1, SRI, GLRX3

3.4 Mitochondrial Function in Neonatal Hearts

Citrate synthase (CS) activity, a marker of mitochondrial content (Larsen et al., 2012), increased with age in hearts of male ($P_{PD} < 0.0001$; Fig. 3.4.1A) and female ($P_{PD} < 0.0001$; Fig. 3.4.1B) offspring. Only male ($P_{ID} = 0.004$; Fig. 3.4.1A), but not female ($P_{ID} = 0.13$; Fig. 3.4.1B), ID offspring had an overall increase in cardiac mitochondrial content. When normalized for CS activity (i.e., mitochondrial content; Fig. 3.4.1), mitochondrial respiration (i.e., oxygen [O_2] flux in pmol/s·IU; Fig. 3.4.2) through the NADH-pathway (electron entrance through complex I; Fig. 3.4.2A, B), the succinate-pathway (electron entrance through complex II; Fig. 3.4.2C, D), and the FAO pathway (electron entrance through complex I and electron transferring flavoprotein (ETF); Fig. 3.4.2E, F) was reduced in ID pups compared to the CTLs, but only in males ($P_{ID} = 0.03$, $P_{ID} = 0.02$, and $P_{ID} = 0.03$, respectively) and not in females ($P_{ID} = 0.12$, $P_{ID} = 0.15$, and $P_{ID} = 0.31$, respectively). Complex IV activity was not affected by ID in either sex (Fig. 3.4.3; $P_{ID} = 0.18$ for males and $P_{ID} = 0.58$ for females). Further, male offspring hearts, but not female hearts, displayed an age-dependent decrease in mitochondrial respiration through the NADH-pathway ($P_{PD} = 0.009$ for males; Fig. 3.4.2A), S-pathway ($P_{PD} = 0.01$ for males; Fig. 3.4.2C), and complex IV ($P_{PD} = 0.005$ for males; Fig. 3.4.3A). In contrast, age did not affect FAO pathway respiration in either sex ($p=0.20$ for males and $p=0.56$ for females; Fig. 3.4.2E, F), though we observed a significant interaction between ID and age in female hearts ($P_{int} = 0.04$; Fig. 3.4.2F).

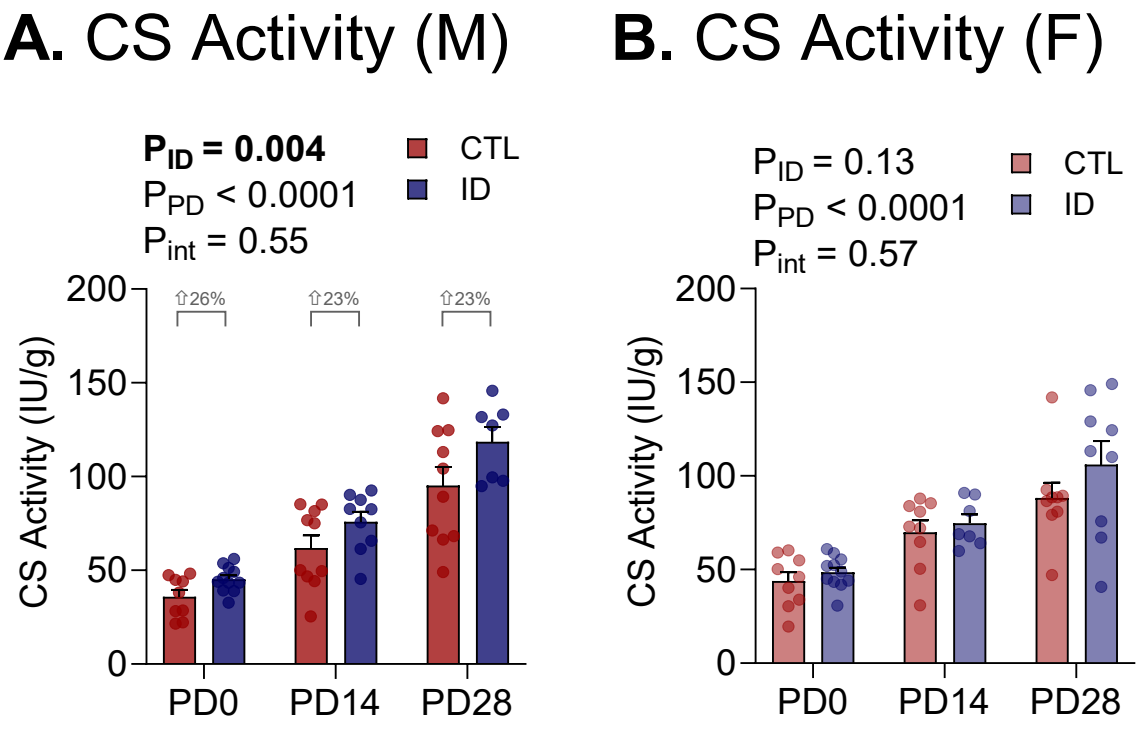

Figure 3.4.1: Citrate synthase (CS) activity in permeabilized cardiac fibers from control (CTL) and iron-deficient (ID) (A) male (M, left) and (B) female (F, right) offspring hearts at postnatal days (PD) 0, 14, and 28.

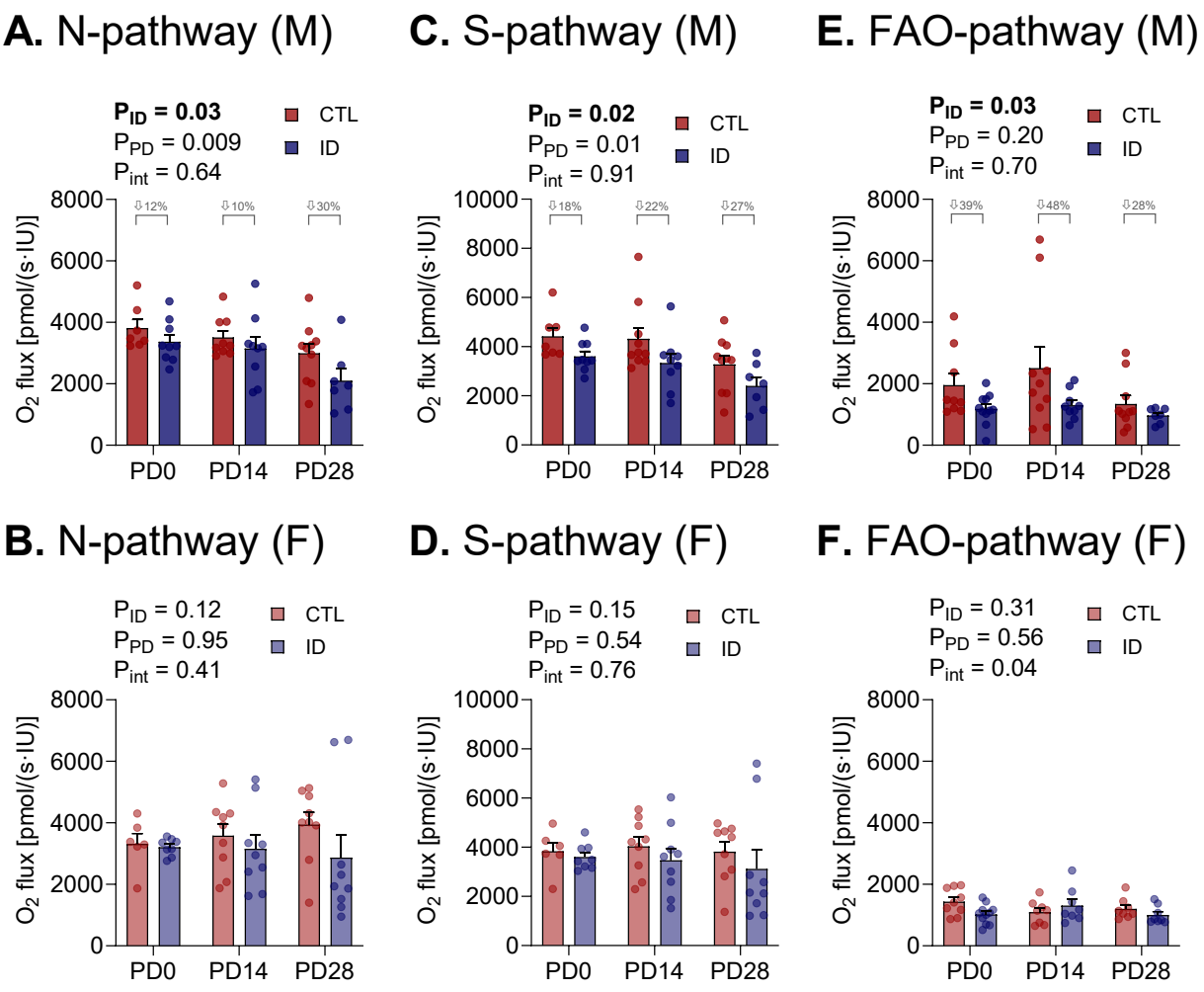

Figure 3.4.2: Mitochondrial respiration of permeabilized cardiac fibers from control (CTL) and iron-deficient (ID) male (M, top row) and female (F, bottom row) offspring hearts at postnatal days (PD) 0, 14, and 28, normalized to citrate synthase activity [pmol/(s·IU)]. From left to right, columns represent oxidative phosphorylation (OXPHOS) through the (A, B) NADH (N), (C, D) succinate (S), and (E, F) fatty acid oxidation (FAO) pathways.

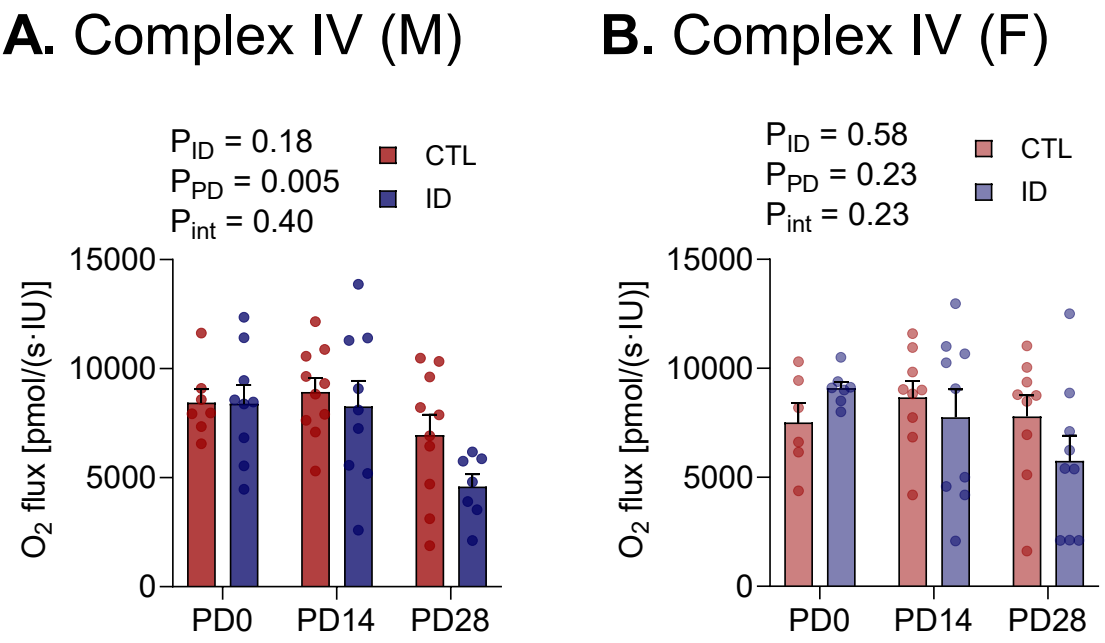

Figure 3.4.3: Complex IV activity of permeabilized cardiac fibers from control (CTL) and iron-deficient (ID) (A) male (M, left) and (B) female (F, right) offspring hearts at postnatal days (PD) 0, 14, and 28.

When mitochondrial respiration was normalized for tissue mass (i.e., oxygen [O_2] flux in pmol/s·mg; Fig. 3.4.4), we observed an age-dependent increase in the NADH-pathway ($P_{PD} < 0.0001$ for males and $P_{PD} < 0.0001$ for females; Fig. 3.4.4A, B), the S-pathway ($P_{PD} < 0.0001$ for males and $P_{PD} = 0.005$ for females; Fig. 3.4.4C, D), and the FAO-pathway ($P_{PD} < 0.0001$ for males and $P_{PD} < 0.0001$ for females; Fig. 3.4.4E, F). Complex IV activity, however, increased with age in male offspring hearts ($P_{PD} = 0.002$ for males; Fig. 3.4.4G), but was unaffected by age in female hearts ($P_{PD} = 0.17$ for females; Fig. 3.4.4H). ID did not affect mitochondrial respiration per tissue mass in either sex (Fig. 3.4.4).

When mitochondrial respiration was normalized to the maximum oxygen flux within the SUIT protocol and expressed as flux control ratios (FCR), we observed no age-dependent alterations in male offspring hearts in any of the studied pathways (Fig. 3.4.5A, C, E, G). Female hearts, however, showed an age-dependent increase in FCRs for the NADH-pathway ($P_{PD} = 0.03$; Fig. 3.4.5B) and the FAO-pathway ($P_{PD} = 0.009$; Fig. 3.4.5F). ID did not affect FCRs in either sex (Fig. 3.4.5).

Given the reductions in mitochondrial respiration expressed per unit of CS activity in the male hearts, we used transmission electron microscopy to assess qualitative changes in mitochondrial morphology in these hearts (Fig. 3.4.6). After consultation from Dr. Hisashi Fujioka at Case Western Reserve University, we concluded that mitochondrial size increased from PD 0 to PD 14, but the number of degraded or degrading mitochondria was increased. Perinatal ID was associated with gross morphological changes in mitochondria, most notably at PD 0, characterized by fewer cristae and more heterogeneity in size and shape.

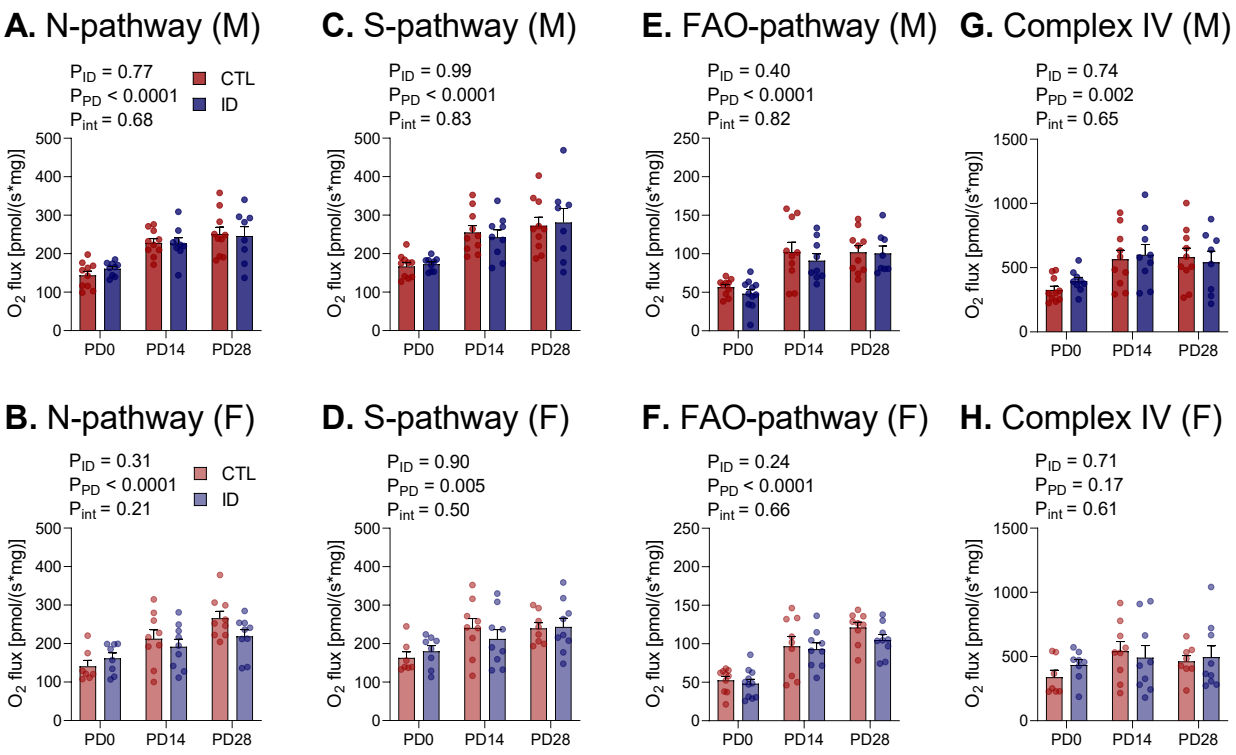

Figure 3.4.4: Mitochondrial respiration of permeabilized cardiac fibers from control (CTL) and iron-deficient (ID) male (M, top row) and female (F, bottom row) offspring at postnatal days (PD) 0, 14, and 28, expressed as oxygen flux normalized to tissue mass (pmol/s·mg). From left to right, columns represent oxidative phosphorylation (OXPHOS) through the (A, B) NADH (N), (C, D) succinate (S), and (E, F) fatty acid oxidation (FAO) pathways, and (G, H) Complex IV activity.

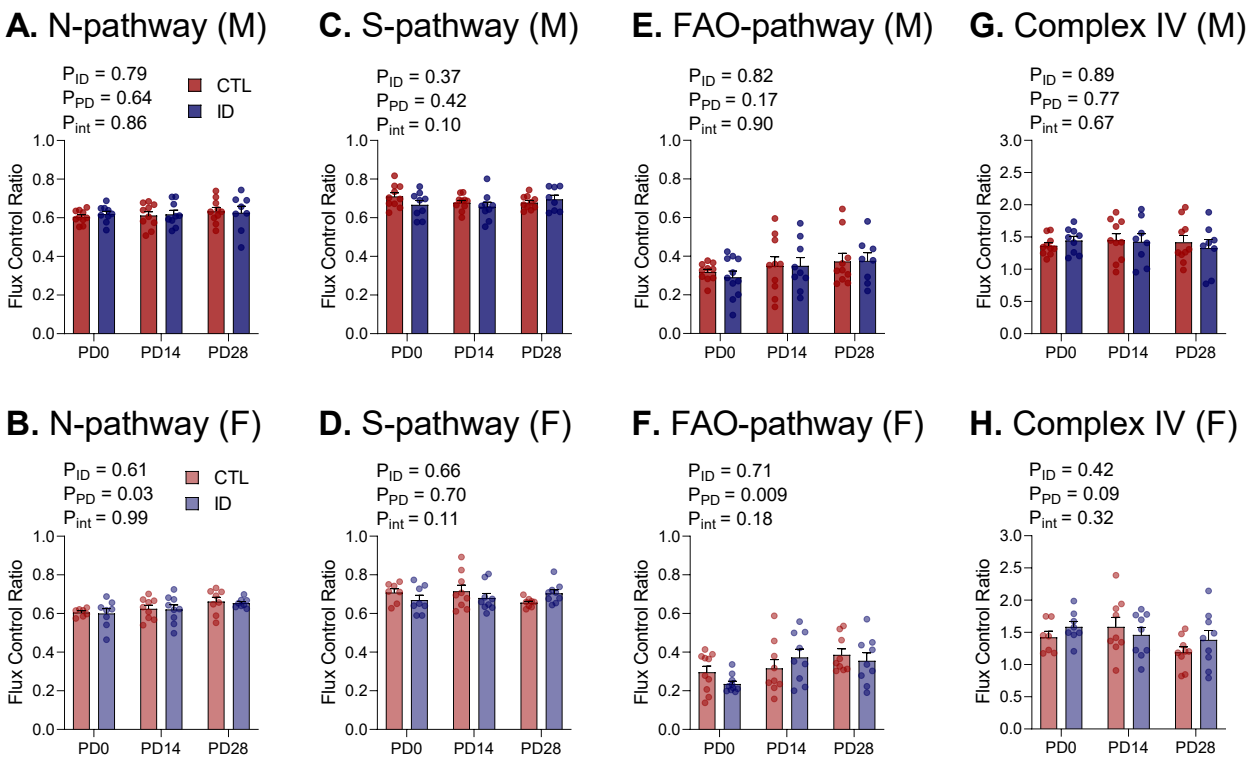

Figure 3.4.5: Mitochondrial respiration of permeabilized cardiac fibers from control (CTL) and iron-deficient (ID) male (M, top row) and female (F, bottom row) offspring at postnatal days (PD) 0, 14, and 28, expressed as flux control ratios. From left to right, columns represent oxidative phosphorylation (OXPHOS) through the (A, B) NADH (N), (C, D) succinate (S), and (E, F) fatty acid oxidation (FAO) pathways, and (G, H) Complex IV activity.

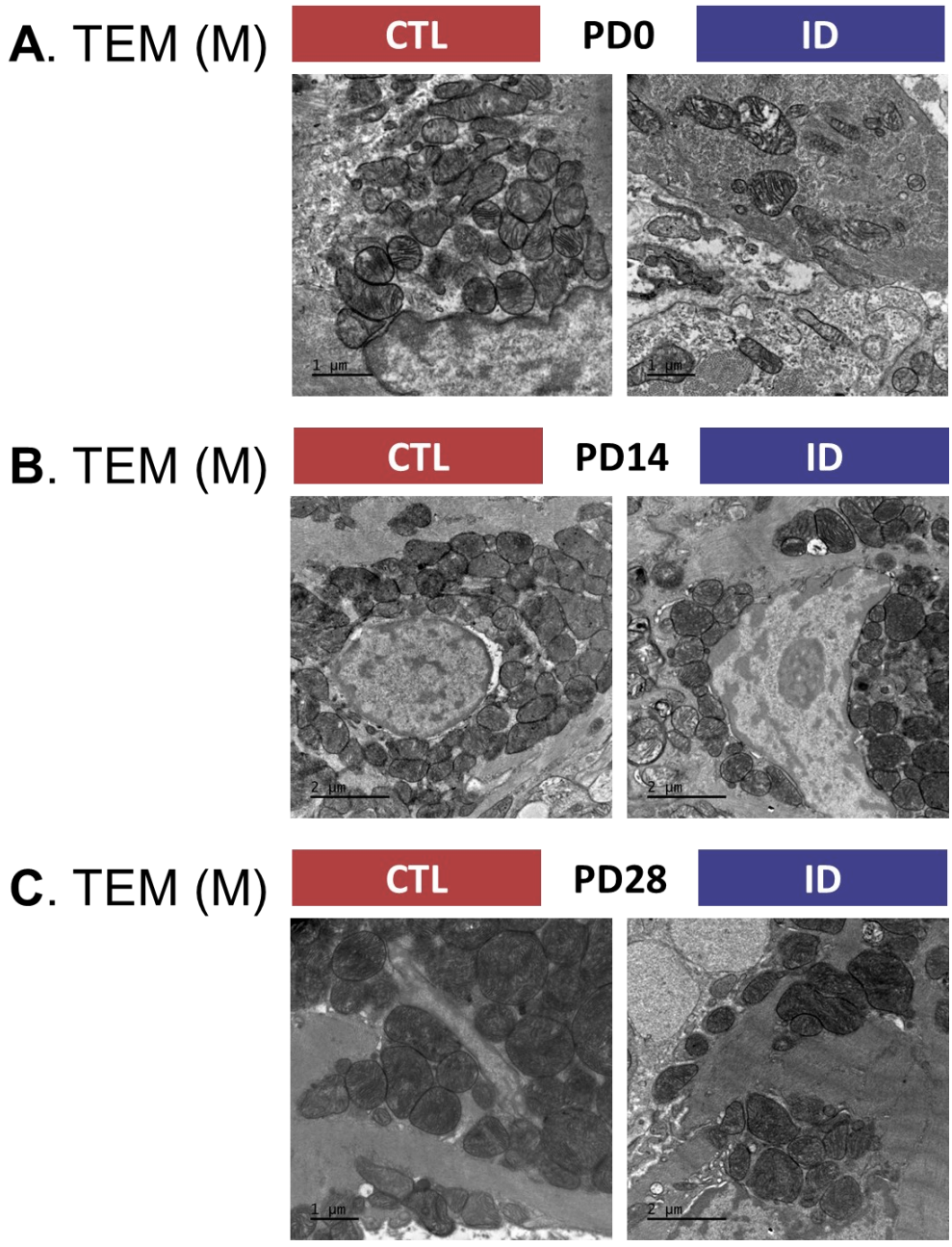

Figure 3.4.6: Transmission electron microscopy (TEM) of control (CTL) and iron-deficient (ID) male (M) offspring hearts at (A) 0, (B) 14, and (C) 28 postnatal days (PD).

3.5 Superoxide Content and mRNA Expression of Antioxidant Enzymes in Neonatal Hearts

We examined perinatal offspring hearts for evidence of excess ROS or a downstream response to ROS production, by assessing DHE fluorescence (Fig. 3.5.1A, B), and gene expression profiles of antioxidant enzymes catalase (Fig. 3.5.2A, B), SOD1 (Fig. 3.5.2C, D) and SOD2 (Fig. 3.5.2E, F). DHE fluorescence was unaffected by age in male offspring hearts ($P_{PD} = 0.17$; Fig. 3.5.1A), but changed with age in female offspring hearts ($P_{PD} = 0.0014$; Fig. 3.5.1B). Both catalase and SOD2 gene expression increased with age in males ($P_{PD} < 0.001$ for catalase and $P_{PD} < 0.001$ for SOD2; Fig. 3.5.2A, E) and females ($P_{PD} = 0.03$ for catalase and $P_{PD} < 0.001$ for SOD2; Fig. 3.5.2B, F), while SOD1 mRNA expression was unaffected by age in either sex ($P_{PD} = 0.57$ for males and $P_{PD} = 0.24$ for females; Fig. 3.5.2C, D). No effect of ID was evident in either DHE staining (Fig. 3.5.1) or gene expression profiles of antioxidant enzymes (Fig. 3.5.2) assessed in male or female offspring hearts.

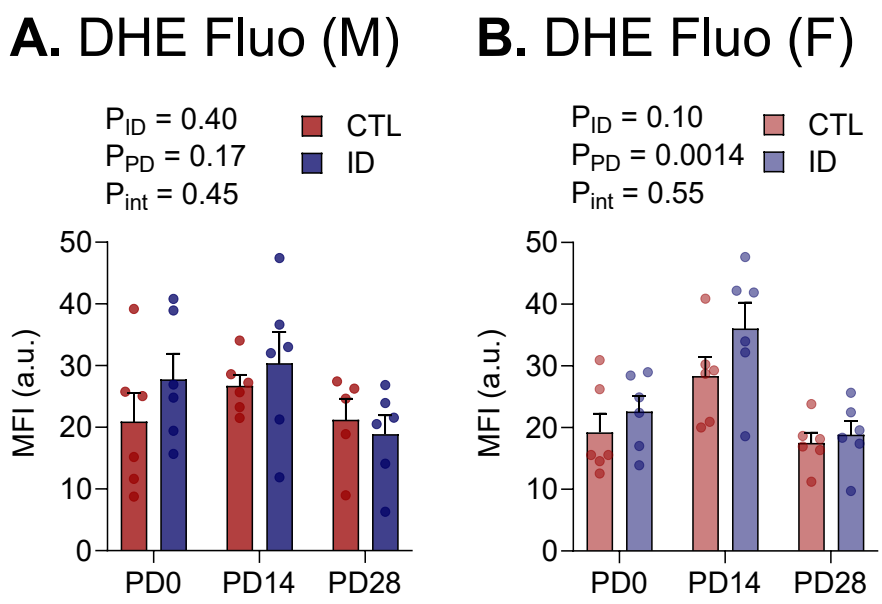

Figure 3.5.1: Superoxide content in control (CTL) versus iron-deficient (ID) (A) male (M, left) and (B) female (F, right) offspring hearts at postnatal days (PD) 0, 14, and 28. Dihydroethidium (DHE) fluorescence for superoxide content expressed as mean fluorescence intensity (arbitrary units, a.u.). Bars show mean±SEM with individual data points (n=7-9). *P<0.05, **P<0.01, ***P<0.001, ****P<0.0001 for multiple comparisons.

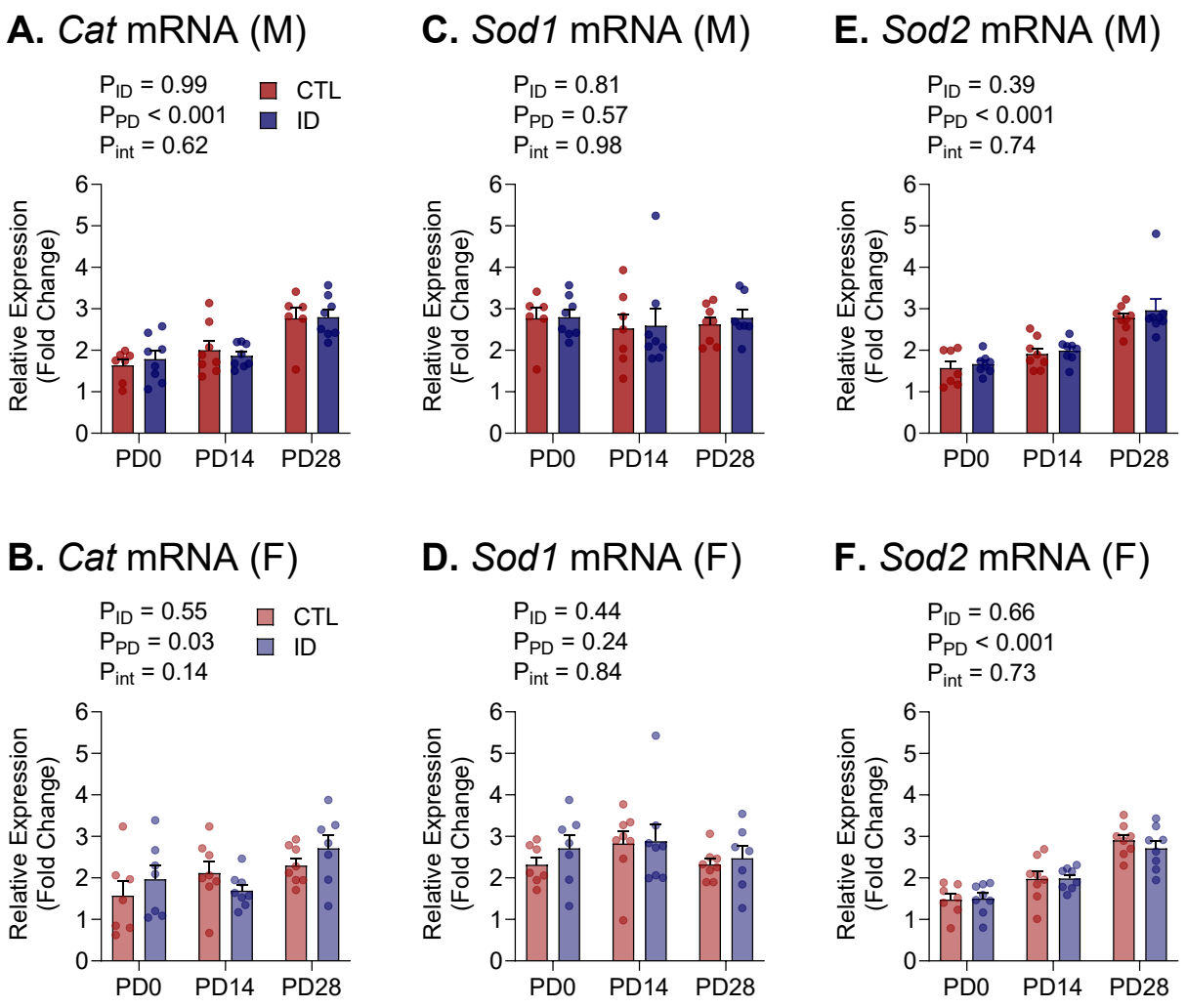

Figure 3.5.2: mRNA expression of antioxidant enzymes in control (CTL) versus iron-deficient (ID) male (M, top row) and female (F, bottom row) offspring hearts at postnatal days (PD) 0, 14, and 28. (A, B) catalase (*Cat*), (C, D) superoxide dismutase 1 (*Sod1*), (E, F) superoxide dismutase 2 (*Sod2*). Bars show mean±SEM with individual data points (n=7-9). *P<0.05, **P<0.01, ***P<0.001, ****P<0.0001 for multiple comparisons.

3.6 mRNA Expression of Iron Metabolism Genes in Neonatal Hearts

We examined gene expression profiles of proteins involved in cellular iron homeostasis in male (Fig. 3.6.1) and female (Fig. 3.6.2) offspring hearts. We observed an age-dependent effect expression of all genes studied in both males and females, excluding *Dmt1* in males ($P_{PD} = 0.10$; Fig. 3.6.1A). The mRNA of iron storage proteins, *Fth* and *Ftl*, decreased with age, while mRNA of proteins involved in iron export from the cell, *Hamp* and *Fpn1*, increased with age (Figs. 3.6.1 and 3.6.2). ID did not change expression of iron metabolism genes in male offspring hearts (Fig. 3.6.1), however, ID female offspring hearts showed increased gene expression of *Tfrc* (Fig. 3.6.2B), most prominently at PD 0.

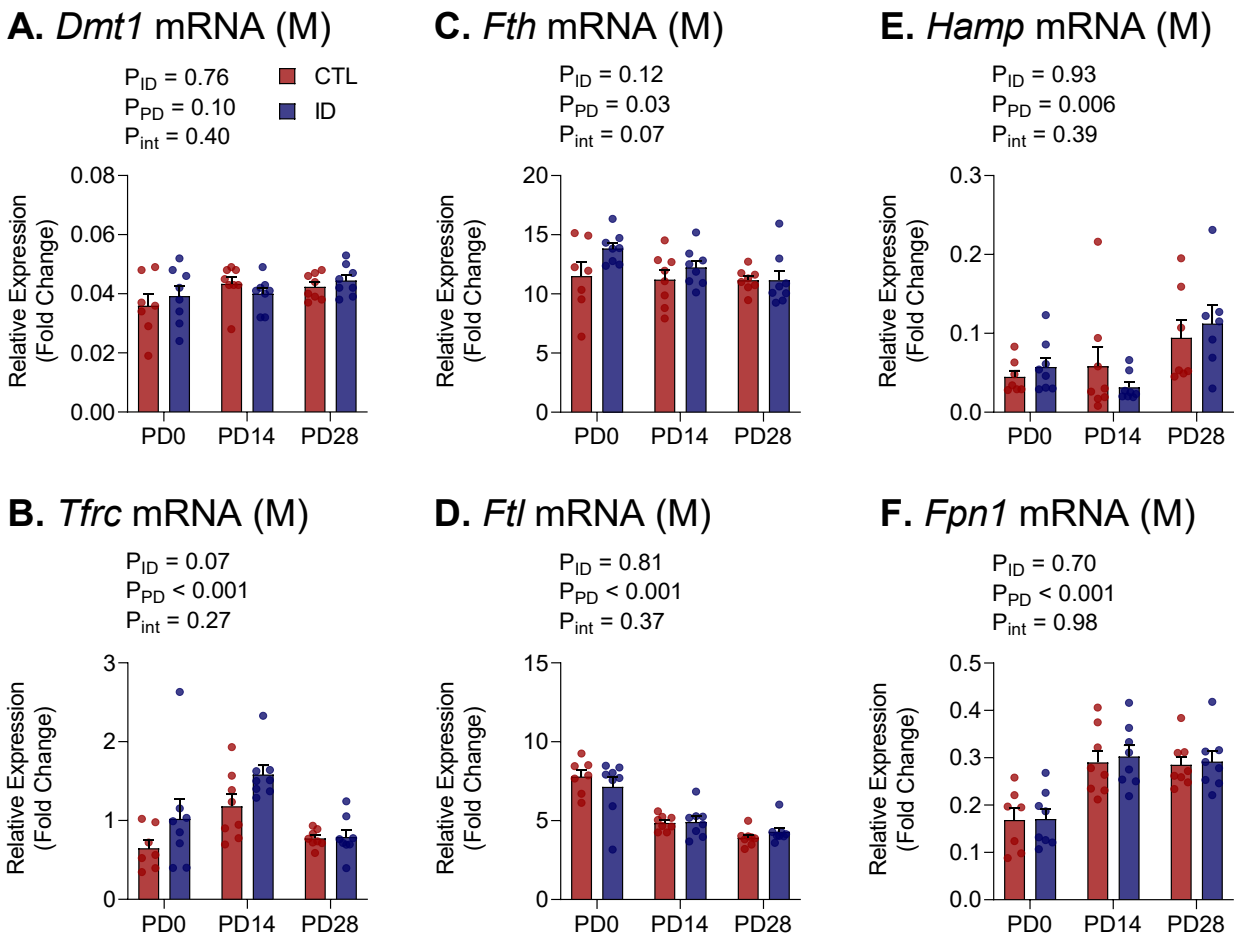

Figure 3.6.1: mRNA expression of cellular iron metabolism proteins in control (CTL) versus iron-deficient (ID) male (M) offspring hearts at postnatal days (PD) 0, 14, and 28. (A) divalent metal transporter 1 (*Dmt1*), (B) transferrin receptor 1 (*Tfrc*), (C) ferritin heavy chain (*Fth*), (D) ferritin light chain (*Ftl*), (E) hepcidin antimicrobial peptide (*Hamp*), (F) ferroportin 1 (*Fpn1*). Bars show mean±SEM with individual data points (n=7-9). *P<0.05, **P<0.01, ***P<0.001, ****P<0.0001 for multiple comparisons.

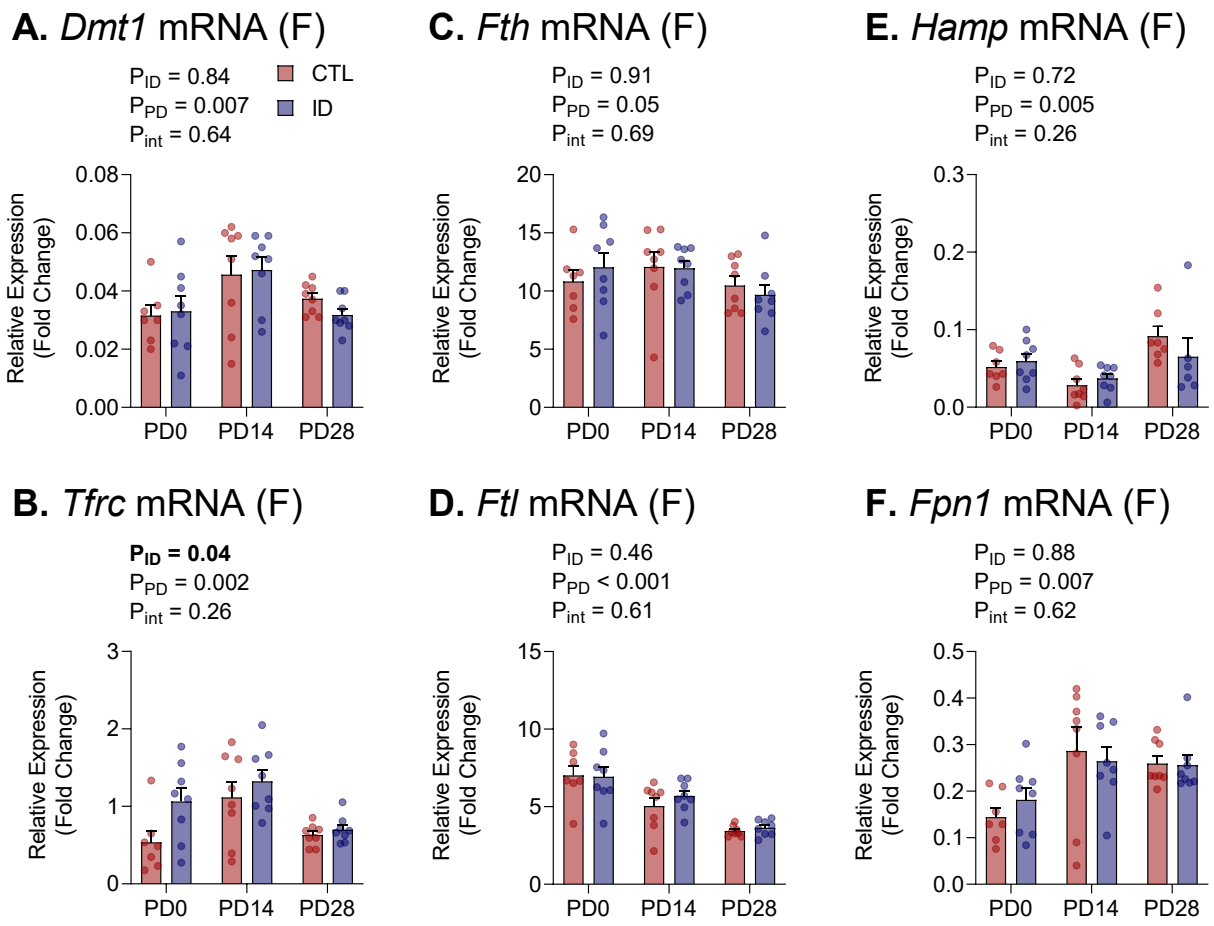

Figure 3.6.2: mRNA expression of cellular iron metabolism proteins in control (CTL) versus iron-deficient (ID) female (F) offspring hearts at postnatal days (PD) 0, 14, and 28. (A) divalent metal transporter 1 (*Dmt1*), (B) transferrin receptor 1 (*Tfrc*), (C) ferritin heavy chain (*Fth*), (D) ferritin light chain (*Ftl*), (E) hepcidin antimicrobial peptide (*Hamp*), (F) ferroportin 1 (*Fpn1*). Bars show mean±SEM with individual data points (n=7-9). *P<0.05, **P<0.01, ***P<0.001, ****P<0.0001 for multiple comparisons.

Chapter 4

Discussion

4.1 Summary of Findings

Developing offspring are particularly vulnerable to ID through the perinatal period, a time at which the developing heart is undergoing substantial metabolic transition to accommodate extrauterine life. Given that OXPHOS proteins incorporate numerous iron prosthetic groups, this shift to primarily mitochondrial energy metabolism in the postnatal heart may be particularly vulnerable to ID. As such, we investigated the effects of maternal iron restriction on neonatal cardiac mitochondria. To summarize, we found that perinatal ID caused (1) anemia and growth restriction with concomitant cardiomegaly in both male and female offspring, (2) age- and sex-specific alterations to the neonatal cardiac proteome that persisted beyond the recovery of anemia and involved various mitochondria-related proteins, (3) changes in mitochondrial function suggestive of altered mitochondrial composition resulting in reduced mitochondrial efficiency, in males but not females offspring, and (4) sex-specific differences in cellular iron metabolism in offspring hearts. Together, these data suggest that perinatal ID is associated with sex-specific cellular responses in the heart, particularly relating to the mitochondria, despite males and females undergoing a similar insult.

4.2 Male and Female Neonates Sustain a Similar Insult During Perinatal Iron Deficiency

Neonatal offspring subjected to perinatal ID showed reduced Hb, growth restriction, and increased relative heart weight compared to CTL counterparts. These results are consistent with those published from our group (Bourque et al., 2008a; Woodman et al., 2018) and others

(Andersen et al., 2006; Gambling et al., 2003; Kochanowski and Rothman, 1985). Importantly, Hb levels were no longer different between ID and CTL pups at PD28, in both sexes, but the growth restriction and increased relative heart weight persisted. Thus, in the following experiments, PD28 was considered a timepoint at which Hb levels had recovered and as such, any differences between CTL and ID offspring were likely to be residual from the ID insult. Further, male and female neonatal offspring sustained a similar insult during perinatal ID, i.e., similar reductions in Hb levels, growth restriction, increases in heart weight relative to body weight throughout the studied timepoints. Since male and female offspring were similarly affected by the perinatal ID insult per these parameters, we were able to consider how male and female offspring hearts responded differentially to perinatal ID at the organ and cell level.

As previously mentioned, (see Section 1.5 Developmental Programming of Cardiovascular Disease by Perinatal Iron Deficiency), cardiomegaly, i.e., an increase in heart size, is a common phenotypic feature of young offspring exposed to perinatal ID. While we saw no changes in absolute heart weight, the proportional weight of the heart when normalized to body weight was increased in perinatal ID offspring. Since the functional capacity of the heart is dependent on its size, the evaluation of heart size must be done in the context of its required workload, i.e., the size of the body it must supply. Notwithstanding, there is a possibility that the proportional increase in heart size reflects an organ sparing effect, as was seen in the brain (Woodman et al., 2017), rather than a compensatory increase. However, clinical studies of anemia without concomitant ID, e.g., Hb Bart's disease (Thammavong et al., 2020), show that the developing heart can compensate in the context of reduced Hb by increasing cardiac output to maintain oxygen and nutrient delivery. The key difference between that model and the model of perinatal ID used here is the biochemical consequences of a lack of iron in the latter. Since iron is essential for energy and DNA metabolism

(see Section 1.2 Iron Homeostasis), a lack of iron in itself may impose constraints on the capacity of the anemic heart to functionally compensate as it otherwise might.

4.3 Perinatal Iron Deficiency Causes Sex- and Age-Specific Changes in the Neonatal Cardiac Proteome

Proteomics analysis revealed that perinatal ID induced age- and sex-specific protein and pathway alterations in the neonatal offspring hearts. Though evident at PD 0, ID-induced alterations were more pronounced at PD 28 in both males and females, despite recovery from anemia by this age. This residual effect could reflect a deficit in functional iron despite recovery from anemia since replenishment of tissue iron levels only occurs after restoration of Hb levels (World Health Organization, 2001). Notably, more pathways, including mitochondria-related proteins, are altered at PD 28 and more proteins directly tied to mitochondrial OXPHOS function are also altered. In males, there is a specific increase in altered complex I subunits, which are known to incorporate iron prosthetic groups. Further, though we observed some functional overlap between groups, gene overlap was minimal, demonstrating unique protein responses between timepoints and between sexes even where similar biological processes were affected. Further, the direction of change also differed between sexes; for example, proteins involved in mitochondrial OXPHOS pathways were upregulated in males while they were downregulated in females. Mitochondria-related proteins were distributed among enriched pathways related to various intracellular functions, nominally those involved in energy metabolism, but also those involved in organelle organization, leading us to believe there may be disturbances in the mitochondrial system. These differences led us to investigate how proteome changes might manifest at the mitochondrial function level in male and female offspring.

4.4 Sex-specific Changes in Mitochondrial Function

The findings that mitochondrial respiration, when normalized to CS activity was decreased in male perinatal ID offspring indicate a compensatory increase in mitochondrial content (shown by CS activity alone), albeit accompanied by a concomitant decrease in mitochondrial efficiency. That ID is associated with increased mitochondrial content may seem counterintuitive, since it constitutes an essential functional component of the ETS, both as iron-sulfur clusters of complexes I, II, and III, and the heme moiety of complexes II, III and IV and cytochrome c (Musallam and Taher, 2018). Despite coordination of the citric acid cycle and ETS for ATP production (whereby proportions of enzymes in each typically remain constant), case of ID represents a prominent exception to this rule (Srere, 1997). Using a model of dietary IDA, Cartier et al. (Cartier et al., 1986) showed that quantities of mitochondrial matrix and respiratory enzymes do not have to remain in constant proportions and are incorporated into mitochondria independently. As a result, mitochondrial protein composition can vary widely in response to different conditions. It was later discovered that the superposition of ID and exercise represents a specific case where the activity of mitochondrial matrix enzymes (including CS activity) is increased while the activity of ETS enzymes, namely NADH dehydrogenase and succinate dehydrogenase, is reduced in skeletal muscle (Hood et al., 1992; Ohira et al., 1987; Willis et al., 1987). Where exercise stimulated mitochondrial biogenesis, and thus an increase in matrix enzyme activity, the lack of iron prevented a corresponding increase in iron-containing ETS enzymes (Ohira et al., 1987), ultimately producing less efficient mitochondria with a disproportionate composition. Our results suggest mitochondria with an altered proportion between CS activity and mitochondrial respiration through various ETS pathways. This is likely due to decreased ETS enzyme activity and/or content of iron containing ETS components secondary to ID (Ackrell et al., 1984; Galan et al., 1984;

Maguire et al., 1982) coupled with the increase in mitochondrial content in an insufficient effort to compensate (Ohira et al., 1987). Thus, in our study, the cardiac mitochondria of ID male offspring may be of abnormal composition, without difference in the intrinsic quality of the OXPHOS pathways shown by the lack of difference in FCRs between CTL and ID offspring. This could be attributed to the fact that in ID conditions, mostly fully functional complexes are incorporated into mitochondria (Ackrell et al., 1984), albeit to a lesser extent in the ID hearts.

Interestingly, cytochrome *c* oxidase or complex IV activity was unaffected by ID in both males and females and in all respiratory parameters studied, including mitochondrial respiration normalized for tissue mass or CS activity, and FCRs. Iron-containing enzymes, particularly those forming the ETS, are known to be differentially affected by ID conditions (Dallman, 1986). More specifically, iron-sulfur (Fe-S) cluster containing ETS enzymes (i.e., complexes I, II, and III) have been shown to be more severely depleted than cytochromes and complex IV, which contain only heme groups (Davies et al., 1982; Galan et al., 1984; McKay et al., 1983). More recent *in vitro* studies using iron chelation in cells also show relatively less effect of ID on heme-exclusive vs. Fe-S cluster-containing ETS complexes (Hoes et al., 2018; Rensvold et al., 2013; Rensvold et al., 2016). In ID, but not anemic mouse hearts (Rineau et al., 2018) and skeletal muscle (Rineau et al., 2021), Rineau and colleagues observed a decrease in complex I activity only, but not complex IV, suggesting differential effects of ID on ETS complexes may depend on the severity of iron depletion. Some reports indicating reduced complex IV activity (Blayney et al., 1976) in ID emphasize the need to consider the severity of ID and the model used in interpretation of results. In studies by Rineau and colleagues, despite the absence of anemia and preservation of complex IV activity, indices of left ventricular dysfunction (Rineau et al., 2018) and decreased physical

endurance (Rineau et al., 2021) were noted, thus overt IDA is not required for functional deficits to occur.

The experimental design adopted in this study examined the changes of ID at various PDs, and therefore did not allow for the direct evaluation of sex-based differences. Notwithstanding, the reduced mitochondrial respiration (notably through the FAO pathway) observed in ID males compared to their respective CTLs was not evident in female ID offspring, despite a comparable severity of anemia. We have no clear explanation for this, though several possibilities exist. First, sex differences in iron utilization have been reported (Kong et al., 2014), and males and females may prioritize iron utilization in cells and tissues differently, with potential functional consequences that depend on the involvement of iron-containing enzymes within a signaling pathway. Further, males and females differ in their postnatal growth trajectories. Males typically grow faster and attain larger body weights than females, which imposes greater iron requirements to sustain tissue growth and blood volume expansion, making them more susceptible to and slower to recover from ID (Domellöf et al., 2002; Ren et al., 2014; Shao et al., 2021). Thus, residual depletion of tissue iron stores in males could affect function, despite the recovery from anemia after weaning. Second, mitochondrial morphology, function, and even metabolic substrate utilization are known to differ between male and females (Khalifa et al., 2017; Ostadal et al., 2019; Wittnich et al., 2013); these adaptations could allow for greater metabolic flexibility and resilience in females in wake of metabolic stressors such as ID and hypoxia. The caveat is that these sex-differences in mitochondria have largely been reported in mature mitochondria, and whether these are evident in fetal or neonatal organelles is not clear.

4.5 Changes in Mitochondrial Proteins and Mitochondrial Function Are Not Associated with Oxidative Stress

No change in the indices of oxidative stress between CTL and ID where measured either in male or female hearts. This agrees with our OXPHOS data, which showed no differences in the quality of mitochondrial OXPHOS pathways. Superoxide content as quantified by DHE staining was the initial factor investigated and yielded no differences. However, given that this marker looked at the whole tissue and superoxide is a highly reactive molecule and generally sequestered to the mitochondria or quickly transformed (Quinlan et al., 2013), potentially obscuring mitochondrial ROS differences or subcellular changes related to efficiency of mitochondrial function, we chose to study mRNA expression of antioxidant enzymes as a more sensitive and more stable marker of responses to oxidative stress. Still, these did not produce any differences between CTL and ID, leading us to conclude that changes in mitochondrial efficiency here were not accompanied by oxidative stress, and/or the system was compensating sufficiently for functional changes.

4.6 Differences in Cardiac Iron Metabolism May Explain Sex-Specific Changes in Mitochondria

The heart may also have specific responses to ID. We explored differences in cellular iron metabolism as a potential explanation for functional differences observed in males and females. Although males and females in our case experience similar Hb reduction, the impact of this at the cellular level may be different. It is suggested that male neonates are at greater risk of developing anemia likely due to a faster growth trajectory compared to females (Domellöf et al., 2002; Kong et al., 2014; Ren et al., 2014). Whole body iron is also managed and distributed differently in males and females (Kong et al., 2014). Since cellular iron metabolism proteins are

transcriptionally regulated (Fig. 1.2.1), we used RT-qPCR to study mRNA expression of key proteins: DMT1, TFR1, FTH and FTL, FPN, and HAMP. We were then able to compare the results of mRNA expression analyses to proteomics and look for congruency between mRNA and protein expression. Our proteomics results showed surprisingly few iron metabolism proteins altered in neonatal hearts; iron metabolism pathways were not enriched at all in male offspring hearts, but prominent iron efflux inhibitor protein, HAMP, was downregulated in PD0 male hearts. Iron metabolism pathways were enriched in females but only at PD0. The minimal response from iron metabolism pathways in the face of perinatal ID may have to do with the immaturity of iron metabolism in the fetus and neonates, which could not only be a systemic immaturity (inability to increase iron uptake in response to low iron), but also differences in distribution and cellular responses to low iron compared to adults.

4.7 Conclusions

In conclusion, the findings presented herein show that perinatal ID causes cardiac adaptations. Although the specific mechanisms underlying these maladaptive changes remain to be clarified, we have identified mitochondrial metabolism as a potential effector, and may contribute to the sex-differences observed in ID offspring. However, contractile and structural pathways were also attenuated in response to ID in our untargeted proteomics analysis, and given their role in dictating muscle contractility, these could also be important contributors to the cardiac dysfunction observed in ID offspring.

4.8 Significance

High rates of ID anemia persist among pregnant women despite iron supplementation. Current treatment strategies, though somewhat effective, are often not well tolerated and must be implemented over a long period, making rapid replenishment of iron stores difficult and potentially

hazardous (Benson et al., 2021; Qassim et al., 2018). Thus, new treatment strategies to prevent the adverse developmental effects of perinatal ID are needed. This study identifies key mechanisms by which perinatal ID alters cardiac mitochondrial function in offspring, and greatly contribute to our understanding of the impact of ID on the development of the offspring. It provides insights into the mechanisms linking perinatal ID with cardiovascular dysfunction, and help identify potential targets for the treatment and prevention of chronic diseases associated with perinatal ID. The results also provide further basis for the testing of novel therapeutics for use in pregnancy to prevent the programming effects of perinatal ID. This study, and following research, will help to identify potential targets and treatments for the prevention of later life CVD associated with perinatal ID and other pregnancy complications with similar etiologies.

4.9 Limitations

While proteomics provides a wealth of information on the identity and quantity of proteins present in a sample, it is important to note that it does not offer information on the function of these proteins. While it may seem to some that there is a discrepancy between our proteomics data and the data presented thereafter (e.g., mitochondrial function), we would offer the perspective that proteomics, as a hypothesis-generating technique, provides insight into only one possible mechanism, i.e., changes in protein quantity, leading to the functional changes observed. Further, in mass spectrometry of complex biological samples, it is possible that lower abundance proteins are masked amongst those that are more abundant; barring any technical issues, which have been excluded as a possibility, this constitutes a possible explanation for the distinctly smaller proteome size in PD0 female hearts compared to the other groups (Fig. 3.3.1).

High-resolution respirometry allows for the study of intact mitochondria, thus providing more integrative insight into the ETS/OXPHOS function and physiology in comparison to

studying protein content or enzyme activity of individual proteins outside their system. However, cell structure and organization of the mitochondrial reticulum are lost during sample preparation. As such, this technique provides an *ex vivo* look at mitochondria but cannot consider the cellular influences on mitochondrial metabolism that exist outside the mitochondria themselves. Further, because substrates are supplied in excess and the conditions created using SUIT protocols are not physiologically accurate in this regard. This must be considered when interpreting high-resolution respirometry data, which can provide insight into intrinsic changes to the function of mitochondrial pathways but may not fully recapitulate how mitochondria are functioning *in vivo*.

4.10 Future Work

Parallel work by Ronan Noble (Noble et al., 2023) explored whether there were cardiac function differences in the CTL versus ID animals of this model. Future studies should include an assessment of ATP levels to determine the relationship between mitochondrial efficiency alterations seen herein and contractile activity. Exploration of calcium signaling in the heart could also further illuminate this functional relationship. Further, proteomics revealed a downregulation of organ structural proteins, which remains to be explored. Although our results suggest that there is no oxidative stress in this context, future studies should consider using more direct measures of reactive oxygen species levels as well as downstream effect of uncontrolled ROS levels, including damage to macromolecules, such a lipid peroxidation, DNA damage, and protein carbonylation. It would be interesting to explore the latter indices of macromolecule damage in the whole tissue/cell, as well as in isolated mitochondria to see whether such changes may be compartmentalized. Should further research conclude that the functional changes are indeed not associated with any sort of oxidative stress, this may be an interesting model in which

to see how mitochondrial dysfunction or dysregulation without accompanying oxidative stress may alter long term cardiac function.

References

Abbaspour, N., Hurrell, R. and Kelishadi, R. (2014). Review on iron and its importance for human health. *J. Res. Med. Sci.* **19**, 164–174.

Ackrell, B. A. C., Maguire, J. J., Dallman, P. R. and Kearney, E. B. (1984). Effect of iron deficiency on succinate- and NADH-ubiquinone oxidoreductases in skeletal muscle mitochondria. *J. Biol. Chem.* **259**, 10053–10059.

Alur, P. (2019). Sex differences in nutrition, growth, and metabolism in preterm infants. *Front. Pediatr.* **7**, 1–9.

Alwan, N. and Hamamy, H. (2015). Maternal Iron Status in Pregnancy and Long-Term Health Outcomes in the Offspring. *J. Pediatr. Genet.* **4**, 111–123.

Andersen, H. S., Gambling, L., Holtrop, G. and Mcardle, H. J. (2006). Maternal Iron Deficiency Identifies Critical Windows for Growth and Cardiovascular Development in the Rat Postimplantation Embryo. *J. Nutr.* **136**, 1171–1177.

Andersen, M. D., Alstrup, A. K. O., Duvald, C. S., Mikkelsen, E. F. R., Vendelbo, M. H., Ovesen, P. G. and Pedersen, M. (2018). Animal Models of Fetal Medicine and Obstetrics. In *Experimental Animal Models of Human Diseases - An Effective Therapeutic Strategy*, pp. 343–373.

Anderson, G. J. and Frazer, D. M. (2017). Current understanding of iron homeostasis. *Am. J. Clin. Nutr.* **106**, 1559S-1566S.

Andreini, C., Putignano, V., Rosato, A. and Banci, L. (2018). The human iron-proteome †. *Metallomics* **10**, 1223–1231.

Anmann, T., Varikmaa, M., Timohhina, N., Tepp, K., Shevchuk, I., Chekulayev, V., Saks,

V. and Kaambre, T. (2014). Formation of highly organized intracellular structure and energy metabolism in cardiac muscle cells during postnatal development of rat heart. *Biochim. Biophys. Acta* **1837**, 1350–1361.

Bailey, R. L. (2015). The Epidemiology of Global Micronutrient Deficiencies. *Ann. Nutr. Metab.* **66**, 22–33.

Baird, J., Jacob, C., Barker, M., Fall, C. H. D., Hanson, M., Harvey, N. C., Inskip, H. M., Kumaran, K. and Cooper, C. (2017). Developmental Origins of Health and Disease: A Lifecourse Approach to the Prevention of Non-Communicable Diseases. *Healthcare* **5**, 1–12.

Balendran, S. and Forsyt (2021). Non-anaemic iron deficiency. *Aust. Prescr.* **44**, 193–196.

Barker, D. J. P. and Osmond, C. (1986). Infant Mortality, Childhood Nutrition, and Ischaemic Heart Disease in England and Wales. *Lancet* **327**, 1077–1081.

Barker, J. P. and Osmond, C. (1987a). Inequalities in health in Britain: Specific explanations in three Lancashire towns. *Br. Med. J. (Clin. Res. Ed).* **294**, 749–752.

Barker, D. J. P. and Osmond, C. (1987b). Death rates from stroke in England and Wales predicted from past maternal mortality. *Br. Med. J. (Clin. Res. Ed).* **295**, 83–86.

Benson, C. S., Shah, A., Frise, M. C. and Frise, C. J. (2021). Iron deficiency anaemia in pregnancy: A contemporary review. *Obstet. Med.* **14**, 67–76.

Blayney, L., Bailey-wood, R., Jacobs, A., Henderson, A. and Muir, J. (1976). The Effects of Iron Deficiency on the Respiratory Function and Cytochrome Content of Rat Heart Mitochondria. *Circ. Res.* **39**, 744–748.

Bourque, S. L. and Davidge, S. T. (2020). Developmental programming of cardiovascular

function: A translational perspective. *Clin. Sci.* **134**, 3023–3046.

Bourque, S. L., Komolova, M., Nakatsu, K. and Adams, M. A. (2008a). Long-term circulatory consequences of perinatal iron deficiency in male wistar rats. *Hypertension* **51**, 154–159.

Bourque, S. L., Iqbal, U., Reynolds, J. N., Adams, M. A. and Nakatsu, K. (2008b). Perinatal Iron Deficiency Affects Locomotor Behavior and Water Maze Performance in Adult Male and Female Rats. *J. Nutr.* **138**, 931–937.

Bourque, S. L., Komolova, M., McCabe, K., Adams, M. A. and Nakatsu, K. (2012). Perinatal iron deficiency combined with a high-fat diet causes obesity and cardiovascular dysregulation. *Endocrinology* **153**, 1174–1182.

Brannon, P. M. and Taylor, C. L. (2017). Iron Supplementation during Pregnancy and Infancy: Uncertainties and Implications for Research and Policy. *Nutrients* **9**, 1–17.

Briguglio, M., Hrelia, S., Malaguti, M., Lombardi, G., Riso, P., Porrini, M., Perazzo, P. and Banfi, G. (2020). The Central Role of Iron in Human Nutrition: From Folk to Contemporary Medicine. *Nutrients* **12**, 1–17.

Brook, W. H., Connell, S., Cannata, J., Maloney, J. E. and Walker, A. M. (1983). Ultrastructure of the myocardium during development from early fetal life to adult life in sheep. *J. Anat.* **137**, 729–741.

Burggren, W. W. and Reyna, K. S. (2011). Developmental trajectories, critical windows and phenotypic alteration during cardio-respiratory development. *Respir. Physiol. Neurobiol.* **178**, 13–21.

Cao, C., Thomas, C., Insogna, K. and O'Brien, K. (2013). Differential effects of hepcidin on

heme and nonheme iron absorption in a rat model of iron overload. *FASEB J.* **27**, 634.18-634.18.

Cao, C., Thomas, C. E., Insogna, K. L. and O'Brien, K. O. (2014). Duodenal Absorption and Tissue Utilization of Dietary Heme and Nonheme Iron Differ in Rats. *J. Nutr. Nutr. Physiol. Metab. Nutr.* **144**, 1710–1717.

Cartier, L. J., Ohira, Y., Chen, M., Cuddihee, R. W. and Holloszy, J. O. (1986). Perturbation of mitochondrial composition in muscle by iron deficiency. Implications regarding regulation of mitochondrial assembly. *J. Biol. Chem.* **261**, 13827–13832.

Cox, J. and Mann, M. (2008). MaxQuant enables high peptide identification rates, individualized p.p.b.-range mass accuracies and proteome-wide protein quantification. *Nat. Biotechnol.* **26**, 1367–1372.

Cox, J., Neuhauser, N., Michalski, A., Scheltema, R. A., Olsen, J. V and Mann, M. (2011). Andromeda: A Peptide Search Engine Integrated into the MaxQuant Environment. *J. Proteome Res.* **10**, 1794–1805.

Crooks, D. R., Maio, N., Lane, A. N., Jarnik, M., Higashi, R. M., Haller, R. G., Yang, Y., Fan, T. W. M., Marston Linehan, W. and Rouault, T. A. (2018). Acute loss of iron–sulfur clusters results in metabolic reprogramming and generation of lipid droplets in mammalian cells. *J. Biol. Chem.* **293**, 8297–8311.

Crowe, C., Dandekar, P., Fox, M., Dhingra, K., Bennet, L. and Hanson, M. A. (1995). The effects of anaemia on heart, placenta and body weight, and blood pressure in fetal and neonatal rats. *J. Physiol.* **488**, 515–519.

Dallman, P. R. (1986). Biochemical basis for the manifestations of iron deficiency. *Annu. Rev.*

Nutr. **6**, 13–40.

Das, N., Menon, N. G., de Almeida, L. G. N., Woods, P. S., Heynen, M. L., Jay, G. D., Caffery, B., Jones, L., Krawetz, R., Schmidt, T. A., et al. (2021). Proteomics Analysis of Tears and Saliva From Sjogren's Syndrome Patients. *Front. Pharmacol.* **12**, 1–17.

Davies, K. J. A., Maguire, J. J. and Brooks, G. A. (1982). Muscle mitochondrial bioenergetics, oxygen supply, and work capacity during dietary iron deficiency and repletion. *Am. J. Physiol. - Endocrinol. Metab.* **5**, E418–E427.

Dickinson, J. E., Sharpe, J., Warner, T. M., Nathan, E. A. and D'Orsogna, L. (2010). Childhood cardiac function after severe maternal red cell isoimmunization. *Obstet. Gynecol.* **116**, 851–857.

Domellöf, M., Lönnerdal, B., Dewey, K. G., Cohen, R. J., Rivera, L. L. and Hernell, O. (2002). Sex Differences in Iron Status During Infancy. *Pediatrics* **110**, 545–552.

Dorn, G. W., Vega, R. B. and Kelly, D. P. (2015). Mitochondrial biogenesis and dynamics in the developing and diseased heart. *Genes Dev.* **29**, 1981–1991.

Dötsch, J. (2014). Perinatal programming - myths, fact, and future of research. 1–4.

Evans, P., Cindrova-davies, T., Muttukrishna, S., Burton, G. J., Porter, J. and Jauniaux, E. (2011). Hepcidin and iron species distribution inside the first-trimester human gestational sac. **17**, 227–232.

Fall, C. and Osmond, C. (2013). Commentary: The developmental origins of health and disease: an appreciation of the life and work of Professor David J.P. Barker, 1938–2013. *Int. J. Epidemiol.* **42**, 1231–1232.

Galan, P., Hercberg, S. and Touitou, Y. (1984). The activity of tissue enzymes in iron-

deficient rat and man: an overview. *Comp. Biochem. Physiol.* **77**, 647–653.

Gambling, L., Dunford, S., Wallace, D. I., Zuur, G., Solanky, N., Srai, S. K. S. and McArdle, H. J. (2003). Iron deficiency during pregnancy affects postnatal blood pressure in the rat. *J. Physiol.* **552**, 603–610.

GBD 2015 DALYs and HALE Collaborators (2016). Global, regional, and national disability-adjusted life-years (DALYs) for 315 diseases and injuries and healthy life expectancy (HALE), 1990–2015: a systematic analysis for the Global Burden of Disease Study 2015. *Lancet* **388**, 1603–1658.

GBD 2017 DALYs and HALE Collaborators (2018). Global, regional, and national disability-adjusted life-years (DALYs) for 359 diseases and injuries and healthy life expectancy (HALE) for 195 countries and territories, 1990-2017: A systematic analysis for the Global Burden of Disease Study 2017. *Lancet* **392**, 1859–1922.

Gilbert, J. S. and Banek, C. T. (2012). Sex Differences in the Developmental Programming of Adult Disease. In *Sex Hormones* (ed. Dubey, R.), pp. 1–28. InTech.

Glancy, B., Hartnell, L. M., Combs, C. A., Fenmou, A., Sun, J., Murphy, E., Subramaniam, S. and Balaban, R. S. (2017). Power Grid Protection of the Muscle Mitochondrial Reticulum. *Cell Rep.* **19**, 487–496.

Gnaiger, E. (2020). *Mitochondrial Pathways and Respiratory Control: An Introduction to OXPHOS Analysis*. 5th ed. Innsbruck, Austria: Bioenergetics Communications.

Gnaiger E, Kuznetsov AV, Schneeberger S, Seiler R, Brandacher G, Steurer W and Margreiter R (2000). Mitochondria in the Cold. In *Life in the Cold*, pp. 431–442. New York.

Godfrey, K. M., Redman, C. W. G., Barker, D. J. P. and Osmond, C. (1991). The effect of maternal anaemia and iron deficiency on the ratio of fetal weight to placental weight. *Br. J. Obstet. Gynaecol.* **98**, 886–891.

Gong, G., Song, M., Csordas, G., Kelly, D. P., Matkovich, S. J. and Dorn, G. W. (2015). Parkin-mediated mitophagy directs perinatal cardiac metabolic maturation in mice. *Science (80-.).* **350**, aad2459.

Goss, C. M. (1938). The First Contractions of the Heart in Rat Embryos. *Anat. Rec.* **70**, 505–524.

Gragasin, F. S., Ospina, M. B., Serrano-Lomelin, J., Kim, S. H., Kokotilo, M., Woodman, A. G., Renaud, S. J., Bourque, S. L., Harris, D. and Kumar, S. (2021). Maternal and Cord Blood Hemoglobin as Determinants of Placental Weight: A Cross-Sectional Study. *J. Clin. Med.* **10**, 997.

Günthel, M., Barnett, P. and Christoffels, V. M. (2018). Development, Proliferation, and Growth of the Mammalian Heart. *Mol. Ther.* **26**, 1599–1609.

Han, X., Ding, S., Lu, J. and Li, Y. (2022). Global, regional, and national burdens of common micronutrient deficiencies from 1990 to 2019: A secondary trend analysis based on the Global Burden of Disease 2019 study. *eClinicalMedicine* **44**, 101299.

Hoes, M. F., Grote Beverborg, N., Kijlstra, J. D., Kuipers, J., Swinkels, D. W., Giepmans, B. N. G., Rodenburg, R. J., van Veldhuisen, D. J., de Boer, R. A. and van der Meer, P. (2018). Iron deficiency impairs contractility of human cardiomyocytes through decreased mitochondrial function. *Eur. J. Heart Fail.* **20**, 910–919.

Hood, D. A., Kelton, R. and Nismo, M. L. (1992). Mitochondrial adaptations to chronic muscle

use: Effect of iron deficiency. *Comp. Biochem. Physiol. -- Part A Physiol.* **101**, 597–605.

Horowitz, K. M., Ingardia, C. J. and Borgida, A. F. (2013). Anemia in Pregnancy. *Clin. Lab. Med.* **33**, 281–291.

Hsu, C. N., & Tain, Y. L. (2019). The Good , the Bad , and the Ugly of Pregnancy. *Nutrients* **11**, 1–21.

Iruretagoyena, J. I., Davis, W., Bird, C., Olsen, J., Radue, R., Teo Broman, A., Kendziorski, C., Splinter Bondurant, S., Golos, T., Bird, I., et al. (2014). Metabolic gene profile in early human fetal heart development. *Mol. Hum. Reprod.* **20**, 690–700.

Jeha, D., Usta, I., Ghulmiyyah, L. and Nassar, A. (2015). A review of the risks and consequences of adolescent pregnancy. *J. Neonatal. Perinatal. Med.* **8**, 1–8.

Juul, S. E., Derman, R. J. and Auerbach, M. (2019). Perinatal Iron Deficiency: Implications for Mothers and Infants. *Neonatology* **115**, 269–274.

Karwi, Q. G., Jörg, A. R. and Lopaschuk, G. D. (2019). Allosteric, transcriptional and post-translational control of mitochondrial energy metabolism. *Biochem. J.* **476**, 1695–1712.

Kassebaum, N. J., Jasrasaria, R., Naghavi, M., Wulf, S. K., Johns, N., Lozano, R., Regan, M., Weatherall, D., Chou, D. P., Eisele, T. P., et al. (2014). A systematic analysis of global anemia burden from 1990 to 2010. *Blood* **123**, 615–624.

Katsarou, A. and Pantopoulos, K. (2020). Basics and principles of cellular and systemic iron homeostasis. *Mol. Aspects Med.* **75**, 1–11.

Khalifa, A. R. M., Abdel-rahman, E. A., Mahmoud, A. M., Ali, M. H., Noureldin, M., Saber, S. H., Mohsen, M. and Ali, S. S. (2017). Sex-specific differences in mitochondria biogenesis, morphology, respiratory function, and ROS homeostasis in young mouse heart

and brain. *Physiol. Rep.* **5**, 1–19.

Kim, H., Kim, D., Lee, I., Rah, B., Sawa, Y. and Schaper, J. (1992). Human Fetal Heart Development after Mid-term: Morphometry and Ultrastructural Study. *J. Cell. Mol. Cardiol.* **24**, 949–965.

Kobak, K. A., Radwa, M., Dzi, M., Kasztura, M. and Josiak, K. (2019). Structural and functional abnormalities in iron-depleted heart. *Heart Fail. Rev.* **24**, 269–277.

Kobayashi, T., Maeda, S., Ichise, N., Sato, T., Iwase, T., Seki, S., Yamada, Y. and Tohse, N. (2011). The beginning of the calcium transient in rat embryonic heart. *J. Physiol. Sci.* **61**, 141–149.

Kochanowski, B. A. and Rothman, A. (1985). Cellular Growth in Iron-Deficient Rats: Effect of Pre-and Postweaning Iron Repletion. *J. Nutr.* **115**, 279–287.

Komolova, M., Bourque, S. L., Nakatsu, K. and Adams, M. A. (2008). Sedentariness and increased visceral adiposity in adult perinatally iron-deficient rats. *Int. J. Obes.* **32**, 1441–1444.

Kong, W.-N., Niu, Q.-M., Ge, L., Zhang, N., Yan, S.-F., Chen, W.-B., Chang, Y.-Z. and Zhao, S.-E. (2014). Sex Differences in Iron Status and Hepcidin Expression in Rats. *Biol. Trace Elem. Res.* **160**, 258–267.

Kulaksiz, H., Theilig, F., Bachmann, S., Gehrke, S. G., Rost, D., Janetzko, A., Cetin, Y. and Stremmel, W. (2005). The iron-regulatory peptide hormone hepcidin : expression and cellular localization in the mammalian kidney. 361–370.

Lai, N., M. Kummitha, C., Rosca, M. G., Fujioka, H., Tandler, B. and Hoppel, C. L. (2019). Isolation of mitochondrial subpopulations from skeletal muscle: Optimizing recovery and

preserving integrity. *Acta Physiol.* **225**, e13182.

Lakhal-Littleton, S. (2019). Mechanisms of cardiac iron homeostasis and their importance to heart function. *Free Radic. Biol. Med.* **133**, 234–237.

Lakhal-Littleton, S. (2021). Advances in understanding the crosstalk between mother and fetus on iron utilization. *Semin. Hematol.* **58**, 153–160.

Lakhal-Littleton, S., Wolna, M., Chung, Y. J., Christian, H. C., Heather, L. C., Brescia, M., Ball, V., Diaz, R., Santos, A., Biggs, D., et al. (2016). An essential cell-autonomous role for hepcidin in cardiac iron homeostasis. *Elife* **5**, 1–25.

Larsen, S., Nielsen, J., Hansen, C. N., Nielsen, L. B., Wibrand, F., Stride, N., Schroder, H. D., Boushel, R., Helge, J. W., Dela, F., et al. (2012). Biomarkers of mitochondrial content in skeletal muscle of healthy young human subjects. *J. Physiol.* **590**, 3349–3360.

Leduc, L., Levy, E., Bouity-Voubou, M. and Delvin, E. (2010). Fetal programming of atherosclerosis: Possible role of the mitochondria. *Eur. J. Obstet. Gynecol. Reprod. Biol.* **149**, 127–130.

Lemieux, H. and Blier, P. U. (2022). Exploring Thermal Sensitivities and Adaptations of Oxidative Phosphorylation Pathways. *Metabolites* **12**, 1–20.

Lemieux, H., Vazquez, E. J., Fujioka, H. and Hoppel, C. L. (2010). Decrease in mitochondrial function in rat cardiac permeabilized fibers correlates with the aging phenotype. *J. Gerontol. Biol. Sci.* **65**, 1157–1164.

Lemieux, H., Semsroth, S., Antretter, H., Höfer, D. and Gnaiger, E. (2011). Mitochondrial respiratory control and early defects of oxidative phosphorylation in the failing human heart. *Int. J. Biochem. Cell Biol.* **43**, 1729–1738.

Lemieux, H., Blier, P. U. and Gnaiger, E. (2017a). Remodelling pathway control of mitochondrial respiratory capacity by temperature in mouse heart: electron flow through the Q-junction in permeabilized fibers. *Sci. Rep.* **7**, 1–13.

Lemieux, H., Blier, P. U. and Gnaiger, E. (2017b). Remodeling pathway control of mitochondrial respiratory capacity by temperature in mouse heart: electron flow through the Q-junction in permeabilized fibers. *Sci. Rep.* **7**, 1–13.

Lewis, R. M., Forhead, A. J., Petry, C. J., Ozanne, S. E. and Nicolas Hales, C. (2002). Long-term programming of blood pressure by maternal dietary iron restriction in the rat. *Br. J. Nutr.* **88**, 283–290.

Lipiński, P., Starzyński, R. R., Canonne-Hergaux, F., Tudek, B., Oliński, R., Kowalczyk, P., Dziaman, T., Thibaudeau, O., Gralak, M. A., Smuda, E., et al. (2010). Benefits and risks of iron supplementation in anemic neonatal pigs. *Am. J. Pathol.* **177**, 1233–1243.

Lisle, S. J. M., Lewis, R. M., Petry, C. J., Ozanne, S. E., Hales, C. N. and Forhead, A. J. (2003). Effect of maternal iron restriction during pregnancy on renal morphology in the adult rat offspring. *Br. J. Nutr.* **90**, 33–39.

Lonnerdal, B. (2017). Excess iron intake as a factor in growth, infections, and development of infants and young children. *Am. J. Clin. Nutr.* **106**, 1681S-1688S.

Lönnerdal, B., Georgieff, M. K. and Hernell, O. (2015). Developmental physiology of iron absorption, homeostasis, and metabolism in the healthy term infant. *J. Pediatr.* **167**, S8–S14.

Lopaschuk, G. D. and Jaswal, J. S. (2010). Energy metabolic phenotype of the cardiomyocyte during development, differentiation, and postnatal maturation. *J. Cardiovasc. Pharmacol.*

56, 130–140.

M G Figueiredo, A. C., Gomes-Filho, I. S., Silva, R. B., S Pereira, P. P., F Da Mata, F. A., Lyrio, A. O., Souza, E. S., Cruz, S. S. and Pereira, M. G. (2018). Maternal Anemia and Low Birth Weight: A Systematic Review and Meta-Analysis. *Nutrients* **10**, 1–17.

Maguire, J. J., Davies, K. J. A., Dallman, P. R. and Packer, L. (1982). Effects of dietary iron deficiency on iron-sulfur proteins and bioenergetic functions of skeletal muscle mitochondria. *Biochim. Biophys. Acta* **679**, 210–220.

Marcela, S. G., Cristina, R. M. M., Angel, P. G. M., Manuel, A. M., Sofía, D. C., Patricia, D. L. R. S., Bladimir, R. R. and Concepción, S. G. (2012). Chronological and Morphological Study of Heart Development in the Rat. *Anat. Rec.* **295**, 1267–1290.

Marin-Garcia, J., Ananthakrishnan, R. and Goldenthal, M. J. (1997). Mitochondrial gene expression in rat heart and liver during growth and development. *Biochem. Cell Biol.* **75**, 137–142.

Markova, V., Holm, C., Pinborg, A. B., Thomsen, L. L. and Moos, T. (2019). Impairment of the Developing Human Brain in Iron Deficiency: Correlations to Findings in Experimental Animals and Prospects for Early Intervention Therapy. *Pharmaceuticals* **12**, 1–16.

McCarthy, R. C. and Kosman, D. J. (2014). Glial Cell Ceruloplasmin and Hepcidin Differentially Regulate Iron Efflux from Brain Microvascular Endothelial Cells. *PLoS One* **9**, e89003.

McKay, R. H., Higuchi, D. A., Winder, W. W., Fell, R. D. and Brown, E. B. (1983). Tissue effects of iron deficiency in the rat. *BBA - Gen. Subj.* **757**, 352–358.

Means, R. T. (2020). Iron deficiency and iron deficiency anemia: Implications and impact in

pregnancy, fetal development, and early childhood parameters. *Nutrients* **12**, 1–15.

Mering, C. Von, Jensen, L. J., Snel, B., Hooper, S. D., Krupp, M., Foglierini, M., Jouffre, N., Huynen, M. A. and Bork, P. (2005). STRING : known and predicted protein – protein associations , integrated and transferred across organisms. **33**, 433–437.

Merle, U., Fein, E., Gehrke, S. G., Stremmel, W. and Kulaksiz, H. (2007). The Iron Regulatory Peptide Hepcidin Is Expressed in the Heart and Regulated by Hypoxia and Inflammation. **148**, 2663–2668.

Michonska, I., Łuszczki, E., Zielinska, M., Oleksy, Ł., Stolarczyk, A. and Deren, K. (2022). Nutritional Programming : History, Hypotheses, and the Role of Prenatal Factors in the Prevention of Metabolic Diseases. *Nutrients* **14**, 1–18.

Miller, E. M. (2016). The reproductive ecology of iron in women. *Am. J. Phys. Anthropol.* **159**, S172–S195.

Muckenthaler, M. U., Rivella, S., Hentze, M. W. and Galy, B. (2017). A Red Carpet for Iron Metabolism. *Cell* **168**, 344–361.

Muñoz, M., Villar, I. and Antonio García-Erce, J. (2009). An update on iron physiology. *World J Gastroenterol* **15**, 4617–4626.

Musallam, K. M. and Taher, A. T. (2018). Iron deficiency beyond erythropoiesis: should we be concerned? *Curr. Med. Res. Opin.* **34**, 81–93.

Nathanielsz, P. W., Poston, L. and Taylor, P. D. (2007). In Utero Exposure to Maternal Obesity and Diabetes: Animal Models That Identify and Characterize Implications for Future Health. *Clin. Perinatol.* **34**, 515–526.

Noble, R. M. N., Holody, C. D., Woodman, A. G., Nie, C., Liu, S. N., Young, D.,

Wiedemeyer, A., Soni, S., Dyck, J. R. B., Graf, D., et al. (2023). Perinatal iron restriction is associated with changes in neonatal cardiac function and structure in a sex-dependent manner. *Clin. Sci. (Lond).* **137**, 1115–1130.

O'Brien, K. O. and Ru, Y. (2017). Iron status of North American pregnant women: an update on longitudinal data and gaps in knowledge from the United States and Canada. *Am. J. Clin. Nutr.* **106**, 1647S-1654S.

Ohira, Y., Cartier, L. J., Chen, M. and Holloszy, J. O. (1987). Induction of an increase in mitochondrial matrix enzymes in muscle of iron-deficient rats. *Am. J. Physiol. - Cell Physiol.* **253**, C639–C644.

Osmond, C., Barker, D. J. P., Winter, P. D., Fall, C. H. D. and Simmonds, S. J. (1993). Early growth and death from cardiovascular disease in women. *Br. Med. J.* **307**, 1519–1524.

Ostadal, B., Drahota, Z., Houstek, J., Milerova, M., Ostadalova, I., Hlavackova, M. and Kolar, F. (2019). Developmental and sex differences in cardiac tolerance to ischemia – reperfusion injury : the role of mitochondria. *Can. J. Physiol. Pharmacol.* **97**, 808–814.

Padmanabhan, V., Cardoso, R. C. and Puttabyatappa, M. (2016). Developmental Programming, a Pathway to Disease. *Endocrinology* **157**, 1328–1340.

Palmer, J. W., Tandler, B. and Hoppel, C. L. (1977). Biochemical properties of subsarcolemmal and interfibrillar mitochondria isolated from rat cardiac muscle. *J. Biol. Chem.* **252**, 8731–8739.

Paul, B. T., Manz, D. H., Torti, F. M. and Torti, S. V (2017). Mitochondria and Iron: Current Questions. *Expert Rev. Hematol.* **10**, 65–79.

Piquereau, J. and Ventura-Clapier, R. (2018). Maturation of Cardiac Energy Metabolism

During Perinatal Development. *Front. Physiol.* **9**, 1–10.

Piquereau, J., Caffin, F., Novotova, M., Lemaire, C., Veksler, V., Garnier, A., Ventura-Clapier, R. and Joubert, F. (2013). Mitochondrial dynamics in the adult cardiomyocytes: which roles for a highly specialized cell? *Front. Physiol.* **4**, 1–12.

Pohjoismäki, J. L. and Goffart, S. (2017). The role of mitochondria in cardiac development and protection. *Free Radic. Biol. Med.* **106**, 345–354.

Pohjoismäki, J., Goffart, S., Taylor, R. W., Turnbull, D. M. and Suomalainen, A. (2010). Developmental and Pathological Changes in the Human Cardiac Muscle Mitochondrial DNA Organization, Replication and Copy Number. *PLoS One* **5**, e10426.

Prabhakar, E. (2022). Iron in Cell Metabolism and Disease. In *Iron Metabolism - A Double-Edged Sword* (ed. Zakaria, M.) and Hassan, T.), pp. 1–17. IntechOpen.

Puig, S., Ramos-Alonso, L., Romero, A. M. and Martínez-Pastor, M. T. (2017). The elemental role of iron in DNA synthesis and repair. *Metallomics* **9**, 1483–1500.

Qassim, A., Mol, B. W., Grivell, R. M. and Grzeskowiak, L. E. (2018). Safety and efficacy of intravenous iron polymaltose, iron sucrose and ferric carboxymaltose in pregnancy: A systematic review. *Aust. New Zeal. J. Obstet. Gynaecol.* **58**, 22–39.

Quezada-Pinedo, H. G., Cassel, F., Duijts, L., Muckenthaler, M. U., Gassmann, M., Jaddoe, V. W. V., Reiss, I. K. M. and Vermeulen, M. J. (2021). Maternal iron status in pregnancy and child health outcomes after birth: A systematic review and meta-analysis. *Nutrients* **13**, 1–17.

Quinlan, C. L., Perevoshchikova, I. V, Hey-mogensen, M., Orr, A. L. and Brand, M. D. (2013). Redox Biology Sites of reactive oxygen species generation by mitochondria

oxidizing different substrates $. *Redox Biol.* **1**, 304–312.

Rao, R. and Georgieff, M. K. (2002). Perinatal aspects of iron metabolism. *Acta Paediatr.* **91**, 124–129.

Ravingerová, T., Kindernay, L., Barteková, M., Ferko, M., Adameová, A., Zohdi, V., Bernátová, I., Ferenczyová, K. and Lazou, A. (2020). The molecular mechanisms of iron metabolism and its role in cardiac dysfunction and cardioprotection. *Int. J. Mol. Sci.* **21**, 1–24.

Reeves, P. G., Nielsen, F. H. and Fahey, G. C. (1993). AIN-93 Purified Diets for Laboratory Rodents: Final Report of the American Institute of Nutrition Ad Hoc Writing Committee on the Reformulation of the AIN-76A Rodent Diet. *J. Nutr* **123**, 1939–1951.

Ren, J., Wu, Q., Wang, Y., Liu, J., Yang, X. and Yang, L. (2014). [Gender differences in iron status in infants 4 and 6 months of age]. *Wei Sheng Yan Jiu* **43**, 357-360,377.

Rensvold, J. W., Ong, S. E., Jeevananthan, A., Carr, S. A., Mootha, V. K. and Pagliarini, D. J. (2013). Complementary RNA and Protein Profiling Identifies Iron as a Key Regulator of Mitochondrial Biogenesis. *Cell Rep.* **3**, 237–245.

Rensvold, J. W., Krautkramer, K. A., Dowell, J. A., Denu, J. M. and Pagliarini, D. J. (2016). Iron deprivation induces transcriptional regulation of mitochondrial biogenesis. *J. Biol. Chem.* **291**, 20827–20837.

Rineau, E., Gaillard, T., Gueguen, N., Procaccio, V., Henrion, D., Prunier, F. and Lasocki, S. (2018). Iron deficiency without anemia is responsible for decreased left ventricular function and reduced mitochondrial complex I activity in a mouse model. *Int. J. Cardiol.* **266**, 206–212.

Rineau, E., Gueguen, N., Procaccio, V., Geneviève, F., Reynier, P., Henrion, D. and Lasocki, S. (2021). Iron Deficiency without Anemia Decreases Physical Endurance and Mitochondrial Complex I Activity of Oxidative Skeletal Muscle in the Mouse.

Rines, A. K. and Ardehali, H. (2013). Transition metals and mitochondrial metabolism in the heart. *J. Mol. Cell. Cardiol.* **55**, 50–57.

Roberts, H., Bourque, S. L. and Renaud, S. J. (2020). Maternal iron homeostasis: effect on placental development and function. *Reproduction* **160**, R65–R78.

Rodríguez-Rodríguez, P., Ramiro-Cortijo, D., Reyes-Hernández, C. G., López de Pablo, A. L., Carmen González, M. and Arribas, S. M. (2018). Implication of oxidative stress in fetal programming of cardiovascular disease. *Front. Physiol.* **9**, 1–13.

Rolph, T. P., Jones, C. T. and Parry, D. (1982). Ultrastructural and enzymatic development of fetal guinea pig heart. *Am. J. Physiol. - Hear. Circ. Physiol.* **243**, H1–H137.

Sánchez-Díaz, M., Ángel Nicolás-Ávila, J., Cordero, M. D. and Hidalgo, A. (2020). Mitochondrial Adaptations in the Growing Heart. *Trends Endocrinol. Metab.* **31**, 308–319.

Sangkhae, V., Ganz, T., Nemeth, E., Sangkhae, V., Fisher, A. L., Wong, S., Koenig, M. D., Tussing-humphreys, L., Chu, A., Lelić, M., et al. (2020). Effects of maternal iron status on placental and fetal iron homeostasis Effects of maternal iron status on placental and fetal iron homeostasis. *J. Clin. Invest.* **130**, e127341.

Schneider, J., Han, W. H., Matthew, R., Sauvé, Y. and Lemieux, H. (2020). Age and sex as confounding factors in the relationship between cardiac mitochondrial function and type 2 diabetes in the Nile Grass rat. *PLoS One* **15**, e0228710.

Schrepper, A. (2016). Cardiac Metabolism During Development and Aging. In *The Scientist's*

Guide to Cardiac Metabolism (ed. Schwarzer, M.) and Doenst, T.), p. 73. Elsevier.

Shao, J., Richards, B., Kaciroti, N., Zhu, B., Clark, K. M. and Lozoff, B. (2021). Contribution of iron status at birth to infant iron status at 9 months: data from a prospective maternal-infant birth cohort in China. *Eur. J. Clin. Nutr.* **75**, 364–372.

Sheldon, C. A., Friedman, W. F., Sybers, H. D. and Friedman, W. F. (1976). Scanning Electron Microscopy of Fetal and Neonatal Lamb Cardiac Cells. *J. Mol. Cell. Cardiol.* **8**, 853–862.

Smith, H. E. and Page, E. (1977). Ultrastructural Changes in Rabbit Heart Mitochondria during the Perinatal Period Neonatal Transition to Aerobic Metabolism. *Dev. Biol.* **57**, 109–117.

Sordahl, L. A., Crow, C. A., Kraft, G. H. and Schwartz, A. (1972). Some Ultrastructural and Biochemical Aspects of Heart Mitochondria Associated with Development: Fetal and Cardiomyopathic Tissue. *J. Mol. Cell. Cardiol.* **4**, 1–10.

Spitzer, M., Wildenhain, J., Rappsilber, J. and Tyers, M. (2014). BoxPlotR: a web tool for generation of box plots. *Nat. Methods* **11**, 121–122.

Srere, P. A. (1997). An exception that proves the rule. *Trends Biochem. Sci.* **22**, 11.

Stevens, G. A., Finucane, M. M., De-Regil, L. M., Paciorek, C. J., Flaxman, S. R., Branca, F., Peña-Rosas, J. P., Bhutta, Z. A. and Ezzati, M. (2013). Global, regional, and national trends in haemoglobin concentration and prevalence of total and severe anaemia in children and pregnant and non-pregnant women for 1995-2011: A systematic analysis of population-representative data. *Lancet Glob. Heal.* **1**, e16-25.

Szklarczyk, D., Gable, A. L., Lyon, D., Junge, A., Wyder, S., Huerta-Cepas, J., Simonovic, M., Doncheva, N. T., Morris, J. H., Jensen, L. J., et al. (2018). STRING v11: protein-

protein association networks with increased coverage, supporting functional discovery in genome-wide experimental datasets. *Nucleic Acids Res.* **47**, 607–613.

Szklarczyk, D., Gable, A. L., Nastou, K. C., Lyon, D., Kirsch, R., Pyysalo, S., Doncheva, N. T., Legeay, M., Fang, T., Jensen, L. J., et al. (2021). The STRING database in 2021: customizable protein-protein networks, and functional characterization of user-uploaded gene/measurement sets. *Nucleic Acids Res.* **49**, 605–612.

Tan, C. M. J. and Lewandowski, A. J. (2020). The Transitional Heart: From Early Embryonic and Fetal Development to Neonatal Life. *Fetal Diagn. Ther.* **47**, 373–386.

Tang, G., Lausman, A., Abdulrehman, J., Petrucci, J., Nisenbaum, R., Hicks, L. K. and Sholzberg, M. (2019). Prevalence of Iron Deficiency and Iron Deficiency Anemia during Pregnancy: A Single Centre Canadian Study. *Blood* **134**, 3389.

Tanne, Z., Coleman, R., Nahir, M., Shomrat, D., Finberg, J. and Youdim, M. (1994). Ultrastructural and cytochemical changes in the heart of iron-deficient rats. *Biochem. Phormacology* **47**, 1759–1766.

Thammavong, K., Luewan, S., Jatavan, P. and Tongsong, T. (2020). Foetal haemodynamic response to anaemia. *ESC Hear. Fail.* **7**, 3473–3482.

Timmis, A., Vardas, P., Townsend, N., Torbica, A., Katus, H., De Smedt, D., Gale, C. P., Maggioni, A. P., Petersen, S. E., Huculeci, R., et al. (2022). European Society of Cardiology: cardiovascular disease statistics 2021. *Eur. Heart J.* **43**, 716–799.

Tzu-hsi Lao, T., Yi Annie Hui, S., Lo Wong, L. and Singh Sahota, D. (2022). Iron deficiency anaemia associated with increased placenta praevia and placental abruption: a retrospective case-control study. *Eur. J. Clin. Nutr.* **76**, 1172–1177.

Van Wilder, L., Clays, E., Devleesschauwer, B., Pype, P., Boeckxstaens, P., Schrans, D. and De Smedt, D. (2020). Health-related quality of life in patients with non-communicable disease: study protocol of a cross-sectional survey. *BMJ Open* **10**, e037131.

Van Wilder, L., Devleesschauwer, B., Clays, E., De Buyser, S., Van Der Heyden, J., Charafeddine, R., Boeckxstaens, P., De Bacquer, D., Vandepitte, S. and De Smedt, D. (2022). The impact of multimorbidity patterns on health-related quality of life in the general population: results of the Belgian Health Interview Survey. *Qual. Life Researcg* **31**, 551–556.

Velayutham, N., Agnew, E. J. and Yutzey, K. E. (2019). Postnatal Cardiac Development and Regenerative Potential in Large Mammals. *Pediatr. Cardiol.* **40**, 1345–1358.

Wallace, A. H., Dalziel, S. R., Cowan, B. R., Young, A. A., Thornburg, K. L. and Harding, J. E. (2017). Long-term cardiovascular outcome following fetal anaemia and intrauterine transfusion: a cohort study. *Arch. Dis. Child.* **102**, 40–45.

Ward, D. M. and Cloonan, S. M. (2019). Mitochondrial Iron in Human Health and Disease. *Annu. Rev. Physiol.* **81**, 453–482.

Watkins, V. Y., Frolova, A. I., Stout, M. J., Carter, E. B., Macones, G. A., Cahill, A. G. and Raghuraman, N. (2021). The relationship between maternal anemia and umbilical cord oxygen content at delivery. *Am. J. Obstet. Gynecol. MFM* **3**, 100270.

Wawer, A. A., Hodyl, N. A., Fairweather-Tait, S. and Froessler, B. (2021). Are Pregnant Women Who Are Living with Overweight or Obesity at Greater Risk of Developing Iron Deficiency/Anaemia? *Nutr. 2021, Vol. 13, Page 1572* **13**, 1572.

Weinstein, E. S., Benson, D. W., Ratcliffe, D. J., Maksem, J. and Fry, D. E. (1984).

Subpopulations of cardiac mitochondria. *Curr. Surg.* **41**, 365–369.

West-Eberhard, M. J. (2003). *Developmental Plasticity and Evolution*. Oxford: Oxford University Press.

West-Eberhard, M. J. (2005). Developmental plasticity and the origin of species differences. *PNAS* **102**, 6543–6549.

Wieringa, F. T., Berger, J., Dijkhuizen, M. A., Hidayat, A., Ninh, N. X., Utomo, B., Wasantwisut, E. and Winichagoon, P. (2007). Sex differences in prevalence of anaemia and iron deficiency in infancy in a large multi-country trial in South-East Asia. *Br. J. Nutr.* **98**, 1070–1076.

Willis, W. T., Brooks, G. A., Henderson, S. A. and Dallman, P. R. (1987). Effects of iron deficiency and training on mitochondrial enzymes in skeletal muscle. *J. Appl. Physiol.* **62**, 2442–2446.

Wittnich, C., Tan, L., Wallen, J. and Belanger, M. (2013). Sex differences in myocardial metabolism and cardiac function : an emerging concept. 719–729.

Wofford, J. D., Chakrabarti, M. and Lindahl, P. A. (2017). Mössbauer spectra of mouse hearts reveal age-dependent changes in mitochondrial and ferritin iron levels. *J. Biol. Chem.* **292**, 5546–5554.

Woodman, A. G., Care, A. S., Mansour, Y., Cherak, S. J., Panahi, S., Gragasin, F. S. and Bourque, S. L. (2017). Modest and severe maternal iron deficiency in pregnancy are associated with fetal anaemia and organ-specific hypoxia in rats. *Sci. Rep.* **7**, 1–10.

Woodman, A. G., Mah, R., Keddie, D., Noble, R. M. N., Panahi, S., Gragasin, F. S., Lemieux, H. and Bourque, S. L. (2018). Prenatal iron deficiency causes sex-dependent

mitochondrial dysfunction and oxidative stress in fetal rat kidneys and liver. *FASEB J.* **32**, 1-10.

Woodman, A. G., Noble, R. M. N., Panahi, S., Gragasin, F. S. and Bourque, S. L. (2019). Perinatal iron deficiency combined with a high salt diet in adulthood causes sex-dependent vascular dysfunction in rats. *J. Physiol.* **597**, 4715–4728.

Woodman, A. G., Mah, R., Keddie, D. L., Noble, R. M. N., Holody, C. D., Panahi, S., Gragasin, F. S., Lemieux, H. and Bourque, S. L. (2020). Perinatal iron deficiency and a high salt diet cause long-term kidney mitochondrial dysfunction and oxidative stress. *Cardiovasc. Res.* **116**, 183–192.

Woodman, A. G., Mah, R. L., Kinney, S., Holody, C. D., Wiedemeyer, A. R., Noble, R. M. N., Clugston, R. D. and Bourque, S. L. (2023). Perinatal iron deficiency causes sex-dependent alterations in renal retinoic acid signaling and nephrogenesis. *J. Nutr. Biochem.* **112**, 109227.

World Health Organization (2001). *Iron deficiency anaemia: Assessment, prevention, and control. A guide for programme managers.* Geneva: World Health Organization.

World Health Organization (2015). *The global prevalence of anaemia in 2011*. Geneva: World Health Organization.

World Health Organization (2017). *Nutritional Anaemias: Tools for Effective Prevention*. Geneva: World Health Organization.

World Health Organization (2018). *Noncommunicable Diseases: Country Profiles 2018*. Geneva: World Health Organization.

World Health Organization (2022a). *Noncommunicable Diseases: Progress Monitor 2022*.

Geneva: World Health Organization.

World Health Organization (2022b). Noncommunicable diseases.

Young, M. F., Oaks, B. M., Tandon, S., Martorell, R., Dewey, K. G. and Wendt, A. S. (2019). Maternal hemoglobin concentrations across pregnancy and maternal and child health: a systematic review and meta-analysis. *Ann. N. Y. Acad. Sci.* **1450**, 47–68.

Zgliczynska, M. and Kosinska-Kaczynska, K. (2021). Micronutrients in Multiple Pregnancies-The Knowns and Unknowns: A Systematic Review. *Nutrients* **13**, 386.

Zhou, Y., Zhou, B., Pache, L., Chang, M., Khodabakhshi, A. H., Tanaseichuk, O., Benner, C. and Chanda, S. K. (2019). Metascape provides a biologist-oriented resource for the analysis of systems-level datasets. *Nat. Commun.* **10**, 1–10.